UNIVERSITÀ
DEGLI STUDI
DI PADOVA

UNIVERSITA' DEGLI STUDI DI PADOVA

Dipartimento di Ingegneria Industriale DII

Corso di Laurea Magistrale in Ingegneria Energetica

A GIS-BASED APPROACH FOR RURAL ELECTRIFICATION AND SOLAR RESOURCE ASSESSMENT: THE CASE STUDY OF A COMMUNITY IN CUBA

Relatore: Prof.ssa Anna Stoppato

Laureando: Carlo Bellini
1178480

Anno Accademico 2019/2020

Abstract

Rural electrification is a crucial step for the socio-economic development of isolated communities. Decentralized power generation, typically more favorable for renewable energies, requires an accurate analysis of the different electrification options, whose convenience depends on multiple factors. The application of Geographical Information System to energy planning allows the assessment at a local level, taking into account the spatial variability of the resources and the distribution of the demand in a territorial context.

The present work proposes a GIS-based model for the calculation of the Levelized Energy Cost (LEC) of several electrification options. The model is implemented in ArcGIS environment and performs the comparison between three power generation options: solar system, diesel generator set and solar-diesel hybrid system. The various configurations can be set by adjusting the input variables, with a special focus on the confrontation between individual systems or centralized mini-grids.

While obtaining one of the required inputs, a solar radiation map, a secondary objective of the research is developed. A method for the creation of high-resolution solar radiation maps is proposed, reducing the approximation due to the extent of the area considered.

The model is finally tested for the case study of the municipality of Guasasa (Cuba), whose electrification is part of the project "HIBRI2". The techno-economic assumptions are facilitated by the background of knowledge provided by previous studies and the simulation leads to reasonable and justifiable results.

The objective is to provide an adequate groundwork for the development of a decision-making tool for the assessment of different rural electrification options, achievable from future studies.

Riassunto esteso

L'elettrificazione rurale rappresenta un passo fondamentale per lo sviluppo socioeconomico delle comunità isolate. La produzione decentralizzata, tipicamente più favorevole alle energie rinnovabili, richiede un'analisi accurata delle varie opzioni di elettrificazione, la cui convenienza dipende da molteplici fattori. Applicare i Sistemi di Informazione Geografica (GIS) alla pianificazione energetica permette una valutazione a livello locale, considerando la variabilità spaziale delle risorse disponibili e la distribuzione della domanda in un contesto territoriale.

Il presente lavoro propone un modello di calcolo del Levelized Energy Cost (LEC) di diverse tipologie d'impianto di generazione elettrica, basato sulla tecnologia GIS. Il modello viene implementato in ambiente ArcGIS e confronta tre opzioni di produzione energetica: sistema fotovoltaico, gruppo diesel o impianto ibrido solare e diesel. Le diverse configurazioni possono essere impostate modificando le variabili di input, con particolare attenzione alla contrapposizione fra soluzione individuale o centralizzata tramite una microrete.

Nel ricavare uno degli input necessari, una mappa della radiazione solare, si è sviluppato un obiettivo secondario della ricerca. Viene proposto un metodo per la creazione di mappe di radiazione solare ad alta risoluzione spaziale, limitando le approssimazioni legate alla vastità dell'area considerata.

Il modello viene infine applicato al caso studio del villaggio di Guasasa (Cuba), la cui elettrificazione è parte del progetto HIBRI2. Le assunzioni tecno-economiche sono agevolate dalla base di conoscenze derivate da ricerche precedenti e la simulazione porta a risultati verosimili e giustificabili.

Il fine è quello di fornire le basi per uno strumento decisionale di valutazione delle opzioni di elettrificazione in un contesto rurale, auspicale da sviluppi futuri.

Aknowledgments

I am grateful for having the opportunity to live an important experience at Ciemat.

I need to express my thanks to my tutor Javier Domínguez for the constant support and to all the people who kindly contributed in my thesis work: Luis Arribas, Luis Zarzalejo, Julio Amador and Ana Martín.

Summary

1 Introduction

Access to electricity is an essential requirement for human development. It is recognized as a basic need to ensure the respect of human rights and the improvement of life quality. According to the World Energy Outlook - 2019, 860 million people in the world are still without access to electricity, of whom almost 600 million are in Sub-Saharan Africa (IEA, 2019).

During the recent years, the worldwide energy policies are strongly committed in reducing this numbers. The trend is positive: in 2017, the population without electricity amounted to almost 1 billion, so the improvement is promising. The progress is concentrated in some areas, especially in Asia, which counts 80% of the 800 million people who gained access since 2000. Nearly two-third of them are attributable to India. The target of reaching 100% of the electrification rate has a major issue: especially in developing countries, the welfare provided by the new energy availability is likely to induce a positive feedback by further increasing the population growth rate, thus increasing the population target. As a consequence, the effort to pursue this challenge must be held constant.

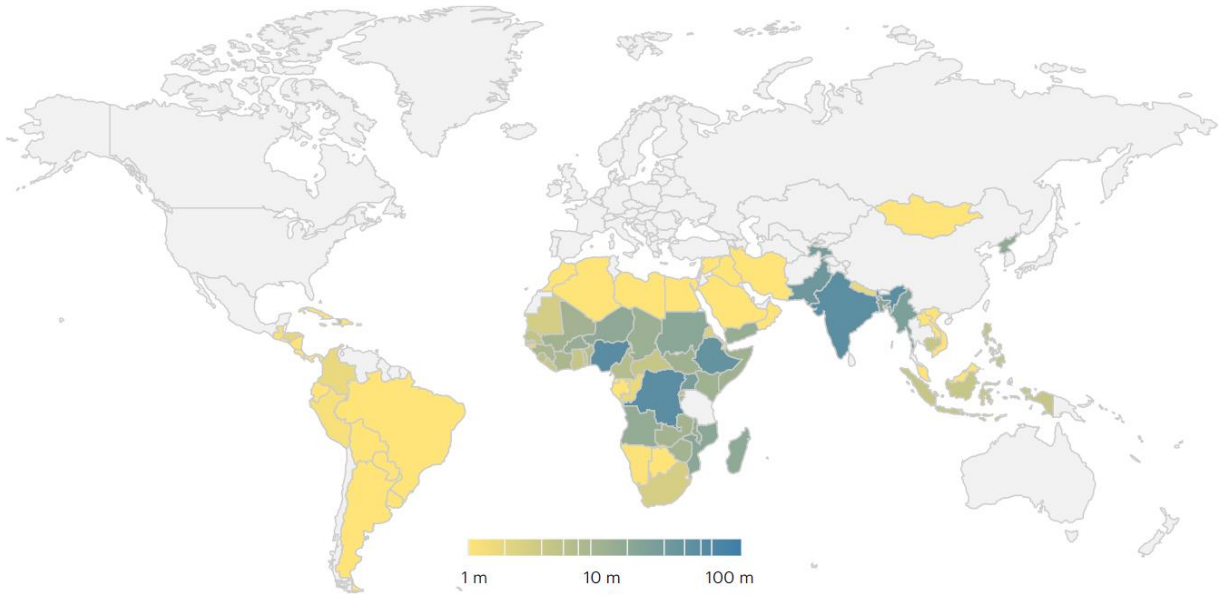

Figure 1.1: World population without access to electricity, divided by countries (2018). Units of million people (IEA,2019).

One of the United Nation's Sustainable Development Goals is to reach universal access to clean and affordable energy by the year 2030. In the Sustainable Development Scenario (SDS)[1],

[1] The International Energy Agency Sustainable Development Scenario outlines a major transformation of the global energy system in order to achieve the three Sustainable Development Goals (SDG) closely related to energy: to achieve universal access to energy (SDG 7), to reduce the severe impact of air pollution (part of SDG 3) and to tackle climate change (SDG 13) (IEA, 2019).

considering an expected strong population growth, this goal would require a cumulative total of more than 1 billion people to be supplied by new energy access. In economic terms, it has been estimated that the process would require an average investment of $40 billion per year (IEA, 2019). According to the Stated Policies Scenario (SPS), so assuming to keep the current and announced policies, the improvements would be considerably slower. In particular, in Sub-Saharan Africa the actual rate of annual connections would require a triplication.

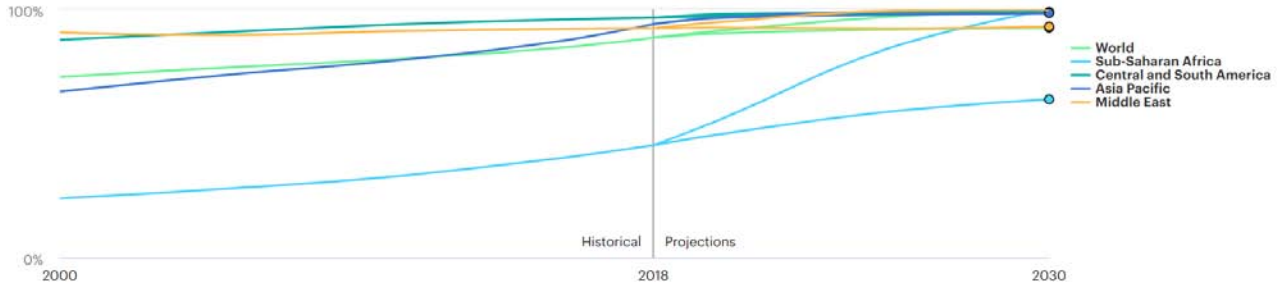

Figure 1.2: Historical and estimated proportion of population without access to electricity of the most critical regions. The lower curves follow the SDS, the upper curves follow the SPS (IEA, 2019).

Renewable energies represent the key to achieve this ambitious target while preserving sustainability. In many areas they would also be the least expensive option.

The advantage of renewable energy in its various form is the unrestricted availability all around the world, even in areas where the distribution of conventional energy sources is inconvenient. The disadvantage is its typical variability, both in time and space, which can undermine a reliable power supply. A careful assessment of the available energy mix is therefore a fundamental step in the early stage of an electrification project. Several factors are involved in this process and they are often detectable at a local level.

The present work aims to provide a decision-making tool for rural electrification projects, using Geographic Information Systems (GIS). It is focused on the economical aspect and on solar energy source, coupled to diesel power generation in different possible configurations.

1.1 Rural electrification

There are two general approaches to electrification: through the extension of the national grid or by the implementation of off-grid systems. The first one is by far the most common, including the 99% of electricity infrastructure investments from utilities and governments (Louie, 2018). The off-grid option prevails when some specific conditions penalize the extension, usually due to an excessive distance from the existing grid.

It is important to be able to estimate the cost associated to both the cases, in order to choose the most convenient option for each case. The cost clearly rises with the increase of the distance to be covered by the grid extension, while the cost of the off-grid option can be

considered independent from the distance. In figure 1.3, the intersection of the cost curves, as a function of the distance from existing grid, indicates the limit which determines whether a system is more economically favorable than the other. To the right of the dot, the off-grid system start being the most cost-effective option for the electrification.

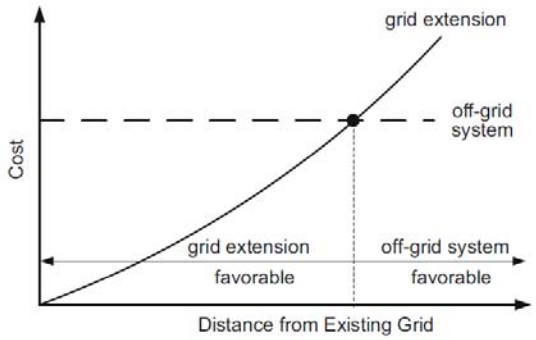

Figure 1.3: Simplified cost curve of grid extension and off-grid systems (Louie, 2018)

It is evident that isolated communities are the most affected by lack of electrification access, due to several aspects that discourage the investors. The main critical aspects of rural electrification are typically the low density load and the high installation, operation and maintenance costs which lead to a long investment return period. As can be noticed in figure 1.4, the gap of rural areas respect to the urban ones is widespread. In 2018, the proportion of the world rural population with access to electricity was 79%, against the 96% of urban population.

Source: IEA, *World Energy Outlook -2019*

Electricity Access, Summary by Region

	Proportion of the population with access to electricity						
	National					Urban	Rural
	2000	2005	2010	2015	2018	2018	2018
WORLD	**73%**	**77%**	**80%**	**85%**	**89%**	**96%**	**79%**
Developing Countries	**64%**	**69%**	**74%**	**80%**	**86%**	**95%**	**77%**
Africa	**36%**	**39%**	**43%**	**49%**	**54%**	**79%**	**35%**
North Africa	91%	96%	>99%	>99%	>99%	>99%	>99%
Sub-Saharan Africa	24%	28%	33%	40%	45%	74%	26%
Developing Asia	**67%**	**74%**	**79%**	**87%**	**94%**	**98%**	**91%**
China	99%	>99%	>99%	>99%	>99%	>99%	>99%
India	43%	58%	68%	79%	95%	>99%	92%
Indonesia	53%	56%	67%	88%	98%	>99%	96%
Other Southeast Asia	65%	76%	79%	85%	90%	97%	83%
Other Developing Asia	38%	46%	57%	74%	79%	89%	73%
Central and South America	**88%**	**91%**	**94%**	**96%**	**97%**	**99%**	**88%**
Middle East	**91%**	**90%**	**91%**	**92%**	**93%**	**98%**	**78%**

Figure 1.4: Proportion of population with access to electricity of the most critical regions (IEA, 2019).

Two main categories of off-grid electrification options can be identified: centralized systems and individual systems. A centralized system requires the construction of a mini-grid that

connects all the loads to the central power plant. In cases of sufficient diversified available energy mix, a hybrid plant, which combines different types of technologies, can be a viable option. Individual systems are designed to supply energy to each load autonomously. Typical examples are: photovoltaic (PV) stand-alone systems, small wind turbines or small diesel generators. The choice of the best option and the most convenient configuration can be challenging. The objective of this work is to facilitate this task.

1.2 Geographic Information Systems (GIS)

Dealing with renewable energy sources (RES), an adequate assessment is fundamental when dealing with coupling the energy demand with the power supply. Spatial and temporal variability play a crucial role in this process. In addition, the integration of a technology has always an important territorial impact, which is not easily detected by a merely technical approach.

Geographical Information Systems (GIS) represents an instrument capable of integrating non-spatial features (technological, economical, etc.) in a local reality, not only intended from a geographical point of view, but also from the perspective of a network of mutually related activities (Domínguez, 2002). The National Center for Geographical Information and Analysis, provides the following definition of a GIS: "A hardware, software and procedure system, designed to enhance access, management, handling, modelling and representation of data output, spatially referenced, to solve complex planning and management problems" (Domínguez, 2000). GIS science allows to combine, manage and analyze a large volume of graphic information (maps) or alphanumeric data (statistics).

The terminology "layer" is commonly used to refer to the mechanism of displaying a geographic dataset. GIS layers are typically classified in two main types: *vector* and *raster*.

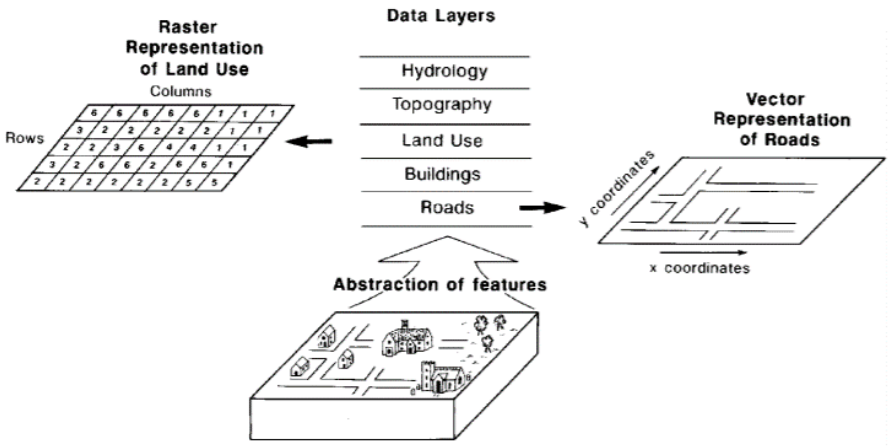

Figure 1.5: Example of raster and vector layer representation of real-world topology (Lovett, 2000).

A vector-based system can depict the characteristics of an area through a series of coordinates couples representing the origin and the end of the feature which is described. In case of point

features, the origin and the end of the vectors coincide. The properties associated to each vector are included in an attribute table. In a matrix system, also called "raster", the area is represented by an array of georeferenced pixels (or cells) associated to one or more attribute values.

A crucial tool of GIS technologies is spatial analysis. Through the topological relations between different elements, it allows to make calculations and create new desired outputs. A first example is the possibility to merge different layers of geographical information according to specific data correlations. Other basic spatial analyst tools allow to create an area of influence with reference to one or more variables of a geographic element. It is the case of buffer creations or dynamic segmentations. Proximity analysis performs an interaction between an element and its surrounding environment, deriving several information. An important potential is the possibility of creating network systems of different types, starting from topological data: hydrographical, transportation, electric, etc. A diffuse means of spatial analysis are the Digital Elevation Models (DEM). They are arrays of regularly spaced elevation values, so a georeferenced representation of the terrain morphology. The cell size of their raster format defines the resolution. From this brief summary of spatial analysis tools, GIS technology result being an ideal instrument for modeling and simulation (Domínguez, 2000).

The wide geographical dispersion that characterizes RES and the importance of evaluating their integration at a local level fit perfectly with the potential of GIS analysis.

1.3 Objectives and method

The objective of this thesis is the development of a GIS-based model for the techno-economic assessment of rural electrification projects, considering the spatial distribution of the demand and the resources. The technologies considered are: photovoltaic system, diesel generator set and their combination in a hybrid system. The resulting comparison of different power plant configurations can be used in a decision-making process for the evaluation of the best electrification option.

Dealing with solar systems modeling, an input layer was required representing the available resource. A high spatial resolution is needed, since the present work is primarily designed for small scale realities. Hence, the high-quality assessment of solar resource represents a secondary objective of the thesis. The proposed approach is not limited in providing useful information for the model. A method is defined for the creation of solar radiation maps, with the purpose of being replicable for any location of interest.

The study is based on the application of the software *ArcGIS* by Esri[2], in the version 10.7.1 of its main component *ArcMap*, used primarily to view, edit, create, and analyze geospatial data. In the first part of the thesis work, one of its tools, called *Area Solar Radiation*,

[2] The Environmental System Research Institute is one of the major producers of GIS softwares.

is used to create a solar radiation raster with a spatial resolution of 30 meters. As reference area, the entire province of Matanzas (Cuba) is considered, a much wider region respect to the one required by the case study, described in the next paragraph. A series of twelve maps, one for each month of the year, are created and merged in order to provide a value for each pixel of the average annual radiation received. The shadows originated by both the morphology and the horizon characteristics are considered in the calculation. The study includes the implementation of a phyton script for the cyclic execution of Area Solar Radiation, with the aim of bypassing the limitation of the tool in performing the calculation for large areas. Indeed, the input settings only allows the insertion of single values for the definition of the atmospheric influence on solar radiation, a condition which may vary considerably over time and space. The validation is conducted through the software *Meteonorm*, version 7.

Meteonorm is a widely used solar radiation data source in the solar energy industry. Its reliable database provides punctual values of solar radiation for any desired site. Selecting an adequate number of locations, it is possible to compare the results with the output derived from the ArcMap calculation. In order to facilitate the comparison, a second phyton script is implemented for the cyclical execution of *Point Solar Radiation*, another ArcMap tool. It has the same architecture of Area Solar Radiation but designed for the calculation on specific point locations. The comparison allows to investigate and perform the necessary corrections on the input tool settings, so that the output of Area Solar Radiation have a minimal error respect to the experimental measurements.

The second part of the thesis is focused on the implementation and the test of the model. One of the input required is the solar radiation map, previously obtained. Another input layer is the distribution of the energy demand, created by a point layer representation of the buildings of the case study. ArcGIS is again the environment of the investigation, making use of its function *ModelBuilder*. The model is designed as a series of calculations between the attributes of the various loads, properly set for each specific simulation. The equations used were extracted from the model proposed by *IntiGIS*[3] and adapted to the structure of the new model. The main result of the set of equations is the *Levelized Energy Cost* (LEC) of the power plant considered for the simulation (also referred as Levelized Electricity Cost or LCOE, Levelized Cost of Energy). The LEC allows the comparison of different methods of electricity generation, based on the sum of all costs which arise throughout the lifetime of the power plant and the sum of the amount of energy produced. It basically measures the average total cost of producing a unit of energy. The immediacy of the information that contains makes it the ideal index to provide a guideline for electrification planning.
Once discussed how the model is structured, it is applied to the case study of the community of Guasasa (Cuba), presented in the next paragraph. The input assumptions are set, drawing

[3] IntiGIS is a model for the evaluation of rural electrification options, developed by CIEMAT research centre.

information from the existing studies. The model is designed with the aim of being adaptable for any case. It has to be seen as the groundwork for a more complete tool derivable from further developments. From this perspective, the results of the simulation are analysed and the different proposed configurations are compared.

In summary, the thesis is structured in three main parts:

- Creation of high-resolution solar radiation maps of Matanzas (Cuba), implementing a method to increase the accuracy for wide areas calculations (Chapter 2);
- Implementation of a model for the LEC calculation of different types of power plant, using Geographical Information Systems (Chapter 3);
- Test of the model for the case study of Guasasa (Chapter 4).

1.4 Context of the case study

The model is tested in the context of the project *HIBRI2*: "Integrated control system for energy supply through hybrid systems in isolated communities in Cuba. Phase II". HIBRI2 is included in the innovation projects promoted by the AECID (Spanish Agency for International Development Cooperation), coordinated by the research centre CIEMAT[4], where the present work took place. The target of the project is to complete the electrification of the small isolated community of Guasasa (Cuba). It constitutes a continuation of the project *HIBRIDUS*, with the objective of promoting the integration of renewable energies in different cuban locations. HIBRIDUS operates actively many projects, among which it is worth mentioning the realization of a cogeneration system to help agricultural exploitations in the municipality of Guama, located in Santiago de Cuba province. HIBRI2 proceed with the same path launched by the previous studies, from which an important background knowledge can be derived. The spanish participants, besides CIEMAT, are the ONG SODEPAZ, in charge of logistic and communication, and BORNAY, responsible for the technical installation of the renewable energy equipment. The cuban institutions included in the project are CUBAENERGÍA, UNE (Unión Eléctrica de Cuba), the municipal government and the Cuban forestry sector (Caballero, 2019).

[4] Centro de Investigaciones Energéticas, Medioambientales y Tecnológicas, a Spanish Public Research Institution dependent on the Ministry of Economy and Competitiveness.

Guasasa is located next to the eastern part of Playa Girón, in Ciénaga de Zapata municipality (province of Matanzas). It is part of the southern coast overlooking the Caribbean Sea and its geographic coordinates are: 22° 38' 0" North; 83° 43' 0" East.

Map 1.1: Location of Guasasa, Cuba (source: Google Maps).

The climate is characterized by warm temperatures during the whole year, with an average annual temperature of 24.5 ℃.

Month	Average temperature (℃)
January	21.1
February	22.3
March	23.8
April	25.3
May	25.9
June	26.3
July	26.3
August	26.4
September	26.1
October	25
November	23.5
December	21.8
Annual average	**24.5**

Table 1.1: Average temperatures in Guasasa, registered during a period of 25 years (1983-2005) (Caballero, 2019).

The population of Guasasa is composed by 214 people and the principal activity of the community is fishing, which constitutes almost the 60% of the economy. The remaining percentage is characterized by forestry service (25%) and other community works (Caballero, 2019).

The actual level of electrification is provided by a diesel generator set which feeds the village for a total of 12 hours a day. The target of HIBRI2 is to provide a continuative energy supply (24 hours a day) through the integration of renewable energies, in order to support the social and economic development of the community. In addition to the direct benefits for Guasasa, the project will constitute an important educational source of information for further applications in other parts of the island.

Figure 1.6: Photos of some examples of typical houses in Guasasa community (Ciemat, 2020).

2 Solar radiation map

One of the inputs required by the LEC model is the spatial distribution of the incoming solar radiation over the study area. In order to reach this data, a viable option could be downloading a solar radiation map in a raster format. The most reliable web sources founded are the following:

- "*Global Solar Atlas*" by the "World bank Group" in collaboration with "SOLARGIS[5]": raster data available in GeoTIFF and AAIGRID (Esri ASCII Grid) format with a spatial resolution (pixel size) of 9 arcsec (nominally 250 m)[6];
- "*NASA Power | Prediction Of Worldwide Energy Resources*": raster data in GeoTIFF format with a spatial resolution of 0.5 degrees[7].

Most of the available maps are created through the interpolation and extrapolation of point-specific measurement, combined with satellites estimations. However, dealing with small and rural areas, a more specific approach would be recommended. Isolated zones are less likely to provide direct measurements, also topographic heterogeneity affects considerably the insolation.

2.1 Area Solar Radiation: an ArcGIS tool

"At a global scale, the latitudinal gradients of insolation, caused by the geometry of Earth's rotation and revolution about the sun, are well known. At the landscape scale, topography is the major factor modifying the distribution of insolation. Variability in elevation, surface orientation (slope and aspect), and shadows cast by topographic features create strong local gradients of insolation." (Fu and Rich, 1999).

Area Solar Radiation is an ArcMap tool, included in the Spatial Analyst extension. It implements a solar radiation model using a digital elevation model (DEM) as input. Its core is the viewshed algorithm, which allows to create maps of global, direct and diffuse radiation for a specific period of time, accounting the site latitude and elevation, shifts in solar angle, atmospheric attenuation, surface orientation and the surrounding topography. It represents an effective tool for the analysis at a local scale, pointing out spatial and temporal variation. For this reason, Area Solar Radiation was chosen to create the insolation map of Guasasa. In addition, the calculation is extended to the entire province of Matanzas and a solar map of a wider area is generated for the benefit of possible future projects or other applications.

[5] SolarGIS is a web service (http://solargis.info) for planning and performance assessment of PV systems.
[6] https://globalsolaratlas.info
[7] https://power.larc.nasa.gov

2.1.1 Viewshed Calculation

A viewshed is the angular distribution of sky obstruction. For every specific position, it provides a raster representation of the visible sky and the sky direction obstructed by the surrounding topography and surface features. For each cell of the input DEM, the viewshed algorithm calculates the maximum angle of sky obstruction (horizon angle) for a specific set of directions around the location of interest (fig. 2.1, left). For all the other directions, the horizon angles are calculated using interpolation (fig. 2.1, right)(Fu & Rich, 1999).

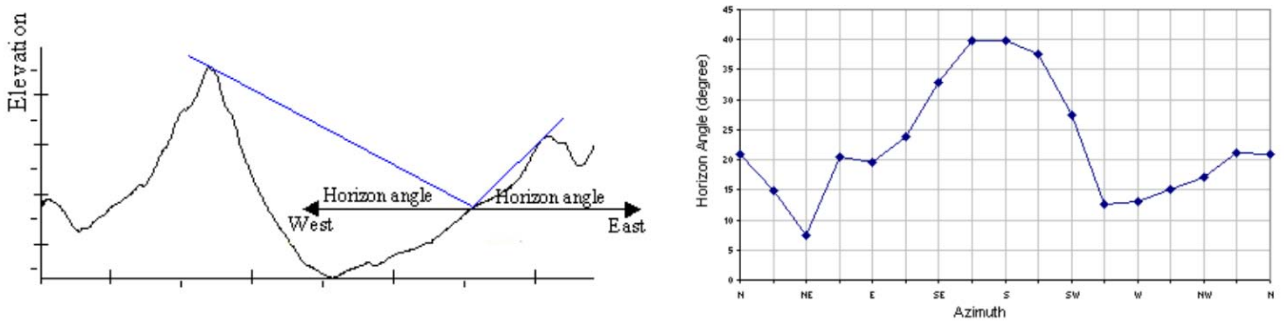

Figure 2.1: Example of horizon angles calculated for two directions (West and East); Horizon angle interpolated for every direction. (Fu and Rich, 1999)

Horizon angles are then projected into a hemispherical coordinate system. Every cell of the viewshed raster grid corresponds to both a zenith angle (θ) (relative to the vertical direction) and an azimuth angle (α) (relative to north direction), allowing to represent a three hemisphere of directions as a two-dimensional grid. Once calculated and converted the horizon angle along the set directions, the sky view associated to each cell of the DEM reminds an upward-looking fisheye photo.

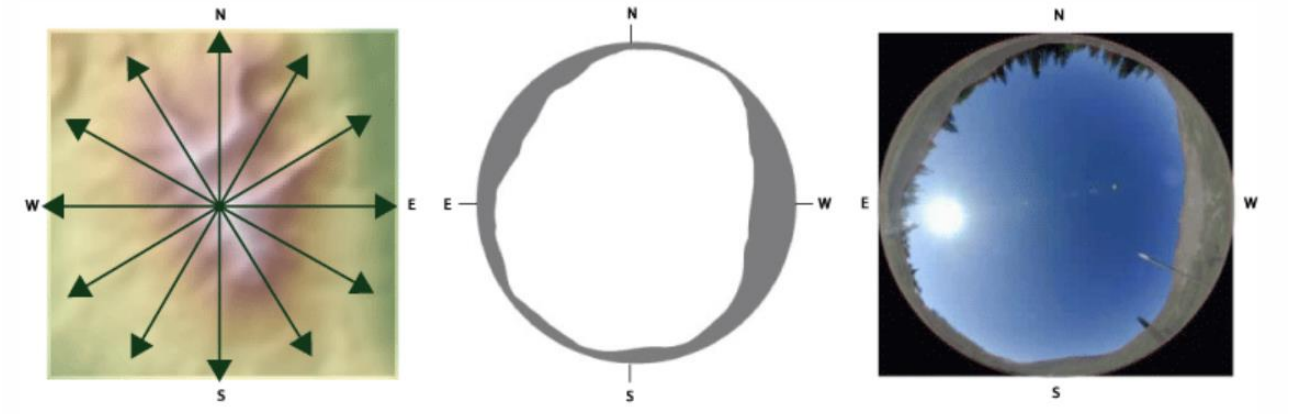

Figure 2.2: direction set for the horizon angle calculation; resultant viewshed (in grey, the obstructed sky sectors) in hemispherical coordinate system; hemispherical (fisheye) photograph (ArcGIS Desktop Help, 2019).

Such viewsheds are then overlayed with a direct sunmap and a diffuse skymap to estimate the direct and diffuse radiation. Repeating the same operation to every raster cell and combining the results will produce an insolation map.

2.1.2 Sun map and Sky map

A sun map represents the apparent position of the sun and its variation over time. It is projected in the same hemispherical coordinates as the viewshed. The sun positions, defined by zenith and azimuth angles, are derived through astronomical equations based on the latitude location and the specific time period. Knowing the sun position, the direct solar radiation can therefore be calculated. A time interval has to be set to define the size of the discrete sky sector which represents the suntrack. Penumbral effects are also accounted, so are the solar disc size variation due to refraction near the horizon.

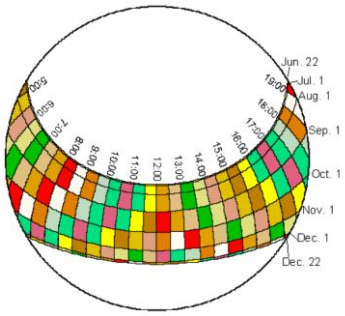

Figure 2.3: Example of a 6 months sun map using a 0.5 hour intervals through the day and month intervals through the year. (Fu and Rich, 1999).

Since diffuse solar radiation is spread along any sky direction, its calculation is related to a different hemispherical raster representation. A sky map represents the entire sky divided into a series of sky sector, which size depends on the number of divisions set for the calculation. Diffuse radiation can be calculated for each sky sector, defined by the zenith and azimuth angles of their centroid and assigned to an identifier value.

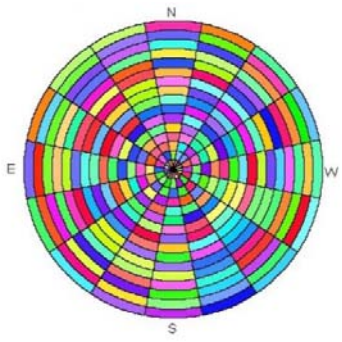

Figure 2.4: A sky map with sky sectors defined by 16 zenith divisions and 16 azimuth divisions. (Fu and Rich, 1999).

Combining viewshed, sun map and sky map, the unobstructed sky area is determined. Hence, the direct and diffuse solar radiations are calculated considering such area only. In particular, the proportion of visible sky is represented by the gap fraction, calculated for each sector as the number of unobstructed cells divided by the total number of cells.

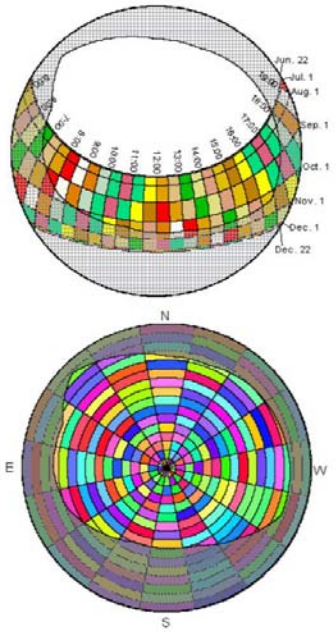

Figure 2.5: Overlay of a viewshed on a sun map (upper) and a sky map (lower). Shaded areas are obstructed sky directions. (Fu and Rich, 1999).

2.1.3 Solar radiation calculation

The incoming global solar radiation (G_{tot}) for a given location during a specific period is calculated as the sum of direct and diffuse radiations.
The contribution of reflected radiation is neglected by the algorithm, since its prediction is complex and it generally constitutes a small proportion of the total.

$$G_{tot} = Dir_{tot} + Dif_{tot} \tag{2.1}$$

Dir_{tot} is the sum of the direct insolation from each sun map sector ($Dir_{\theta,\alpha}$).

$$Dir_{tot} = \Sigma\, Dir_{\theta,\alpha} \tag{2.2}$$

Dif_{tot} is the sum of the diffuse insolation from each sky map sector ($Dif_{\theta,\alpha}$).

$$Dif_{tot} = \Sigma\, Dif_{\theta,\alpha} \tag{2.3}$$

The direct solar radiation from the sun map sector with a centroid at zenith angle (θ) and azimuth angle (α) is calculated as follows.

$$Dir_{\theta,\alpha} = S_{Const} \cdot \beta^{m(\theta)} \cdot SunDur_{\theta,\alpha} \cdot SunGap_{\theta,\alpha} \cdot cos(AngIn_{\theta\alpha,}) \quad (2.4)$$

Where:

- S_{Const} is the Solar Constant, representing the solar flux outside the atmosphere. The value considered is at the mean earth-sun distance and, according to the World Radiation Center (WRC), it is equal to 1367 W/m²;
- β is the transmittivity of the atmosphere (averaged over all wavelengths) for the shortest path (in direction of the zenith);
- $m(\theta)$ is the relative optical path length, as a proportion of the zenith path length. For zenith angles lower than 80° it can be calculated by the following equation;

$$m(\theta) = \frac{e^{-0.000118 \cdot Elev - 1.638 \cdot 10^{-9} \cdot Elev^2}}{cos(\theta)} \quad (2.5)$$

- $Elev$ is the ground elevation above the sea level;
- $SunDur_{\theta,\alpha}$ is the equivalent time duration of the sky sector;
- $SunGap_{\theta,\alpha}$ is the gap fraction of the sun map sector (introduced in 2.1.2);
- $AngIn_{\theta\alpha}$ is the angle of incidence between the centroid of the sky sector and the axis normal to the surface. Multiplying by the cosine of this angle, the effect of the surface orientation is taken into account;

$$AngIn_{\theta,\alpha} = arcos[cos(\theta) \cdot cos(G_z) + sin(\theta) \cdot sin(G_z) \cdot cos(\alpha - G_a)] \quad (2.6)$$

- G_z is the surface zenith angle;
- G_a is the surface azimuth angle;

The diffuse solar radiation from the sky map sector with the centroid at a certain zenith angle (θ) and azimuth angle ($\propto$), is calculated as follows.

$$Dif_{\theta,\alpha} = R_g \cdot P_{dif} \cdot Dur \cdot SkyGap_{\theta,\alpha} \cdot Weight_{\theta,\alpha} \cdot cos(AngIn_{\theta,\alpha}) \quad (2.7)$$

Where:

- P_{dif} is the diffuse proportion, indicating the fraction of global normal radiation which is diffuse;

- R_g is the global normal radiation, calculable as the sum of the direct radiation from every sector without correction for angle of incidence and divided by the proportion of direct radiation $(1 - P_{dif})$;

$$R_g = \frac{S_{Const}\,\Sigma\left(\beta^{m(\theta)}\right)}{1 - P_{dif}} \tag{2.8}$$

- $Weight_{\theta,\alpha}$ is the proportion of diffuse radiation related to a sky sector with respect to all the sectors.
  For the uniform sky diffuse model, it is calculated as:

$$Weight_{\theta,\alpha} = \frac{(cos\theta_2 - cos\theta_1)}{Div_{azi}} \tag{2.9}$$

  For the standard overcast sky model, it is calculated as:

$$Weight_{\theta,\alpha} = \frac{(2cos\theta_2 + cos2\theta_2 - 2cos\theta_1 - cos2\theta_1)}{4 \cdot Div_{azi}} \tag{2.10}$$

- $\theta_1$and θ_2 are the bounding zenith angles of the sky sector;
- Div_{azi} is the number of azimuthal divisions of the sky sector.

2.2 Input settings

The solar radiation tool requires some user-defined input parameters. For the present study, the parameters are set aiming a good trade-off between accuracy of results and reasonable time of calculation. DEM, Latitude, Transmittivity and Diffuse proportion will be introduced in the next paragraphs. The rest of the input settings are introduced in table 1:

Sky size / Resolution	200
Time configuration	Multiple days in a year (2020, Start day, End day)
Day interval	3
Hour interval	0.5
Z factor	1
Slope and aspect input type	FLAT_SURFACE
Calculation directions	32
Zenith divisions	16
Azimuth divisions	16
Diffuse model type	STANDARD_OVERCAST_SKY

Table 2.1: Some of the chosen inputs setting for the solar analysis.

- The Sky size defines the resolution of the viewshed, the sun map and the sky map rasters. Its value refers to the number of grid cells per side (rows and columns). “A 200 x 200 sky size is sufficient for most purposes. Increasing sky size beyond this does not significantly improve model accuracy, but greatly increases computation time.” (Fu & Rich, 1999). A value of 200 is therefore chosen for the sky size, being a good compromise between time consumption and accuracy.
- The time configuration specifies the time for which insolation is to be calculated. The chosen periods are monthly intervals, selecting the number of start and end day out of 365 (366 for leap years, as in the case of 2020). Notice that the end day is exclusive in the period considered (e.g. January Start-End days are: 1-32).
- The time interval is used for the calculation of sky sectors for the sun map. To ensure a high precision, a daily interval through the year and a 0.5 hour interval through the day has been chosen. “In general, […] a 0.5 hour interval is sufficient for multi-day calculations” (Fu and Rich, 1999).
- Selecting “FLAT_SURFACE” option, the calculation will be performed considering the irradiation on a horizontal surface.
- The Z factor has the function to convert the surface z units when they differ from the ground x,y units. Converting all the data in a meters projected coordinate system, Z factor can be set with the value of 1.
- The number of directions refers to the viewshed calculation. “Natural terrain at 30-meters resolution is usually quite smooth, so fewer directions are sufficient for most situations (16 or 32)” (ArcGis Desktop Help, 2019).
- The values of azimuth and zenith divisions, used to create sky sectors in the sky map, needs to be a multiple of 8. “In most situations 8 x 8 sky divisions is sufficient. In cases where diffuse radiation is of major interest, skymap divisions should be increased to 16 x 16 or even more” (Fu and Rich, 1999).
- Selecting the “STANDARD_OVERCAST_SKY” diffuse model type, the incoming diffuse radiation flux varies with the zenith angle.

2.2.1 Digital Elevation Model

“A Digital Elevation Model (DEM) represents the 3D shape of a terrain in a digital format. A terrain is mathematically modelled as a function $z = f(x, y)$ which maps each point (x, y) in a planar domain D into an elevation value $f(x, y)$. In this view, the terrain is the graph of function f over D” (De Floriani & Magillo, 2018).

In other words, a DEM data set is composed by points or grid cells associated to latitude-longitude location references and the respective value of altitude.

It is possible to make a distinction between two types of models: Digital Terrain Model (DTM) and Digital Surface Model (DSM). While the first one refers exclusively to the ground surface, a DSM also includes vegetation and anthropic elements. The main index of DEM quality is its cell resolution. Of course, minimizing the topographic generalization is a key step in order to obtain a high-quality calculation.

The "Advance Land Observation System (ALOS) World 3D – 30 m (AW3D30) Digital Surface Model" is a global digital surface model dataset with a horizontal resolution of approximately 30 m (1 arcsec). It was released in 2015 by the Japan Aerospace Exploration Agency (JAXA) Earth Observation Research Centre, in a free of charge version available upon registration[8]. A mosaic of the area which includes the province of Matanzas has been downloaded and properly cut and merged through ArcMap tools. Since the insolation is influenced by the horizon angle, which depends on the surrounding topography, the area considered was extended beyond the borders of the province itself.
In figure 2.6, the MDS used as input for "Area Solar Radiation" calculation. Each pixel of the map represents an area of 30x30 meters approximately. To highlight the effective study area, a map of the province of Matanzas was overlaid.

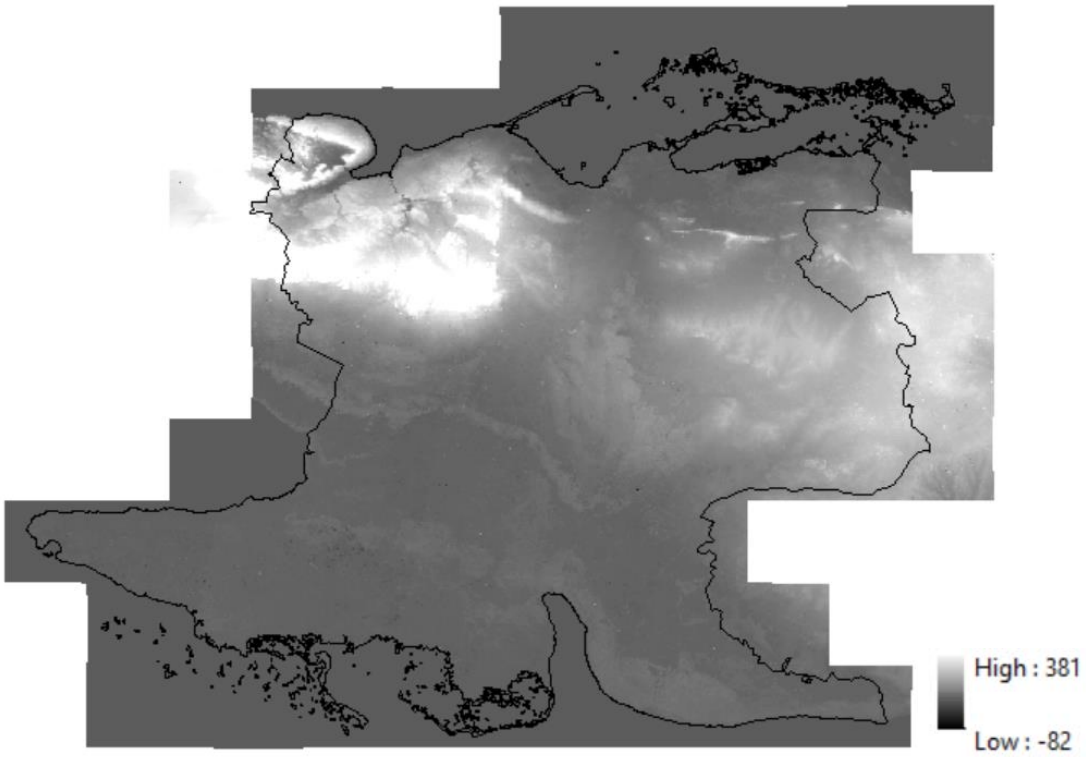

Figure 2.6: DSM including the province of Matanzas. Units of meters (own elaboration by ArcMap).

[8] http://www.eorc.jaxa.jp/ALOS/en/aw3d30/

2.2.2 Diffuse proportion and Transmittivity

The ArgGIS help library reports the following definition of Diffuse proportion and Transmittivity, two important input parameters required by Area Solar Radiation tool.

"The diffuse proportion is the fraction of global normal radiation flux that is diffuse. Values range from 0 to 1. This value should be set according to atmospheric conditions. Typical values are 0.2 for very clear sky conditions and 0.3 for generally clear sky conditions" (ArcGis Desktop Help, 2019).

"The amount of solar radiation received by the surface is only a portion of what would be received outside the atmosphere. Transmittivity is a property of the atmosphere that is expressed as the ratio of the energy (averaged overall wavelengths) reaching the earth's surface to that which is received at the upper limit of the atmosphere (extraterrestrial). Values range from 0 (no transmission) to 1 (complete transmission). Typically observed values are 0.6 or 0.7 for very clear sky conditions and 0.5 for only a generally clear sky. The value for the energy received at the earth's surface is at the shortest path through the atmosphere (that is, the sun is at the zenith, or directly overhead) and for sea level. For areas beyond Tropic of Capricorn and Tropic of Cancer, the sun can never be at the exact zenith, not even at noon; however, this value still refers to the moment when the sun is at the zenith. Because the algorithm corrects for elevation effects, transmittivity should always be given for sea level. Transmittivity has an inverse relation with the diffuse proportion parameter" (ArcGis Desktop Help, 2019).

Basically, the requested value of the transmittivity refers to an optical air mass[9] equal to 1 (AM1) disregarding the elevation effect. This is justified by the correction made by the relative optical path length $m(\theta)$ in (2.4), which will convert the transmittivity into the effective value, referred to the actual sunlight path for the time considered. In this way, the dependence on the zenith angle is eliminated and so is the connection to geographical position and time period. However, both parameters are strongly dependent on weather and atmospheric conditions. Not considering their variations over time and space would clearly lead to some approximations, in contrast with the level of accuracy reached up to this point of the study. We will go deeper into this topic in paragraph 2.3.

[9] The air mass (m) defines the optical path length through the atmosphere. It can be expressed as the relation between the effective path covered by the sunlights and the shortest possible path through the atmosphere. Considering s atmosphere thickness and θ solar zenith angle, it can be derived by trigonometric identities. The following equation is not valid for zenith angles above 80°, due to the significant earth's curvature (Comini & Savino, 2013):

$$m = \frac{m \cdot s}{m} = \frac{1}{\cos(\theta)} = \sec(\theta)$$

2.2.3 Latitude

The tool does not allow to set multiple values of transmittivity and diffuse ratio, since the solar analyst was mainly designed for landscapes and local scales. The same consideration is valid for the site latitude, which is automatically set based on the geographic coordinates of the centroid of the DEM uploaded. When the study area is small, considering the same latitude for every cell is an acceptable approximation in the calculation of solar position and declination. The province of Matanzas, that is a substantially larger area, was divided into smaller areas for this purpose. The DSM presented in fig. 2.7, has been divided into 80 squared areas with a size of 0.15x0.15 decimal degrees. Each block has been numbered proceeding from west to east and from south to north.

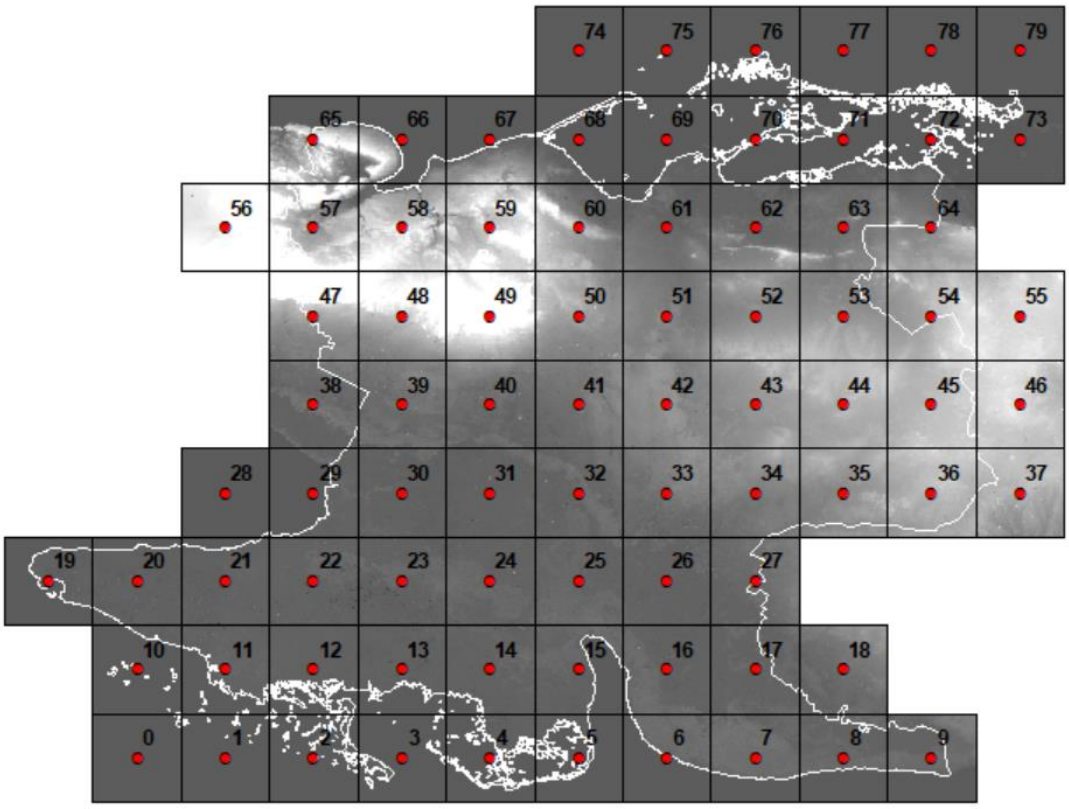

Figure 2.7: DSM including the province of Matanzas, divided into 80 zones (own elaboration from ArcMap).

The red points highlight the center of each zone, whose latitudes and longitudes are presented in the table 2.2.

n°	Lat	Long	n°	Lat	Long	n°	Lat	Long	n°	Lat	Long
0	22.075	-81.975	20	22.375	-81.975	40	22.675	-81.375	60	22.975	-81.225
1	22.075	-81.825	21	22.375	-81.825	41	22.675	-81.225	61	22.975	-81.075
2	22.075	-81.675	22	22.375	-81.675	42	22.675	-81.075	62	22.975	-80.925
3	22.075	-81.525	23	22.375	-81.525	43	22.675	-80.925	63	22.975	-80.775
4	22.075	-81.375	24	22.375	-81.375	44	22.675	-80.775	64	22.975	-80.625
5	22.075	-81.225	25	22.375	-81.225	45	22.675	-80.625	65	23.125	-81.675
6	22.075	-81.075	26	22.375	-81.075	46	22.675	-80.475	66	23.125	-81.525
7	22.075	-80.925	27	22.375	-80.925	47	22.825	-81.675	67	23.125	-81.375
8	22.075	-80.775	28	22.525	-81.825	48	22.825	-81.525	68	23.125	-81.225
9	22.075	-80.625	29	22.525	-81.675	49	22.825	-81.375	69	23.125	-81.075
10	22.225	-81.975	30	22.525	-81.525	50	22.825	-81.225	70	23.125	-80.925
11	22.225	-81.825	31	22.525	-81.375	51	22.825	-81.075	71	23.125	-80.775
12	22.225	-81.675	32	22.525	-81.225	52	22.825	-80.925	72	23.125	-80.625
13	22.225	-81.525	33	22.525	-81.075	53	22.825	-80.775	73	23.125	-80.475
14	22.225	-81.375	34	22.525	-80.925	54	22.825	-80.625	74	23.275	-81.225
15	22.225	-81.225	35	22.525	-80.775	55	22.825	-80.475	75	23.275	-81.075
16	22.225	-81.075	36	22.525	-80.625	56	22.975	-81.825	76	23.275	-80.925
17	22.225	-80.925	37	22.525	-80.475	57	22.975	-81.675	77	23.275	-80.775
18	22.225	-80.775	38	22.675	-81.675	58	22.975	-81.525	78	23.275	-80.625
19	22.375	-82.125	39	22.675	-81.525	59	22.975	-81.375	79	23.275	-80.475

Table 2.2: Latitude and longitude values (in decimal degrees coordinates) of the 80 areas composing the surface of Matanzas.

2.3 Local K_t and K_d calculation

Crossing the atmosphere and colliding against its molecules and particles, a portion of the solar flux is affected by phenomena of absorption and scattering. This interaction is responsible for the attenuation of the solar radiation hitting the Earth's surface and involves gases (CO_2 , O_2 , O_3, other air molecules), solid particulate matter, liquid particles (aerosols, including non-condensed water) and clouds (condensed water) (De C. Alves *et al*, 2013). The influence of this factors is higher when the probability of interaction with the solar flux increases, so it depends on the distance crossed by the sunbeams, the variability in air composition (e.g. due to pollution) and weather conditions.

The Solar Analyst does not consider the variability of atmospheric conditions in time and space, a limitation highlihted by the developers themselves: "The Solar Analyst does not currently model clouds [..] Clouds are extremely hard to model or predict, and detailed information, such as clouds distribution, thickness, cloud type, are not available for most areas. [..] For many purposes, in particular involving multi-day insolation calculation, cloud effects can be included by using an appropriate transmittivity and diffuse proportion." (Fu & Rich, 1999). In order to deal with this aspect, the current analysis set different values of input transmittivity and diffuse proportion for each of the 80 divisions and in relation to the time period considered.

The atmospheric clearness index (K_T), also known as atmospheric transmissivity or atmospheric transmission coefficient (Mora-Lopez *et al*, 2010) can be defined as the ratio between the radiation on a horizontal surface (H) and the extraterrestrial radiation (H_o) referred to the same location and averaged over a time period. The Monthly average clearness index (Duffie & Beckman, 2013):

$$\overline{K_T} = \frac{\overline{H}}{\overline{H_0}} \tag{2.11}$$

The diffuse fraction (K_D), can be defined as the ratio between the diffuse radiation (H_d) and the radiation on a horizontal surface (H) referred to the same location and averaged over a time period. The monthly average diffuse fraction (Duffie & Beckman, 2013):

$$\overline{K_D} = \frac{\overline{H_d}}{\overline{H}} \tag{2.12}$$

The scientific literature proposes many models for the prediction of K_T and K_D, influenced by the stochastic nature of cloud attenuation process. Statistical time series models can be reliable to forecast the clearness index in the long term, while more recent forecasting models based on machine learning approaches are more effective for short term predictions (Lopez *et al*, 2010). The atmospheric transmissivity, according to the Lambert-Beer Law of radiation extinction, has an inverse exponential relationship with the atmospheric optical depth[10], which can be seen as the sum of the optical depth of each atmosphere components[11]. (Singh *et al*, 2013). However, due to complexity and lack of data, which in this analysis should be spatially distributed, an empirical approach was preferred. Starting from historical data of solar radiation (collected by meteorological station), it is possible to derive the monthly average clearness index and diffuse ratio related to each area considered.

From this point of the dissertation on, the ArcGIS input parameters "transmittivity" and "diffuse proportion" will be referred as K_T and K_D. To be noticed that the input required by "Area Solar radiation" refers to an hypothetical condition of AM 1 and sea level, while the calculated clearness index for each time and area, refers to the effective optical path length and altitude.

[10] "When light or other radiation passes through a partially transparent medium, its intensity is diminished by scattering and/or absorption. The effect of the medium can be characterized by an attenuation coefficient α, defined as the fraction of intensity lost per unit distance traveled. The integration of this attenuation over the total path through the medium is called the optical depth" (Simpson, 1997).

[11] The clearness index, or transmissivity (T) is equal to:

$$K_T = T = \exp\left[-m\left(\tau_a + \tau_g + \tau_{NO_2} + \tau_\omega + \tau_{O_3} + \tau_r\right)\right]$$

Where: m is air mass factor and $\tau_a, \tau_g, \tau_{NO_2}, \tau_\omega, \tau_{O_3}, \tau_r$ are optical depth of aerosol, gases, nitrous oxide, water, ozone and Rayleigh scattering from oxygen and nitrogen (Singh *et al*, 2013).

2.3.1 Meteonorm

The calculation of the average monthly values of K_T and K_D, requires the investigation of the average monthly global horizontal and diffuse radiation for the 80 areas selected. This data has been provided by the software "Meteonorm" (version 7.1.10).

Meteonorm is a comprehensive meteorological database containing climatological data for solar engineering applications at any location in the world. Combining its large data storage from all parts of the world with numerous computational models, the program can produce results which statistically represents a typical year of the time period set in the desired location. The radiation database refers to 20 years measurements periods, while the others meteorological parameters are based on monthly averages calculated over 1961-1990 and 2000-2009 periods. Such weather stations data are adapted to every location through space dependent interpolation, taking altitude, topography, region etc. into account. In particular, for global radiation the interpolation procedure is a 3-D inverse distance model (Shepard's gravity interpolation) (Meteonorm Handbook part I, 2016). Diffuse radiation is derived from global radiation through the dynamic model of Perez *et al*[12], which takes into account its anisotropic behavior concentrated in the circumsolar zone and near the horizon (Duffie & Beckman, 2013). Depending on the availability of input data, it makes use of two to four parameters. The two required input are solar zenith angle and global horizontal radiation, or alternatively, normalized clearness index (k_t') calculated by a formula independent by the zenith angle (Perez *et al.* 1990b). When time series of global radiation is available, their dynamics allow to calculate a stability index (Δk_t')[13]. When the dew point temperature is available, it can be used to estimate the water content (humidity) in atmosphere, providing useful information about the level of absorption and production of aerosol (Meteonorm Handbook part II, 2015). Perez model was derived empirically from a large series of data and covers a wide set of sky conditions for a range of climatic regions. The extraterrestrial solar radiation can be computed by astronomical equations.

---

[12] The model developed by Perez *et al* establishes a relationship between sky conditions and a geometric representation of the sky emisphere, described by the cone of circumsolar radiation and a horizon band over an isotropic background. The sky conditions are parametrised by the zenith angle (θ), the sky clearness (ε') and the sky brightness (Δ):

$$\varepsilon' = \frac{[(D_h+B_n)/D_h+\theta^3\cdot 1.041]}{1+\theta^3\cdot 1.041}; \quad \Delta = \frac{D_h\cdot AM}{G_o}$$

Where: D_h is the diffuse irradiance, B_n is the normal beam irradiance, G_o is the extraterrestrial irradiance and AM is the air mass (Padovan & Del Col, 2010).

[13] $\Delta k_t' = 0.5\cdot\left(\left|k_{t_i}' - k_{t_{i+1}}'\right| + \left|k_{t_i}' - k_{t_{i-1}}'\right|\right)$, where *i*, *i*-1 and *i*+1 refer to present, previous and subsequent hour (Meteonorm Handbook part II, 2015).

"The solar constant I_{sc} is the energy from the sun per unit time received on a unit area of surface perpendicular to the direction of propagation of the radiation at mean earth-sun distance outside the atmosphere" (Duffie & Beckman, 2013). Meteonorm considers the following solar constant value:

$$I_{sc} = 1366 \frac{W}{m^2} \tag{2.13}$$

Considering the variation of the earth-sun distance, due to the eccentricity of the terrestrial orbit, a correction factor ε accounts the actual solar distance at any time in the year. I_0 is therefore the extraterrestrial normal solar irradiance at the actual earth-sun distance at any point in time:

$$I_0 = I_{sc}\, \varepsilon \tag{2.14}$$

The equation used by Meteonorm to calculate the factor ε, relative to the n-th day of the year, is (Meteonorm Handbook part II, 2015):

$$\varepsilon = 1 + 0.0334 \cdot \cos\left(n \cdot \frac{2\pi}{365.25} - 0.048869\right) \tag{2.15}$$

$I_{0,h}$ is the extraterrestrial radiation for a horizontal surface, obtainable combining G_0 with the solar zenith angle θ_z:

$$I_{0,h} = I_0 \cos(\theta_z) \tag{2.17}$$

The calculation of the daily irradiation requires the introduction of the sunset hour angle ω_s, with equal modulus and opposite sign of the sunrise hour angle:

$$\omega_s = \left|\omega_{sunset,sunrise}\right| = \omega_{sunset} = -\omega_{sunrise}$$

$$\omega_s = \cos^{-1}(-\tan\delta \tan\varphi) \tag{2.17}$$

φ is the latitude angle for the location (in degrees) and δ is the declination angle (in degrees) for the n day of the year considered:

$$\delta = 23.45 \cdot \sin\left(360° \frac{284+n}{365}\right) \tag{2.18}$$

Integrating $I_{0,h}$ over the time period from sunrise to sunset, the daily extraterrestrial irradiation on a horizontal plane $(H_{0,h})$ can be calculated. Applying the variable substitution from time t (in hours units) to hour angle(ω) $\left(dt = \frac{24}{2\pi} d\omega\right)$, the integral equation is the following:

$$H_{0,h} = \frac{24}{2\pi} \int_{-\omega_s}^{\omega_s} I_{0,h}\, d\omega \tag{2.19}$$

Remembering the equation that define the zenith angle (calling T_h=$\sin\delta\sin\varphi$ and U_h=$\cos\delta\cos\varphi$):

$$\cos(\theta_z) = (\sin\delta\sin\varphi) + (\cos\delta\cos\varphi)\cos\omega = T_h + U_h\cos\omega \tag{2.20}$$

Substituting (2.19) in (2.15), (2.18) can be calculated as follows:

$$H_{0,h} = \frac{24}{2\pi} I_0 \int_{-\omega_s}^{\omega_s} (T_h + U_h\cos(\omega_s))d\omega = \frac{24}{2\pi} I_0 \left[2T_h \frac{\pi}{180^\circ}\omega_s + 2U_h\sin(\omega_s)\right] \tag{2.21}$$

Substituting T_h and U_h and expressing ω_s in [°] and I_0 in [W/m^2], the daily extraterrestrial irradiance on a horizontal plane $\left[\frac{Wh}{m^2 d}\right]$ is (Comini & Savino, 2013):

$$H_{0,h} = \frac{24}{\pi} I_0 \left[\frac{\pi}{180^\circ}\omega_s\sin\delta\sin\varphi + \cos\delta\cos\varphi\sin\omega_s\right] \tag{2.22}$$

Once imported the list of 80 locations using the batch mode function of Meteonorm, the calculation settings have to be defined.

- The field "Future" has been selected as climatological time period, allowing to choose between three different future scenarios from the IPCC report 2007 (Meehl *et al*, 2007): B1 (low), A1B (mid), A2(high). The option A1B (year 2020) has been chosen, characterized by a forecast of a more integrated world, with a balanced emphasis on all energy sources.
- The field "Interpolated" has been set for the atmospheric turbidity, basing on satellite data from the satellite experiment MISR and MODIS (Meteonorm Handbook part I, 2016).
- A personalized output format has been selected, setting monthly Global (H_h), Diffuse ($H_{d,h}$), and Extraterrestrial radiation ($H_{0,h}$) as output format of the calculation.

In the first step of the calculation, the software searches for the closest weather stations to each selected location and their long-term monthly means are interpolated. The whole set of weather station used by the current calculation are the following: La Fe, Havana/Jose Marti, Casa Blanca, Camaguey, Key West FL. In a second step, the interpolated monthly data are run by a stochastic weather generator to create a typical mean year of data with the selected time resolution (hourly). The results have finally been exported and used to calculate the monthly mean K_T and K_D value for each location, using (2.11) and (2.12). Table 2.3 includes all the clearness index and diffuse fractions calculated, per month and location.

n°	Lat [°]	Long [°]	Jan		Feb		Mar		Apr		May		Jun	
			K_T	K_D	K_T	K_D	K_T	K_D	K_T	K_D	K_T	K_D	K_T	K_D
0	22.075	-81.975	0.559	0.363	0.554	0.414	0.564	0.407	0.570	0.444	0.521	0.492	0.486	0.469
1	22.075	-81.825	0.563	0.352	0.554	0.414	0.568	0.417	0.573	0.403	0.526	0.413	0.489	0.479
2	22.075	-81.675	0.572	0.402	0.558	0.433	0.574	0.429	0.579	0.383	0.532	0.453	0.492	0.518
3	22.075	-81.525	0.572	0.386	0.554	0.429	0.574	0.424	0.579	0.399	0.535	0.451	0.498	0.500
4	22.075	-81.375	0.572	0.402	0.546	0.427	0.571	0.420	0.576	0.401	0.532	0.475	0.502	0.497
5	22.075	-81.225	0.577	0.383	0.546	0.435	0.578	0.409	0.579	0.410	0.532	0.486	0.508	0.497
6	22.075	-81.075	0.581	0.395	0.546	0.427	0.578	0.427	0.576	0.434	0.532	0.464	0.511	0.476
7	22.075	-80.925	0.577	0.391	0.533	0.461	0.568	0.375	0.566	0.447	0.529	0.456	0.511	0.476
8	22.075	-80.775	0.572	0.402	0.529	0.472	0.564	0.383	0.563	0.399	0.529	0.489	0.511	0.459
9	22.075	-80.625	0.572	0.402	0.533	0.461	0.568	0.369	0.563	0.421	0.532	0.481	0.511	0.459
10	22.225	-81.975	0.563	0.368	0.558	0.425	0.574	0.376	0.579	0.366	0.534	0.456	0.492	0.524
11	22.225	-81.825	0.568	0.397	0.558	0.433	0.574	0.412	0.582	0.370	0.537	0.492	0.495	0.509
12	22.225	-81.675	0.577	0.391	0.558	0.440	0.581	0.401	0.585	0.378	0.540	0.462	0.498	0.494
13	22.225	-81.525	0.577	0.375	0.554	0.429	0.578	0.415	0.579	0.399	0.537	0.443	0.498	0.518
14	22.225	-81.375	0.577	0.383	0.542	0.438	0.571	0.408	0.573	0.409	0.534	0.451	0.505	0.470
15	22.225	-81.225	0.581	0.395	0.542	0.438	0.574	0.400	0.576	0.423	0.531	0.414	0.508	0.479
16	22.225	-81.075	0.581	0.395	0.542	0.438	0.574	0.424	0.576	0.429	0.531	0.475	0.508	0.462
17	22.225	-80.925	0.572	0.394	0.533	0.461	0.568	0.387	0.563	0.449	0.528	0.472	0.511	0.476
18	22.225	-80.775	0.568	0.405	0.529	0.425	0.564	0.401	0.560	0.435	0.528	0.494	0.511	0.482
19	22.375	-82.125	0.561	0.411	0.556	0.459	0.571	0.432	0.581	0.426	0.545	0.430	0.502	0.491
20	22.375	-81.975	0.561	0.355	0.556	0.406	0.571	0.420	0.581	0.426	0.543	0.454	0.495	0.533
21	22.375	-81.825	0.561	0.363	0.552	0.386	0.571	0.408	0.578	0.423	0.540	0.451	0.495	0.521
22	22.375	-81.675	0.561	0.363	0.548	0.389	0.571	0.414	0.578	0.434	0.540	0.435	0.495	0.521
23	22.375	-81.525	0.561	0.363	0.544	0.408	0.568	0.417	0.571	0.450	0.534	0.473	0.495	0.515
24	22.375	-81.375	0.561	0.371	0.531	0.433	0.561	0.458	0.562	0.458	0.531	0.470	0.498	0.494
25	22.375	-81.225	0.561	0.355	0.531	0.433	0.561	0.446	0.562	0.452	0.528	0.461	0.502	0.473
26	22.375	-81.075	0.566	0.368	0.527	0.444	0.561	0.404	0.562	0.379	0.528	0.489	0.505	0.524
27	22.375	-80.925	0.561	0.363	0.523	0.472	0.557	0.430	0.556	0.474	0.528	0.483	0.508	0.479
28	22.525	-81.825	0.536	0.407	0.542	0.426	0.563	0.404	0.571	0.439	0.545	0.484	0.502	0.461
29	22.525	-81.675	0.541	0.429	0.538	0.422	0.563	0.416	0.568	0.447	0.543	0.470	0.502	0.503
30	22.525	-81.525	0.541	0.387	0.538	0.430	0.563	0.404	0.565	0.416	0.543	0.470	0.502	0.461
31	22.525	-81.375	0.545	0.383	0.534	0.433	0.559	0.436	0.562	0.390	0.540	0.473	0.502	0.479
32	22.525	-81.225	0.545	0.383	0.529	0.437	0.559	0.442	0.559	0.392	0.537	0.443	0.502	0.503
33	22.525	-81.075	0.550	0.372	0.529	0.437	0.559	0.412	0.562	0.424	0.537	0.459	0.502	0.521
34	22.525	-80.925	0.550	0.380	0.521	0.468	0.556	0.421	0.568	0.419	0.543	0.427	0.508	0.485
35	22.525	-80.775	0.550	0.372	0.517	0.480	0.556	0.463	0.565	0.399	0.540	0.462	0.508	0.503
36	22.525	-80.625	0.545	0.383	0.517	0.496	0.556	0.445	0.562	0.418	0.540	0.429	0.508	0.533
37	22.525	-80.475	0.541	0.412	0.513	0.451	0.549	0.426	0.556	0.451	0.537	0.464	0.505	0.530
38	22.675	-81.675	0.534	0.427	0.538	0.445	0.563	0.392	0.571	0.450	0.551	0.420	0.505	0.512
39	22.675	-81.525	0.539	0.407	0.538	0.430	0.563	0.410	0.568	0.447	0.548	0.476	0.505	0.470
40	22.675	-81.375	0.543	0.387	0.538	0.430	0.563	0.404	0.565	0.433	0.545	0.468	0.508	0.479
41	22.675	-81.225	0.543	0.378	0.534	0.441	0.559	0.424	0.565	0.421	0.543	0.470	0.505	0.554
42	22.675	-81.075	0.548	0.383	0.534	0.417	0.559	0.455	0.565	0.388	0.543	0.459	0.505	0.470
43	22.675	-80.925	0.548	0.383	0.521	0.435	0.556	0.384	0.571	0.428	0.545	0.484	0.508	0.491
44	22.675	-80.775	0.548	0.375	0.517	0.480	0.556	0.451	0.571	0.378	0.545	0.435	0.508	0.521
45	22.675	-80.625	0.548	0.375	0.517	0.488	0.556	0.445	0.568	0.408	0.543	0.459	0.508	0.450
46	22.675	-80.475	0.539	0.432	0.508	0.504	0.549	0.432	0.559	0.386	0.540	0.467	0.505	0.524
47	22.825	-81.675	0.534	0.427	0.544	0.481	0.566	0.443	0.581	0.393	0.560	0.414	0.512	0.491
48	22.825	-81.525	0.534	0.427	0.544	0.481	0.566	0.425	0.581	0.399	0.560	0.414	0.512	0.491
49	22.825	-81.375	0.543	0.403	0.549	0.400	0.569	0.381	0.581	0.410	0.560	0.455	0.512	0.450
50	22.825	-81.225	0.548	0.375	0.549	0.423	0.573	0.402	0.581	0.393	0.557	0.416	0.512	0.474
51	22.825	-81.075	0.548	0.375	0.549	0.446	0.569	0.387	0.581	0.393	0.557	0.405	0.509	0.471
52	22.825	-80.925	0.548	0.375	0.544	0.442	0.569	0.446	0.584	0.391	0.557	0.437	0.515	0.465
53	22.825	-80.775	0.553	0.380	0.540	0.461	0.569	0.411	0.587	0.405	0.557	0.463	0.518	0.428
54	22.825	-80.625	0.553	0.372	0.540	0.406	0.569	0.423	0.587	0.411	0.557	0.432	0.518	0.491
55	22.825	-80.475	0.548	0.383	0.536	0.409	0.566	0.437	0.584	0.424	0.554	0.423	0.518	0.457
56	22.975	-81.825	0.532	0.431	0.549	0.462	0.568	0.377	0.590	0.398	0.569	0.402	0.518	0.486
57	22.975	-81.675	0.532	0.431	0.549	0.446	0.568	0.389	0.587	0.405	0.566	0.394	0.515	0.523
58	22.975	-81.525	0.537	0.427	0.549	0.454	0.571	0.375	0.590	0.392	0.569	0.397	0.518	0.480
59	22.975	-81.375	0.546	0.370	0.557	0.379	0.575	0.420	0.594	0.380	0.569	0.407	0.521	0.466
60	22.975	-81.225	0.546	0.370	0.557	0.439	0.578	0.424	0.594	0.380	0.569	0.469	0.521	0.448
61	22.975	-81.075	0.550	0.375	0.557	0.439	0.578	0.418	0.594	0.385	0.569	0.402	0.521	0.489
62	22.975	-80.925	0.550	0.367	0.553	0.443	0.578	0.418	0.597	0.356	0.569	0.423	0.527	0.455
63	22.975	-80.775	0.550	0.383	0.553	0.420	0.578	0.435	0.600	0.370	0.569	0.397	0.527	0.483
64	22.975	-80.625	0.555	0.372	0.553	0.359	0.578	0.400	0.600	0.392	0.569	0.402	0.530	0.497
65	23.125	-81.675	0.539	0.410	0.551	0.438	0.568	0.431	0.590	0.382	0.569	0.418	0.521	0.477
66	23.125	-81.525	0.539	0.393	0.551	0.462	0.571	0.423	0.594	0.374	0.572	0.395	0.524	0.451
67	23.125	-81.375	0.544	0.381	0.555	0.450	0.571	0.440	0.597	0.399	0.572	0.405	0.524	0.469
68	23.125	-81.225	0.548	0.387	0.555	0.405	0.575	0.432	0.597	0.399	0.572	0.405	0.527	0.489
69	23.125	-81.075	0.548	0.370	0.555	0.405	0.575	0.396	0.600	0.407	0.572	0.451	0.527	0.460
70	23.125	-80.925	0.553	0.375	0.559	0.417	0.578	0.382	0.600	0.370	0.575	0.403	0.533	0.455
71	23.125	-80.775	0.553	0.383	0.555	0.420	0.578	0.382	0.600	0.376	0.578	0.396	0.533	0.449
72	23.125	-80.625	0.553	0.375	0.559	0.417	0.578	0.388	0.603	0.368	0.578	0.411	0.536	0.441
73	23.125	-80.475	0.553	0.383	0.555	0.427	0.582	0.386	0.606	0.387	0.575	0.413	0.536	0.469
74	23.275	-81.225	0.544	0.381	0.555	0.450	0.571	0.429	0.600	0.397	0.575	0.398	0.530	0.514
75	23.275	-81.075	0.548	0.370	0.555	0.405	0.575	0.420	0.603	0.384	0.575	0.423	0.530	0.463
76	23.275	-80.925	0.548	0.387	0.555	0.420	0.575	0.396	0.603	0.368	0.581	0.434	0.536	0.430
77	23.275	-80.775	0.548	0.378	0.555	0.405	0.578	0.388	0.603	0.374	0.581	0.439	0.536	0.447
78	23.275	-80.625	0.548	0.378	0.555	0.405	0.578	0.382	0.606	0.372	0.581	0.429	0.539	0.444
79	23.275	-80.475	0.548	0.387	0.555	0.405	0.578	0.418	0.606	0.372	0.578	0.401	0.539	0.478

n°	Lat [°]	Long [°]	Jul		Aug		Sep		Oct		Nov		Dec	
			K_T	K_D	K_T	K_D	K_T	K_D	K_T	K_D	K_T	K_D	K_T	K_D
0	22.075	-81.975	0.515	0.509	0.489	0.534	0.458	0.585	0.491	0.523	0.549	0.407	0.547	0.397
1	22.075	-81.825	0.521	0.446	0.489	0.540	0.461	0.574	0.491	0.508	0.549	0.382	0.542	0.409
2	22.075	-81.675	0.526	0.480	0.489	0.503	0.468	0.565	0.498	0.507	0.554	0.395	0.542	0.383
3	22.075	-81.525	0.526	0.486	0.489	0.509	0.468	0.536	0.494	0.489	0.549	0.447	0.538	0.404
4	22.075	-81.375	0.529	0.450	0.498	0.512	0.468	0.558	0.487	0.527	0.545	0.426	0.533	0.398
5	22.075	-81.225	0.532	0.470	0.498	0.488	0.471	0.540	0.491	0.470	0.549	0.423	0.533	0.434
6	22.075	-81.075	0.532	0.436	0.511	0.488	0.475	0.536	0.494	0.541	0.554	0.387	0.533	0.389
7	22.075	-80.925	0.532	0.453	0.520	0.485	0.475	0.521	0.487	0.534	0.549	0.431	0.524	0.450
8	22.075	-80.775	0.532	0.453	0.523	0.494	0.475	0.564	0.483	0.523	0.545	0.451	0.519	0.473
9	22.075	-80.625	0.532	0.442	0.520	0.439	0.475	0.500	0.480	0.543	0.545	0.418	0.519	0.455
10	22.225	-81.975	0.525	0.492	0.502	0.485	0.475	0.586	0.502	0.526	0.556	0.419	0.550	0.405
11	22.225	-81.825	0.528	0.472	0.495	0.540	0.475	0.543	0.498	0.455	0.556	0.387	0.545	0.426
12	22.225	-81.675	0.531	0.481	0.492	0.512	0.475	0.543	0.502	0.474	0.561	0.376	0.545	0.417
13	22.225	-81.525	0.531	0.481	0.489	0.497	0.471	0.540	0.494	0.489	0.556	0.427	0.536	0.407
14	22.225	-81.375	0.531	0.464	0.498	0.506	0.468	0.565	0.487	0.550	0.547	0.459	0.531	0.429
15	22.225	-81.225	0.531	0.442	0.498	0.488	0.468	0.580	0.491	0.508	0.552	0.390	0.536	0.460
16	22.225	-81.075	0.531	0.475	0.508	0.503	0.471	0.518	0.491	0.508	0.552	0.431	0.536	0.398
17	22.225	-80.925	0.531	0.459	0.520	0.497	0.475	0.550	0.487	0.550	0.547	0.426	0.526	0.441
18	22.225	-80.775	0.531	0.448	0.523	0.494	0.475	0.521	0.483	0.492	0.543	0.421	0.521	0.436
19	22.375	-82.125	0.528	0.456	0.526	0.468	0.481	0.549	0.504	0.444	0.552	0.423	0.543	0.395
20	22.375	-81.975	0.531	0.448	0.520	0.532	0.481	0.556	0.500	0.463	0.552	0.431	0.538	0.442
21	22.375	-81.825	0.531	0.470	0.514	0.515	0.478	0.567	0.496	0.459	0.552	0.366	0.533	0.482
22	22.375	-81.675	0.531	0.470	0.511	0.482	0.475	0.493	0.496	0.496	0.552	0.431	0.533	0.375
23	22.375	-81.525	0.528	0.456	0.502	0.467	0.468	0.522	0.489	0.511	0.547	0.393	0.529	0.450
24	22.375	-81.375	0.525	0.480	0.508	0.479	0.461	0.559	0.481	0.504	0.538	0.483	0.519	0.450
25	22.375	-81.225	0.525	0.486	0.502	0.503	0.458	0.563	0.481	0.512	0.538	0.475	0.519	0.495
26	22.375	-81.075	0.525	0.447	0.505	0.482	0.458	0.607	0.481	0.519	0.538	0.417	0.519	0.459
27	22.375	-80.925	0.531	0.453	0.511	0.482	0.468	0.551	0.481	0.504	0.534	0.429	0.514	0.481
28	22.525	-81.825	0.540	0.424	0.520	0.509	0.481	0.549	0.481	0.473	0.527	0.453	0.510	0.477
29	22.525	-81.675	0.540	0.467	0.514	0.497	0.478	0.525	0.481	0.527	0.532	0.432	0.510	0.421
30	22.525	-81.525	0.537	0.454	0.514	0.497	0.478	0.482	0.481	0.473	0.532	0.432	0.510	0.458
31	22.525	-81.375	0.537	0.415	0.514	0.467	0.475	0.514	0.481	0.512	0.532	0.441	0.510	0.421
32	22.525	-81.225	0.534	0.429	0.508	0.527	0.471	0.547	0.481	0.519	0.532	0.432	0.510	0.477
33	22.525	-81.075	0.534	0.495	0.508	0.509	0.468	0.507	0.474	0.583	0.527	0.444	0.510	0.430
34	22.525	-80.925	0.537	0.432	0.508	0.479	0.475	0.564	0.478	0.555	0.523	0.466	0.500	0.438
35	22.525	-80.775	0.534	0.489	0.511	0.494	0.475	0.550	0.478	0.555	0.523	0.405	0.500	0.467
36	22.525	-80.625	0.534	0.434	0.514	0.485	0.471	0.554	0.474	0.512	0.523	0.483	0.495	0.490
37	22.525	-80.475	0.531	0.464	0.508	0.473	0.468	0.500	0.470	0.548	0.514	0.491	0.486	0.520
38	22.675	-81.675	0.545	0.441	0.523	0.459	0.490	0.521	0.483	0.512	0.525	0.466	0.507	0.443
39	22.675	-81.525	0.545	0.446	0.520	0.439	0.490	0.514	0.483	0.566	0.529	0.462	0.507	0.462
40	22.675	-81.375	0.543	0.470	0.520	0.468	0.486	0.573	0.483	0.512	0.529	0.436	0.507	0.500
41	22.675	-81.225	0.540	0.457	0.514	0.503	0.483	0.500	0.483	0.473	0.529	0.470	0.507	0.443
42	22.675	-81.075	0.540	0.424	0.511	0.482	0.476	0.579	0.476	0.520	0.529	0.419	0.507	0.472
43	22.675	-80.925	0.540	0.478	0.511	0.512	0.480	0.610	0.479	0.523	0.525	0.440	0.502	0.419
44	22.675	-80.775	0.537	0.454	0.511	0.500	0.476	0.471	0.479	0.500	0.520	0.443	0.498	0.433
45	22.675	-80.625	0.537	0.475	0.514	0.485	0.473	0.525	0.476	0.528	0.520	0.452	0.498	0.510
46	22.675	-80.475	0.534	0.467	0.505	0.506	0.469	0.471	0.472	0.556	0.511	0.407	0.478	0.570
47	22.825	-81.675	0.554	0.413	0.535	0.483	0.503	0.486	0.479	0.539	0.520	0.452	0.505	0.457
48	22.825	-81.525	0.554	0.407	0.532	0.463	0.503	0.547	0.483	0.496	0.525	0.422	0.510	0.453
49	22.825	-81.375	0.557	0.400	0.529	0.477	0.507	0.490	0.487	0.500	0.529	0.436	0.514	0.439
50	22.825	-81.225	0.554	0.439	0.523	0.523	0.503	0.486	0.487	0.531	0.529	0.444	0.514	0.439
51	22.825	-81.075	0.551	0.457	0.523	0.535	0.500	0.469	0.483	0.473	0.529	0.419	0.514	0.458
52	22.825	-80.925	0.551	0.484	0.520	0.515	0.497	0.548	0.483	0.496	0.529	0.419	0.505	0.476
53	22.825	-80.775	0.551	0.447	0.520	0.503	0.493	0.476	0.483	0.512	0.529	0.402	0.500	0.471
54	22.825	-80.625	0.551	0.447	0.523	0.535	0.493	0.497	0.487	0.523	0.529	0.453	0.500	0.442
55	22.825	-80.475	0.551	0.447	0.538	0.463	0.497	0.493	0.487	0.446	0.520	0.409	0.490	0.451
56	22.975	-81.825	0.566	0.440	0.550	0.453	0.517	0.454	0.485	0.504	0.518	0.491	0.507	0.419
57	22.975	-81.675	0.563	0.438	0.547	0.467	0.514	0.477	0.485	0.481	0.518	0.412	0.507	0.467
58	22.975	-81.525	0.566	0.451	0.547	0.456	0.517	0.526	0.489	0.485	0.523	0.435	0.507	0.448
59	22.975	-81.375	0.566	0.399	0.550	0.492	0.524	0.442	0.492	0.519	0.527	0.448	0.512	0.443
60	22.975	-81.225	0.563	0.438	0.547	0.494	0.524	0.435	0.492	0.550	0.532	0.427	0.517	0.486
61	22.975	-81.075	0.563	0.411	0.544	0.419	0.520	0.464	0.492	0.527	0.532	0.436	0.517	0.458
62	22.975	-80.925	0.566	0.461	0.550	0.481	0.517	0.441	0.492	0.420	0.536	0.424	0.507	0.467
63	22.975	-80.775	0.569	0.412	0.547	0.467	0.517	0.474	0.492	0.504	0.536	0.432	0.502	0.442
64	22.975	-80.625	0.569	0.423	0.550	0.442	0.517	0.441	0.500	0.496	0.541	0.429	0.502	0.452
65	23.125	-81.675	0.567	0.443	0.559	0.446	0.524	0.435	0.489	0.492	0.518	0.456	0.507	0.390
66	23.125	-81.525	0.567	0.438	0.559	0.457	0.527	0.516	0.489	0.492	0.523	0.435	0.507	0.438
67	23.125	-81.375	0.570	0.441	0.559	0.451	0.531	0.385	0.492	0.519	0.527	0.431	0.512	0.434
68	23.125	-81.225	0.570	0.405	0.562	0.465	0.531	0.468	0.492	0.489	0.532	0.479	0.512	0.472
69	23.125	-81.075	0.570	0.385	0.559	0.467	0.534	0.459	0.496	0.447	0.536	0.415	0.512	0.453
70	23.125	-80.925	0.570	0.436	0.559	0.462	0.534	0.452	0.500	0.481	0.541	0.454	0.507	0.457
71	23.125	-80.775	0.573	0.434	0.562	0.449	0.534	0.452	0.504	0.478	0.541	0.403	0.507	0.476
72	23.125	-80.625	0.573	0.429	0.562	0.465	0.534	0.452	0.508	0.481	0.545	0.408	0.502	0.452
73	23.125	-80.475	0.573	0.444	0.565	0.446	0.537	0.475	0.515	0.504	0.550	0.430	0.498	0.466
74	23.275	-81.225	0.573	0.444	0.562	0.411	0.536	0.484	0.498	0.515	0.530	0.422	0.510	0.476
75	23.275	-81.075	0.573	0.408	0.565	0.452	0.539	0.468	0.498	0.508	0.534	0.504	0.510	0.467
76	23.275	-80.925	0.573	0.383	0.565	0.414	0.539	0.468	0.506	0.500	0.543	0.437	0.510	0.448
77	23.275	-80.775	0.573	0.413	0.565	0.435	0.539	0.462	0.509	0.504	0.543	0.429	0.510	0.457
78	23.275	-80.625	0.573	0.429	0.565	0.446	0.539	0.475	0.513	0.485	0.548	0.417	0.505	0.471
79	23.275	-80.475	0.573	0.429	0.565	0.419	0.539	0.449	0.521	0.507	0.553	0.405	0.500	0.495

Table 2.3: Monthly clearness index and diffuse ratio calculated for the 80 sites considered

2.3.2 Point Solar Radiation tool

The values of K_T and K_D need to be validate before being used as transmittivity and diffuse proportion input for the execution of Area Solar Radiation. An effective method is to run the calculation and compare the outputs with the results provided by Meteonorm, which represents a reliable source, according to the previous paragraph.

Point Solar Radiation is an ArcMap tool belonging to the same Spatial Analyst extension as Area Solar Radiation. The required input parameters and the equations used are the same for both the tools, except the location where the calculation is run: Point Solar Radiation derives incoming solar radiation for specific locations that can be loaded in the format of point feature class or table of point coordinates. This implies short calculation time and allows to directly compare the results with the expected values. Like in Meteonorm calculation, the centroid coordinates of each of the 80 zones is set as input location for a Point Solar Radiation calculation. This step requires the creation of series of vector data (in shapefile format) defined by the coordinates of the central point of each zone, and sequentially numbered from 0 to 79. Before using such files as input location for the calculation, they need to be projected into metric coordinate system, in order to avoid conversion errors. The reference geodetic system for the Area of Cuba is: WGS 1984 UTM Zone 17N. At this point, the main issue is the necessity of running a calculation with multiple input setting with a tool which only allows to set a unique value of transmittivity and diffuse ratio.

The problem can be solved implementing a phyton script that cyclically execute the function PointSolarRadiation from the arcpy environment. All the fixed parameters are set according to paragraph 2.2 and using the code language suggested by the "ArcGis Desktop help". Each of the variable parameters dependent on the location has been saved in a text file in the same numerical order of the correspondent reference zone:

- "Lat.txt" representing the location latitudes;
- "Kt_monthname.txt" representing the transmittivity for the specific month;
- "Kd_monthname.txt" representing the diffuse proportion for the specific month.

Each value of the text files is loaded sequentially as input of the calculation by means of a for-loop. For the i-th cycle, a suffix "i" included between 0 and 79 is added to the name of each loaded variable parameters. Associating the i-th variables to the location shapefile identified by the same number, ensures to execute the calculation for every i-th zone with the respective input parameter. For example, considering zone number 0 in January: "Lat0", "kt_jan0", "Kd_jan0", "0.shp" and "dsm_split0.TIF" are associated to the same i element of the list called "dictList[i]". "0.shp" is the point location file, while "dsm_split0" is the DSM raster file of the zone in which the point is located (derived from the cut of the total DSM through raster split ArcMap tool). Once calculated the monthly global, direct and diffuse radiation for each of the 80 points, the outputs are merged into three single files. The script is run for every

month of the year, properly selecting the time period and the text files. In figure 2.8, the flowchart of the script, while an example of the script can be found in Appendix 1.

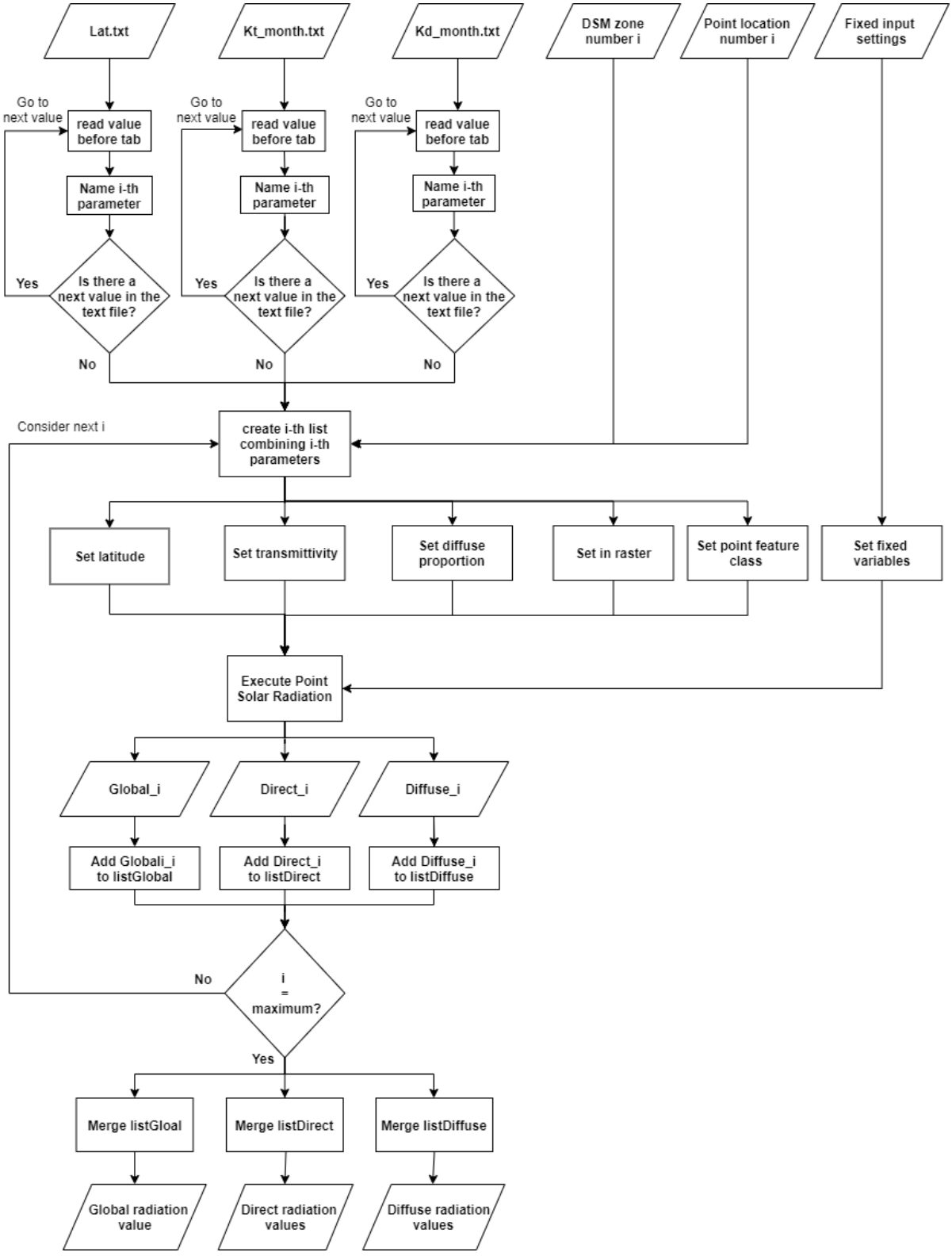

Figure 2.8: Flowchart of the script for the Point Solar Radiation calculation.

2.3.3 Corrections

The output radiation generated by the script execution differs significantly from the value estimated by Meteonorm. The monthly mean error, calculated as a percentage of the Meteonorm values and averaged for all the 80 study areas, is presented in table 2.4, separating global (err% glob), direct (err% dir) and diffuse (err% diff) radiation.

Month	JAN	FEB	MAR	APR	MAY	JUN	JUL	AUG	SEP	OCT	NOV	DEC
err% glob	-8.683	12.027	18.624	23.895	30.116	23.532	30.404	37.196	35.395	21.883	-0.373	-20.036
errr% dir	-12.226	17.648	28.907	39.924	46.504	30.512	46.224	57.412	54.267	32.095	-1.420	-36.895
errr% diff	-2.652	4.671	4.037	0.836	10.174	16.710	11.464	16.332	18.905	12.543	1.676	1.107

Table 2.4: mean percentage error of the Point Solar Radiation calculation in relation to the monthly Meteonorm values.

As can be noticed in equation 2.4, the calculation of direct radiation depends on a fixed solar constant, without taking into account how the Earth's orbital eccentricity influences the incoming irradiance. Considering the effect of the sun distance variability over the year represents a first correction factor to reduce the error. Using the equations proposed by Spencer (1971) (Duffie & Beckman, 2013) to calculate the extraterrestrial normal radiation $I_{0,n}$ from the solar constant I_{sc} :

$$I_{0,n} = I_{sc}\left(1 + 0.033\cos\frac{360\cdot n}{365}\right) \tag{2.23}$$

Every monthly direct radiation calculation can be corrected by a factor equal to $\left(1 + 0.033\cos\frac{360\cdot n}{365}\right)$, using the middle day of every month as n value. Accounting the eccentricity effect on direct radiation direct results to have an effect of mitigation of the error as can be seen in table 2.5:

Month	JAN	FEB	MAR	APR	MAY	JUN	JUL	AUG	SEP	OCT	NOV	DEC
err% glob	-5.818	14.548	19.692	22.880	27.161	19.646	26.284	34.026	34.286	22.914	1.949	-17.515
errr% dir	-9.570	20.296	30.068	38.778	43.177	26.406	41.604	53.774	53.003	33.213	0.878	-34.905
errr% diff	-0.461	7.027	4.973	0.010	7.672	13.038	7.942	13.644	17.931	13.495	4.046	4.295

Table 2.5: mean percentage error of the 80 Point Solar Radiation calculations, accounting the eccentricity effect, compared to the monthly Meteonorm values.

A correction of the input values of transmittivity and diffuse proportion is still needed to minimize the discrepancy and achieve a better accuracy.

As already discussed in paragraph 2.2.2, the input transmissivity required by the ArcMap tool, refers to a condition of AM1 and zero altitude, while the calculated K_T refers to the actual conditions of the respective sites. An average error was therefore predictable. However, the existing heterogeneity across the different areas, reflects a good approximation of the variability due to weather conditions forecast. Applying the same correction factor to every area, such variability accuracy is preserved.

A first step is focused on minimizing the percentual error of direct radiation. The K_T values have been modified with a per cent variation of ±5% and different execution of the script have been done, investigating the modified K_T which produces the most accurate direct radiation output (in comparison to Meteonorm values) for each month. In table 2.6, the errors of the outputs produced by using $K_{T,mod}$ and K_D as input of the calculation, where $K_{T,mod}$ is the clearness index value which minimizes the direct radiation error. The second row shows the applied variation from the original K_T values.

Month	JAN	FEB	MAR	APR	MAY	JUN	JUL	AUG	SEP	OCT	NOV	DEC
Kt mod	+5%	-10%	-20%	-20%	-25%	-15%	-25%	-30%	-25%	-15%	-	+25%
err% glob	2.578	-2.662	-9.460	-8.057	-11.995	-3.036	-7.841	-15.379	-9.242	-4.204	1.949	25.608
errr% dir	-1.711	2.769	-0.455	3.041	0.098	3.152	-1.151	-1.611	4.340	4.387	0.878	-1.367
errr% diff	9.475	-9.764	-22.337	-27.002	-27.169	-9.534	-26.991	-30.026	-21.919	-12.595	4.046	58.417

Table 2.6: mean percentage error of the 80 Point Solar Radiation calculations compared to the monthly Meteonorm values, using the modified clearness index ($K_{T,mod}$) as input transmissivity.

Diffuse radiation is calculated depending on global normal radiation R_g (eq. 2.7) which also depends on direct radiation, as can be seen in eq. 2.8. For this reason, direct radiation needs to be corrected first. A second step is to minimize the gap of diffuse radiation. Following the same procedure, modified values of K_D with per cent variation of ±5% have been tested, coupled with $K_{T,mod}$ as input of the point solar radiation script. The chosen couples of $K_{T,mod}$ and $K_{D,mod}$ are the ones which produced the minimum error, as reported in the table 2.7.
The second row shows the applied variation respect the original K_T and K_D values, respectively.

Month	JAN	FEB	MAR	APR	MAY	JUN	JUL	AUG	SEP	OCT	NOV	DEC
Kt_m ; Kd_m	+5% ; -5%	-10% ; +5%	-20% ; +15%	-20% ; +15%	-25% ; +20%	-15% ; +5%	-25% ; +20%	-30% ; +20%	-25% ; +10%	-15% ; +5%	- ; -	+25% ; -25%
err% glob	-0.777	0.988	-0.196	0.680	2.041	1.472	1.611	0.947	0.329	0.586	1.949	-1.439
errr% dir	-1.711	2.769	-0.455	3.041	0.098	3.152	-1.151	-1.611	4.340	4.387	0.878	-1.367
errr% diff	0.809	-1.419	-0.033	-6.354	4.240	-0.278	4.762	3.560	-3.583	-3.195	4.046	-1.473

Table 2.7: mean percentage error of the 80 Point Solar Radiations calculation compared to the monthly Meteonorm values, using the modified clearness index ($K_{T,mod}$) as input transmissivity and the modified diffuse ratio ($K_{D,mod}$) as input diffuse proportion.

A comparison is useful to visualize the trend and the correction. The monthly global, direct and diffuse horizontal irradiation has been calculated for the 80 point-locations identified along the province of Matanzas. The average values between the 80 locations have been used to compare the output calculated by Point Solar Radiation with the reference values calculated by Meteonorm. Properly adjusting the input values of transmittivity and diffuse proportion, the error between the two calculations has been minimized.
In the following tables and graphs, "Point solar" refers to the outputs calculated before the correction, while "Corrected" refers to the outputs calculated using the modified $K_{T,mod}$ and $K_{D,mod}$.

GLOBAL IRRADIATION [kWh/m²]												
Month	JAN	FEB	MAR	APR	MAY	JUN	JUL	AUG	SEP	OCT	NOV	DEC
Meteonorm	121.588	129.275	167.763	182.738	187.438	170.550	186.125	172.738	145.025	130.813	118.850	107.663
Point Solar	111.029	144.823	199.006	226.403	243.886	210.683	242.715	236.990	196.356	159.438	118.407	86.091
Corrected	120.643	130.552	167.434	183.979	191.263	173.060	189.123	174.373	145.502	131.579	121.166	106.113

Table 2.8: Monthly global horizontal irradiation calculated through: Meteonorm (first row), Point Solar with original values of K_T and K_D (second row), Point Solar with corrected values $K_{T,mod}$ and $K_{D,mod}$ (third row).

DIRECT IRRADIATION [kWh/m²]												
Month	JAN	FEB	MAR	APR	MAY	JUN	JUL	AUG	SEP	OCT	NOV	DEC
Meteonorm	74.638	73.138	98.513	108.775	104.550	88.000	103.075	89.600	70.963	64.713	67.525	59.463
Point Solar	65.512	86.045	126.990	152.202	153.170	114.850	150.721	141.041	109.471	85.482	66.566	37.524
Corrected	73.361	75.163	98.064	112.082	104.653	90.774	101.889	88.156	74.042	67.551	68.118	58.649

Table 2.9: Monthly direct horizontal irradiation calculated through: Meteonorm (first row), Point Solar with original values of K_T and K_D (second row), Point Solar with corrected values $K_{T,mod}$ and $K_{D,mod}$ (third row).

DIFFUSE IRRADIATION [kWh/m²]												
Month	JAN	FEB	MAR	APR	MAY	JUN	JUL	AUG	SEP	OCT	NOV	DEC
Meteonorm	46.988	56.188	69.363	74.075	82.950	82.500	83.163	83.113	74.050	66.150	51.275	48.250
Point Solar	45.741	58.812	72.162	74.694	91.389	96.285	92.697	96.687	88.049	74.447	52.134	48.784
Corrected	47.368	55.390	69.340	69.369	86.467	82.271	87.123	86.071	71.397	64.037	53.349	47.539

Table 2.10: Monthly diffuse irradiation calculated through: Meteonorm (first row), Point Solar with original values of K_T and K_D (second row), Point Solar with corrected values $K_{T,mod}$ and $K_{D,mod}$ (third row).

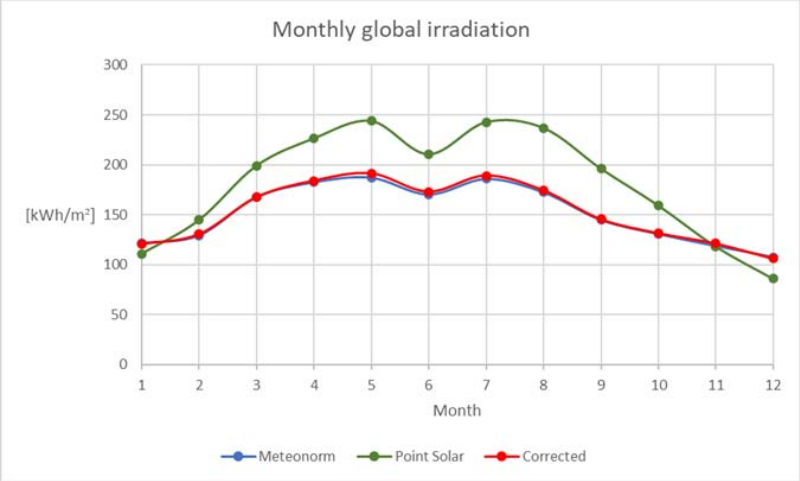

Figure 2.9: Trend of the monthly global horizontal irradiation calculated through: Meteonorm (blue), Point Solar with original values of K_T and K_D (green), Point Solar with corrected values $K_{T,mod}$ and $K_{D,mod}$ (red).

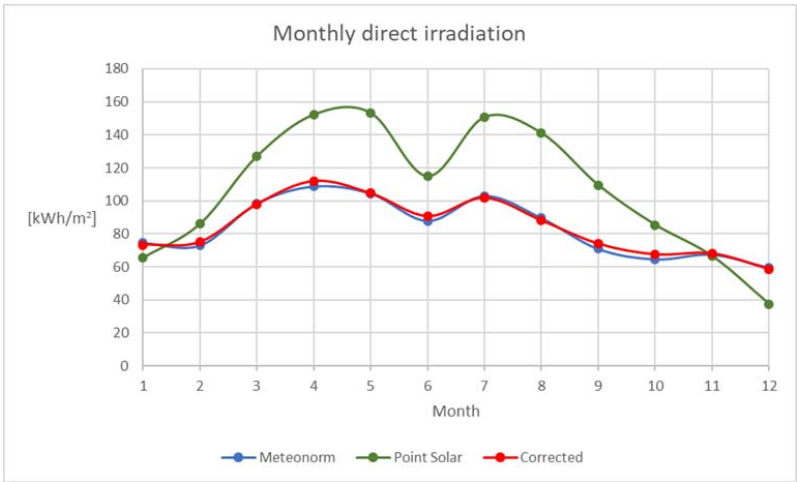

Figure 2.10: Trend of the monthly direct horizontal irradiation calculated through: Meteonorm (blue), Point Solar with original values of K_T and K_D (green), Point Solar with corrected values $K_{T,mod}$ and $K_{D,mod}$ (red).

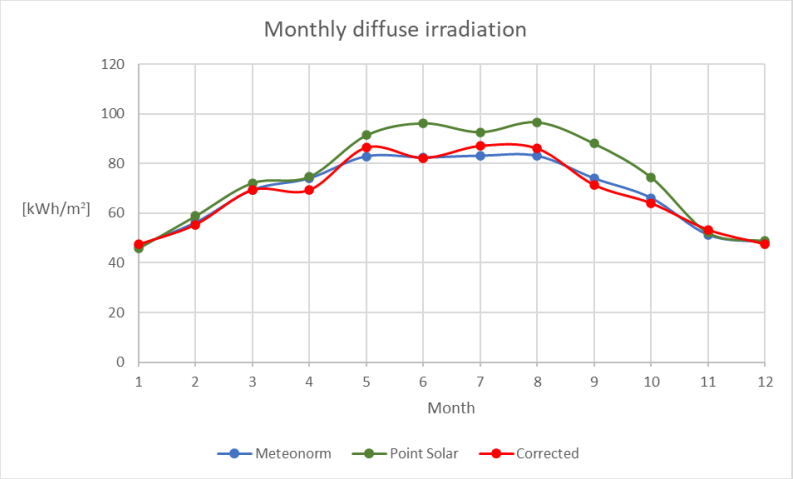

Figure 2.11: : Trend of the monthly diffuse irradiation calculated through: Meteonorm (blue), Point Solar with original values of K_T and K_D (green), Point Solar with corrected values $K_{T,mod}$ and $K_{D,mod}$ (red).

2.4 Results

Once the input parameters required by Area Solar Radiation tool are provided, it is possible to proceed to the creation of the solar maps. All the corrected value of monthly clearness index and diffuse ratio to be set as transmissivity and diffuse proportion of the 80 zones are listed in table 2.11.

n°	Lat [°]	Long [°]	Jan		Feb		Mar		Apr		May		Jun	
			K_{T_mod}	K_{D_mod}	K_{T_mod}	K_{D_mod}	K_{T_mod}	K_{D_mod}	K_{T_mod}	K_{D_mod}	K_{T_mod}	K_{D_mod}	K_{T_mod}	K_{D_mod}
0	22.075	-81.975	0.586	0.345	0.499	0.434	0.451	0.468	0.456	0.511	0.390	0.590	0.414	0.493
1	22.075	-81.825	0.591	0.334	0.499	0.434	0.454	0.479	0.458	0.464	0.395	0.496	0.416	0.502
2	22.075	-81.675	0.601	0.381	0.503	0.454	0.459	0.494	0.463	0.440	0.399	0.544	0.419	0.544
3	22.075	-81.525	0.601	0.367	0.499	0.450	0.459	0.487	0.463	0.459	0.401	0.541	0.424	0.525
4	22.075	-81.375	0.601	0.381	0.491	0.449	0.457	0.483	0.461	0.461	0.399	0.570	0.426	0.522
5	22.075	-81.225	0.605	0.364	0.491	0.457	0.462	0.471	0.463	0.471	0.399	0.583	0.431	0.522
6	22.075	-81.075	0.610	0.376	0.491	0.449	0.462	0.491	0.461	0.499	0.399	0.557	0.434	0.500
7	22.075	-80.925	0.605	0.371	0.480	0.484	0.454	0.431	0.453	0.514	0.397	0.547	0.434	0.500
8	22.075	-80.775	0.601	0.381	0.476	0.496	0.451	0.441	0.451	0.459	0.397	0.587	0.434	0.482
9	22.075	-80.625	0.601	0.381	0.480	0.484	0.454	0.424	0.451	0.485	0.399	0.577	0.434	0.482
10	22.225	-81.975	0.591	0.350	0.503	0.447	0.459	0.433	0.463	0.421	0.400	0.547	0.419	0.551
11	22.225	-81.825	0.596	0.377	0.503	0.454	0.459	0.474	0.466	0.425	0.402	0.590	0.421	0.535
12	22.225	-81.675	0.605	0.371	0.503	0.462	0.465	0.461	0.468	0.435	0.405	0.554	0.424	0.519
13	22.225	-81.525	0.605	0.356	0.499	0.450	0.462	0.477	0.463	0.459	0.402	0.531	0.424	0.544
14	22.225	-81.375	0.605	0.364	0.488	0.460	0.457	0.470	0.458	0.470	0.400	0.541	0.429	0.494
15	22.225	-81.225	0.610	0.376	0.488	0.460	0.459	0.460	0.461	0.487	0.398	0.497	0.431	0.503
16	22.225	-81.075	0.610	0.376	0.488	0.460	0.459	0.487	0.461	0.493	0.398	0.570	0.431	0.485
17	22.225	-80.925	0.601	0.374	0.480	0.484	0.454	0.445	0.451	0.517	0.396	0.567	0.434	0.500
18	22.225	-80.775	0.596	0.385	0.476	0.446	0.451	0.461	0.448	0.500	0.396	0.593	0.434	0.506
19	22.375	-82.125	0.589	0.391	0.501	0.482	0.457	0.497	0.465	0.490	0.409	0.516	0.426	0.516
20	22.375	-81.975	0.589	0.337	0.501	0.426	0.457	0.483	0.465	0.490	0.407	0.545	0.421	0.560
21	22.375	-81.825	0.589	0.345	0.497	0.406	0.457	0.470	0.462	0.487	0.405	0.541	0.421	0.547
22	22.375	-81.675	0.589	0.345	0.493	0.409	0.457	0.476	0.462	0.499	0.405	0.522	0.421	0.547
23	22.375	-81.525	0.589	0.345	0.490	0.428	0.454	0.479	0.457	0.518	0.400	0.567	0.421	0.541
24	22.375	-81.375	0.589	0.352	0.478	0.455	0.449	0.527	0.450	0.526	0.398	0.564	0.424	0.519
25	22.375	-81.225	0.589	0.337	0.478	0.455	0.449	0.513	0.450	0.520	0.396	0.553	0.426	0.497
26	22.375	-81.075	0.594	0.350	0.474	0.467	0.449	0.464	0.450	0.435	0.396	0.587	0.429	0.550
27	22.375	-80.925	0.589	0.345	0.471	0.496	0.446	0.495	0.444	0.545	0.396	0.580	0.431	0.503
28	22.525	-81.825	0.563	0.386	0.488	0.448	0.450	0.464	0.457	0.505	0.409	0.581	0.426	0.484
29	22.525	-81.675	0.568	0.407	0.484	0.443	0.450	0.478	0.455	0.514	0.407	0.564	0.426	0.528
30	22.525	-81.525	0.568	0.367	0.484	0.451	0.450	0.464	0.452	0.478	0.407	0.564	0.426	0.484
31	22.525	-81.375	0.573	0.364	0.480	0.455	0.447	0.502	0.450	0.448	0.405	0.567	0.426	0.503
32	22.525	-81.225	0.573	0.364	0.476	0.458	0.447	0.509	0.447	0.451	0.402	0.531	0.426	0.528
33	22.525	-81.075	0.578	0.353	0.476	0.458	0.447	0.474	0.450	0.487	0.402	0.551	0.426	0.547
34	22.525	-80.925	0.578	0.361	0.469	0.491	0.445	0.484	0.455	0.482	0.407	0.512	0.431	0.509
35	22.525	-80.775	0.578	0.353	0.465	0.504	0.445	0.533	0.452	0.459	0.405	0.554	0.431	0.528
36	22.525	-80.625	0.573	0.364	0.465	0.521	0.445	0.512	0.450	0.481	0.405	0.515	0.431	0.559
37	22.525	-80.475	0.568	0.391	0.461	0.473	0.439	0.490	0.444	0.519	0.402	0.557	0.429	0.556
38	22.675	-81.675	0.561	0.406	0.484	0.468	0.450	0.450	0.457	0.518	0.413	0.504	0.429	0.538
39	22.675	-81.525	0.566	0.386	0.484	0.451	0.450	0.471	0.455	0.514	0.411	0.571	0.429	0.494
40	22.675	-81.375	0.571	0.367	0.484	0.451	0.450	0.464	0.452	0.497	0.409	0.561	0.431	0.503
41	22.675	-81.225	0.571	0.359	0.480	0.463	0.447	0.488	0.452	0.485	0.407	0.564	0.429	0.581
42	22.675	-81.075	0.575	0.364	0.480	0.438	0.447	0.523	0.452	0.446	0.407	0.551	0.429	0.494
43	22.675	-80.925	0.575	0.364	0.469	0.457	0.445	0.442	0.457	0.492	0.409	0.581	0.431	0.516
44	22.675	-80.775	0.575	0.356	0.465	0.504	0.445	0.519	0.457	0.434	0.409	0.523	0.431	0.547
45	22.675	-80.625	0.575	0.356	0.465	0.512	0.445	0.512	0.455	0.469	0.407	0.551	0.431	0.472
46	22.675	-80.475	0.566	0.411	0.458	0.529	0.439	0.497	0.447	0.444	0.405	0.561	0.429	0.550
47	22.825	-81.675	0.561	0.406	0.490	0.505	0.453	0.510	0.465	0.452	0.420	0.496	0.435	0.516
48	22.825	-81.525	0.561	0.406	0.490	0.505	0.453	0.489	0.465	0.459	0.420	0.496	0.435	0.516
49	22.825	-81.375	0.571	0.383	0.494	0.420	0.456	0.438	0.465	0.471	0.420	0.547	0.435	0.473
50	22.825	-81.225	0.575	0.356	0.494	0.444	0.458	0.463	0.465	0.452	0.418	0.499	0.435	0.497
51	22.825	-81.075	0.575	0.356	0.494	0.468	0.456	0.445	0.465	0.452	0.418	0.486	0.433	0.494
52	22.825	-80.925	0.575	0.356	0.490	0.464	0.456	0.513	0.467	0.450	0.418	0.524	0.438	0.488
53	22.825	-80.775	0.580	0.361	0.486	0.484	0.456	0.472	0.470	0.466	0.418	0.556	0.440	0.449
54	22.825	-80.625	0.580	0.353	0.486	0.427	0.456	0.486	0.470	0.472	0.418	0.518	0.440	0.516
55	22.825	-80.475	0.575	0.364	0.482	0.430	0.453	0.503	0.467	0.488	0.416	0.508	0.440	0.479
56	22.975	-81.825	0.559	0.409	0.494	0.485	0.454	0.434	0.472	0.458	0.427	0.482	0.440	0.510
57	22.975	-81.675	0.559	0.409	0.494	0.468	0.454	0.448	0.470	0.466	0.424	0.473	0.438	0.549
58	22.975	-81.525	0.564	0.406	0.494	0.477	0.457	0.431	0.472	0.451	0.427	0.476	0.440	0.504
59	22.975	-81.375	0.573	0.351	0.501	0.398	0.460	0.483	0.475	0.437	0.427	0.489	0.443	0.489
60	22.975	-81.225	0.573	0.351	0.501	0.461	0.463	0.487	0.475	0.437	0.427	0.563	0.443	0.471
61	22.975	-81.075	0.578	0.356	0.501	0.461	0.463	0.480	0.475	0.443	0.427	0.482	0.443	0.513
62	22.975	-80.925	0.578	0.348	0.497	0.465	0.463	0.480	0.477	0.410	0.427	0.507	0.448	0.477
63	22.975	-80.775	0.578	0.364	0.497	0.441	0.463	0.501	0.480	0.426	0.427	0.476	0.448	0.507
64	22.975	-80.625	0.583	0.353	0.497	0.377	0.463	0.460	0.480	0.450	0.427	0.482	0.450	0.522
65	23.125	-81.675	0.566	0.390	0.496	0.460	0.454	0.496	0.472	0.439	0.427	0.501	0.443	0.501
66	23.125	-81.525	0.566	0.374	0.496	0.485	0.457	0.486	0.475	0.430	0.429	0.474	0.445	0.474
67	23.125	-81.375	0.571	0.362	0.500	0.473	0.457	0.507	0.477	0.459	0.429	0.486	0.445	0.492
68	23.125	-81.225	0.576	0.367	0.500	0.425	0.460	0.497	0.477	0.459	0.429	0.486	0.448	0.513
69	23.125	-81.075	0.576	0.351	0.500	0.425	0.460	0.456	0.480	0.469	0.429	0.542	0.448	0.483
70	23.125	-80.925	0.581	0.356	0.503	0.438	0.463	0.440	0.480	0.426	0.431	0.484	0.453	0.478
71	23.125	-80.775	0.581	0.364	0.500	0.441	0.463	0.440	0.480	0.432	0.433	0.475	0.453	0.472
72	23.125	-80.625	0.581	0.356	0.503	0.438	0.463	0.446	0.483	0.424	0.433	0.493	0.456	0.463
73	23.125	-80.475	0.581	0.364	0.500	0.449	0.465	0.444	0.485	0.446	0.431	0.496	0.456	0.493
74	23.275	-81.225	0.571	0.362	0.500	0.473	0.457	0.493	0.480	0.456	0.431	0.478	0.450	0.540
75	23.275	-81.075	0.576	0.351	0.500	0.425	0.460	0.483	0.483	0.442	0.431	0.508	0.450	0.486
76	23.275	-80.925	0.576	0.367	0.500	0.441	0.460	0.456	0.483	0.424	0.435	0.521	0.456	0.452
77	23.275	-80.775	0.576	0.359	0.500	0.425	0.463	0.446	0.483	0.430	0.435	0.527	0.456	0.469
78	23.275	-80.625	0.576	0.359	0.500	0.425	0.463	0.440	0.485	0.427	0.435	0.515	0.458	0.467
79	23.275	-80.475	0.576	0.367	0.500	0.425	0.463	0.480	0.485	0.427	0.433	0.481	0.458	0.502

n°	Lat [°]	Long [°]	Jul		Aug		Sep		Oct		Nov		Dec	
			K_T	K_D	K_T	K_D	K_T	K_D	K_T	K_D	K_T	K_D	K_T	K_D
0	22.075	-81.975	0.386	0.610	0.343	0.641	0.343	0.644	0.417	0.549	0.549	0.407	0.684	0.297
1	22.075	-81.825	0.390	0.536	0.343	0.648	0.346	0.631	0.417	0.533	0.549	0.382	0.678	0.307
2	22.075	-81.675	0.395	0.577	0.343	0.604	0.351	0.622	0.423	0.533	0.554	0.395	0.678	0.287
3	22.075	-81.525	0.395	0.583	0.343	0.611	0.351	0.590	0.420	0.513	0.549	0.447	0.672	0.303
4	22.075	-81.375	0.397	0.540	0.349	0.615	0.351	0.614	0.414	0.553	0.545	0.426	0.666	0.299
5	22.075	-81.225	0.399	0.564	0.349	0.585	0.353	0.594	0.417	0.493	0.549	0.423	0.666	0.325
6	22.075	-81.075	0.399	0.524	0.357	0.586	0.356	0.589	0.420	0.568	0.554	0.387	0.666	0.292
7	22.075	-80.925	0.399	0.544	0.364	0.582	0.356	0.574	0.414	0.561	0.549	0.431	0.654	0.338
8	22.075	-80.775	0.399	0.544	0.366	0.593	0.356	0.621	0.411	0.549	0.545	0.451	0.649	0.355
9	22.075	-80.625	0.399	0.530	0.364	0.526	0.356	0.550	0.408	0.570	0.545	0.418	0.649	0.341
10	22.225	-81.975	0.394	0.590	0.351	0.582	0.356	0.644	0.427	0.552	0.556	0.419	0.687	0.304
11	22.225	-81.825	0.396	0.567	0.347	0.648	0.356	0.597	0.423	0.478	0.556	0.387	0.681	0.320
12	22.225	-81.675	0.398	0.577	0.345	0.615	0.356	0.597	0.427	0.498	0.561	0.376	0.681	0.313
13	22.225	-81.525	0.398	0.577	0.343	0.596	0.353	0.594	0.420	0.513	0.556	0.427	0.669	0.305
14	22.225	-81.375	0.398	0.557	0.349	0.607	0.351	0.622	0.414	0.577	0.547	0.459	0.664	0.321
15	22.225	-81.225	0.398	0.530	0.349	0.585	0.351	0.638	0.417	0.533	0.552	0.390	0.669	0.345
16	22.225	-81.075	0.398	0.570	0.355	0.604	0.353	0.570	0.417	0.533	0.552	0.431	0.669	0.299
17	22.225	-80.925	0.398	0.550	0.364	0.596	0.356	0.605	0.414	0.577	0.547	0.426	0.658	0.331
18	22.225	-80.775	0.398	0.537	0.366	0.593	0.356	0.574	0.411	0.517	0.543	0.421	0.652	0.327
19	22.375	-82.125	0.396	0.547	0.368	0.562	0.361	0.604	0.428	0.467	0.552	0.423	0.679	0.296
20	22.375	-81.975	0.398	0.537	0.364	0.639	0.361	0.612	0.425	0.486	0.552	0.431	0.673	0.332
21	22.375	-81.825	0.398	0.564	0.360	0.618	0.358	0.624	0.422	0.482	0.552	0.366	0.667	0.362
22	22.375	-81.675	0.398	0.564	0.357	0.579	0.356	0.542	0.422	0.521	0.552	0.431	0.667	0.281
23	22.375	-81.525	0.396	0.547	0.351	0.560	0.351	0.574	0.415	0.537	0.547	0.393	0.661	0.338
24	22.375	-81.375	0.394	0.577	0.355	0.575	0.346	0.615	0.409	0.529	0.538	0.483	0.649	0.337
25	22.375	-81.225	0.394	0.583	0.351	0.604	0.343	0.619	0.409	0.537	0.538	0.475	0.649	0.372
26	22.375	-81.075	0.394	0.536	0.353	0.578	0.343	0.668	0.409	0.545	0.538	0.417	0.649	0.344
27	22.375	-80.925	0.398	0.544	0.357	0.579	0.351	0.606	0.409	0.529	0.534	0.429	0.643	0.361
28	22.525	-81.825	0.405	0.509	0.364	0.611	0.361	0.604	0.409	0.497	0.527	0.453	0.637	0.357
29	22.525	-81.675	0.405	0.561	0.360	0.596	0.358	0.577	0.409	0.553	0.532	0.432	0.637	0.315
30	22.525	-81.525	0.402	0.544	0.360	0.596	0.358	0.530	0.409	0.497	0.532	0.432	0.637	0.343
31	22.525	-81.375	0.402	0.498	0.360	0.561	0.356	0.566	0.409	0.537	0.532	0.441	0.637	0.315
32	22.525	-81.225	0.400	0.514	0.355	0.632	0.353	0.601	0.409	0.545	0.532	0.432	0.637	0.357
33	22.525	-81.075	0.400	0.593	0.355	0.611	0.351	0.558	0.403	0.612	0.527	0.444	0.637	0.322
34	22.525	-80.925	0.402	0.518	0.355	0.575	0.356	0.621	0.406	0.582	0.523	0.466	0.625	0.329
35	22.525	-80.775	0.400	0.587	0.357	0.593	0.356	0.605	0.406	0.582	0.523	0.405	0.625	0.350
36	22.525	-80.625	0.400	0.521	0.360	0.582	0.353	0.609	0.403	0.537	0.523	0.483	0.619	0.368
37	22.525	-80.475	0.398	0.557	0.355	0.568	0.351	0.550	0.400	0.575	0.514	0.491	0.607	0.390
38	22.675	-81.675	0.409	0.529	0.366	0.551	0.367	0.573	0.411	0.537	0.525	0.466	0.634	0.333
39	22.675	-81.525	0.409	0.535	0.364	0.526	0.367	0.565	0.411	0.594	0.529	0.462	0.634	0.347
40	22.675	-81.375	0.407	0.564	0.364	0.561	0.365	0.631	0.411	0.537	0.529	0.436	0.634	0.375
41	22.675	-81.225	0.405	0.548	0.360	0.604	0.362	0.550	0.411	0.497	0.529	0.470	0.634	0.333
42	22.675	-81.075	0.405	0.509	0.357	0.579	0.357	0.636	0.404	0.546	0.529	0.419	0.634	0.354
43	22.675	-80.925	0.405	0.574	0.357	0.614	0.360	0.671	0.407	0.550	0.525	0.440	0.628	0.314
44	22.675	-80.775	0.402	0.544	0.357	0.600	0.357	0.519	0.407	0.525	0.520	0.443	0.622	0.325
45	22.675	-80.625	0.402	0.570	0.360	0.582	0.355	0.578	0.404	0.554	0.520	0.452	0.622	0.382
46	22.675	-80.475	0.400	0.560	0.353	0.607	0.352	0.518	0.401	0.583	0.511	0.407	0.598	0.428
47	22.825	-81.675	0.416	0.495	0.374	0.580	0.378	0.535	0.407	0.566	0.520	0.452	0.631	0.343
48	22.825	-81.525	0.416	0.489	0.372	0.555	0.378	0.602	0.411	0.521	0.525	0.422	0.637	0.340
49	22.825	-81.375	0.418	0.480	0.370	0.572	0.380	0.539	0.414	0.525	0.529	0.436	0.643	0.329
50	22.825	-81.225	0.416	0.527	0.366	0.628	0.378	0.535	0.414	0.557	0.529	0.444	0.643	0.329
51	22.825	-81.075	0.413	0.549	0.366	0.642	0.375	0.516	0.411	0.497	0.529	0.419	0.643	0.343
52	22.825	-80.925	0.413	0.581	0.364	0.618	0.372	0.603	0.411	0.521	0.529	0.419	0.631	0.357
53	22.825	-80.775	0.413	0.536	0.364	0.604	0.370	0.523	0.411	0.537	0.529	0.402	0.625	0.353
54	22.825	-80.625	0.413	0.536	0.366	0.642	0.370	0.546	0.414	0.549	0.529	0.453	0.625	0.332
55	22.825	-80.475	0.413	0.536	0.377	0.556	0.372	0.542	0.414	0.468	0.520	0.409	0.613	0.338
56	22.975	-81.825	0.424	0.528	0.385	0.544	0.388	0.499	0.412	0.529	0.518	0.491	0.634	0.314
57	22.975	-81.675	0.422	0.525	0.383	0.560	0.385	0.525	0.412	0.505	0.518	0.412	0.634	0.350
58	22.975	-81.525	0.424	0.541	0.383	0.547	0.388	0.579	0.415	0.509	0.523	0.435	0.634	0.336
59	22.975	-81.375	0.424	0.479	0.385	0.590	0.393	0.486	0.419	0.545	0.527	0.448	0.640	0.333
60	22.975	-81.225	0.422	0.525	0.383	0.593	0.393	0.479	0.419	0.577	0.532	0.427	0.646	0.364
61	22.975	-81.075	0.422	0.494	0.381	0.503	0.390	0.510	0.419	0.553	0.532	0.436	0.646	0.343
62	22.975	-80.925	0.424	0.553	0.385	0.577	0.388	0.485	0.419	0.441	0.536	0.424	0.634	0.350
63	22.975	-80.775	0.427	0.495	0.383	0.560	0.388	0.521	0.419	0.529	0.536	0.432	0.628	0.332
64	22.975	-80.625	0.427	0.507	0.385	0.530	0.388	0.485	0.425	0.521	0.541	0.429	0.628	0.339
65	23.125	-81.675	0.425	0.532	0.391	0.535	0.393	0.479	0.415	0.517	0.518	0.456	0.634	0.293
66	23.125	-81.525	0.425	0.526	0.391	0.548	0.395	0.568	0.415	0.517	0.523	0.435	0.634	0.329
67	23.125	-81.375	0.428	0.529	0.391	0.541	0.398	0.423	0.419	0.545	0.527	0.431	0.640	0.325
68	23.125	-81.225	0.428	0.486	0.394	0.558	0.398	0.515	0.419	0.513	0.532	0.479	0.640	0.354
69	23.125	-81.075	0.428	0.462	0.391	0.561	0.401	0.504	0.422	0.469	0.536	0.415	0.640	0.340
70	23.125	-80.925	0.428	0.523	0.391	0.554	0.401	0.497	0.425	0.505	0.541	0.454	0.634	0.343
71	23.125	-80.775	0.430	0.520	0.394	0.538	0.401	0.497	0.428	0.501	0.541	0.403	0.634	0.357
72	23.125	-80.625	0.430	0.514	0.394	0.558	0.401	0.497	0.431	0.506	0.545	0.408	0.628	0.339
73	23.125	-80.475	0.430	0.533	0.396	0.535	0.403	0.522	0.438	0.529	0.550	0.430	0.622	0.350
74	23.275	-81.225	0.430	0.533	0.394	0.493	0.402	0.532	0.423	0.541	0.530	0.422	0.637	0.357
75	23.275	-81.075	0.430	0.490	0.396	0.542	0.404	0.515	0.423	0.533	0.534	0.504	0.637	0.350
76	23.275	-80.925	0.430	0.459	0.396	0.497	0.404	0.515	0.430	0.525	0.543	0.437	0.637	0.336
77	23.275	-80.775	0.430	0.496	0.396	0.523	0.404	0.508	0.433	0.529	0.543	0.429	0.637	0.343
78	23.275	-80.625	0.430	0.514	0.396	0.535	0.404	0.522	0.436	0.510	0.548	0.417	0.631	0.353
79	23.275	-80.475	0.430	0.514	0.396	0.503	0.404	0.494	0.443	0.533	0.553	0.405	0.625	0.371

Table 2.11: corrected vales of monthly clearness index and diffuse ratio for each of the 80 zones considered in the province of Matanzas

2.4.1 Script

Similarly to the Point Solar tool, a script is required to run the calculation with different inputs for each zone. The two scripts have a similar structure: a number of fixed input settings (defined in paragraph 2.2) are combined to variable input settings which are iteratively taken from a text file. In this case, all the variable inputs are contained in a single file (var_"month".txt) and ordered in a precise sequence, with every row related to a different zone. Associating a floating "i" number to every value separated by a tab and reading the text line by line, the script converts the text into an array in which every row is a list of parameters of a single zone. Each list is used in a loop to set the missing input required by Area Solar Radiation: latitude, transmittivity and diffuse proportion. In addition to them, further four values are taken from the text file to set the extent environmet. The Output Extent environment setting defines what portion of raster will be processed by the tool. For each loop generated by the script, the extent area needs to be defined by setting the coordinates of their opposites corners (in meters coordinate system). In this way the calculation is run for a sequence of portions of the total DSM, which is loaded together with the fixed inputs. Every time the command "Area Solar" is executed, it generates a portion of global solar map, which is numbered with an "i" value and added to a list. When the loop comes to the last iteration (zone 79) all the portions are merged in a single raster by the tool "Mosaic to new raster". The setting chosen for the mosaic are: pixel type 32_BIT_FLOATING; number of bands 1; mosaic method MEAN; mosaic color map mode FIRST. This means that the output cell values of the overlapping areas are the average value of the overlapping cell and the color map of the first raster dataset will be applied to all the raster mosaic (ArcGis Desktop Help, 2019). The extent environment borders exceeds the size area of each zone, in order to flatten the gap between contiguous areas. The 80 zones identified in figure 7 have a size of 0.15x0.15 decimal degrees, while the chosen size of the extent area is 0.225x0.225 decimal degrees. Figure 2.13 represent the flowchart of the script which resumes all its steps and an example of the script can be found in appendix 2.

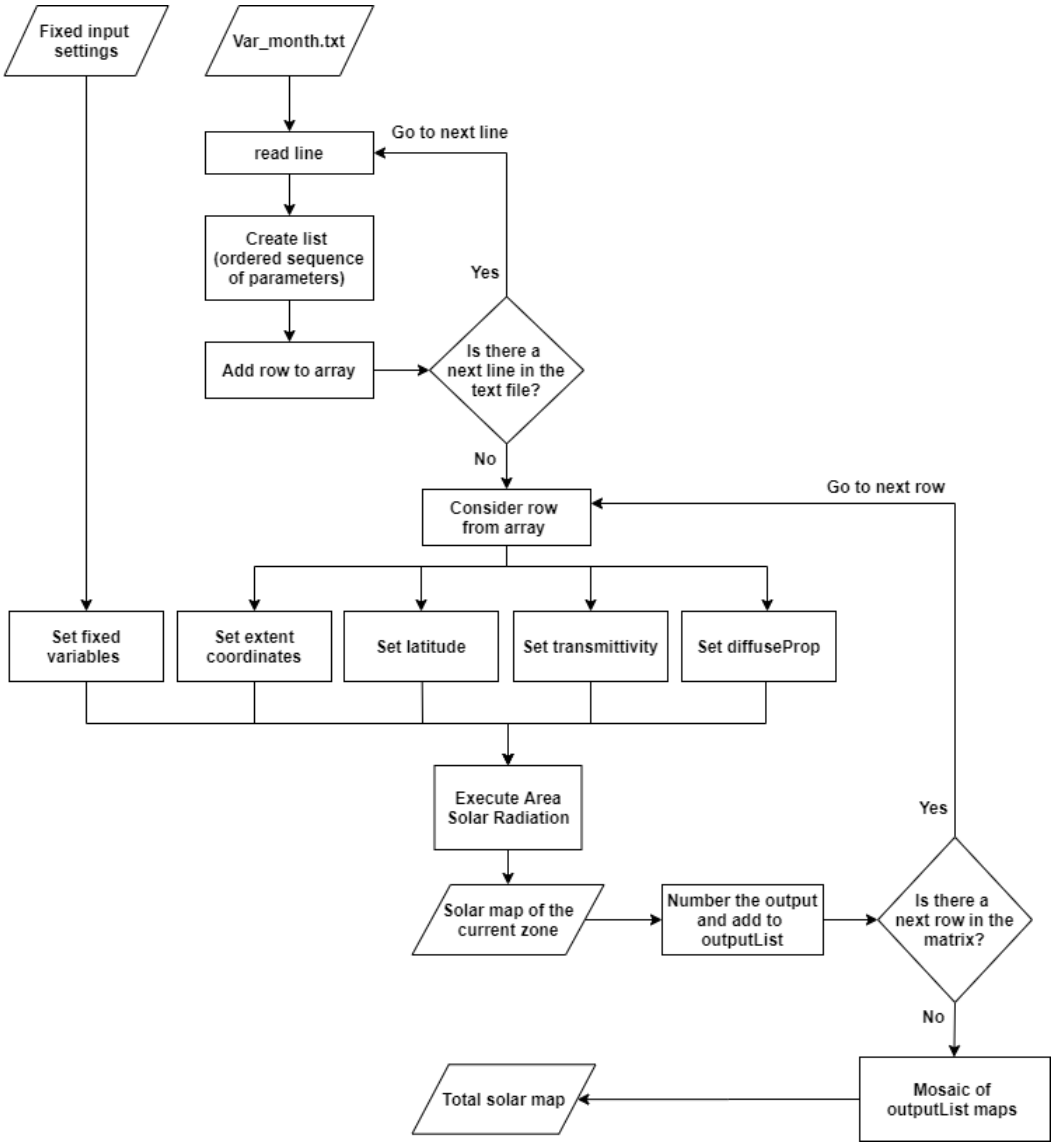

Figure 2.12: Flowchart of the script for the Area Solar Radiation calculation.

2.4.2 Irradiation maps

The resulting monthly solar maps of Matanzas are summed (through the raster calculator tool) and merged. The map obtained (map 2.1) represents the Annual Global Horizontal Irradiation in Matanzas, calculated through the Area Solar Radiation tool.

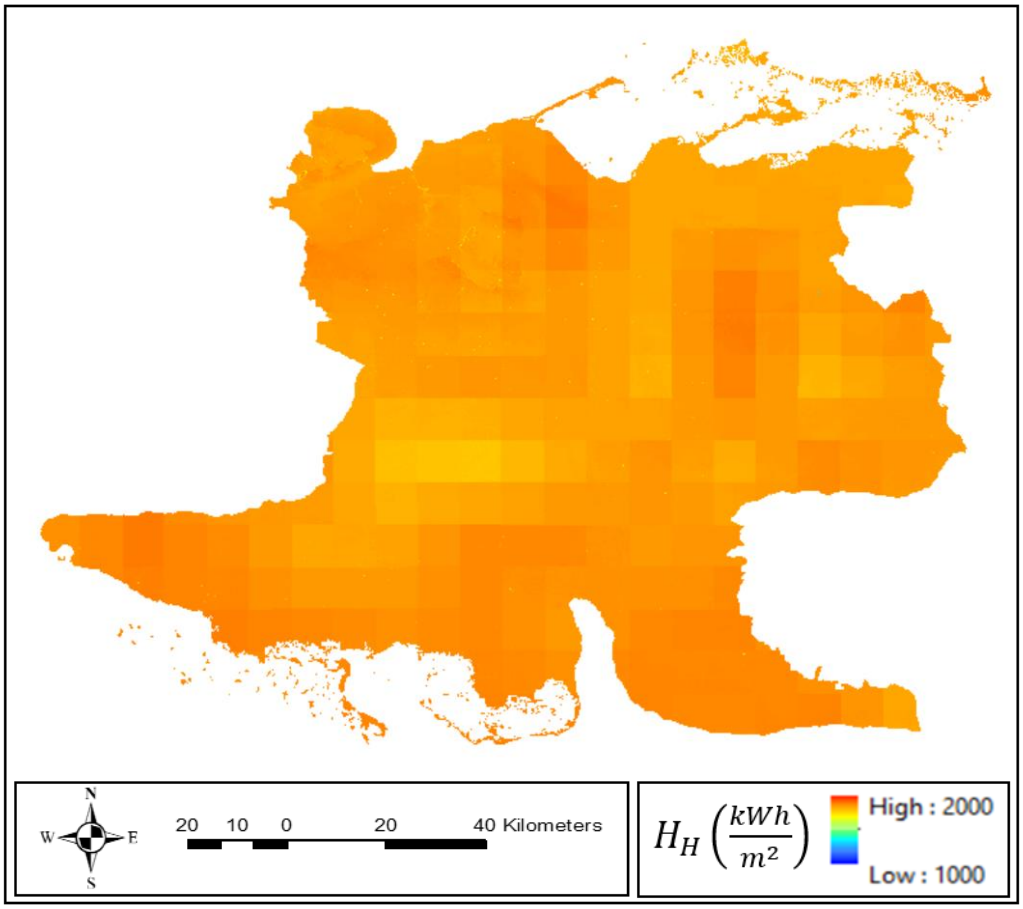

Map 2.1: Annual Global Horizontal Irradiation in Matanzas (own elaboration through ArcMap).

The high-resolution is hidden by the large scale of the area considered. A closer view would highlight the variation of the solar radiation pixel by pixel. In the northern part of the province, characterized by a mountain landscape, a higher level of radiation is visible along the slopes. The relevance of this result is that any portion of this wide area can be extracted and used for eventual future studies.

The calculated monthly solar maps of Matanza can be found from Appendix 3 to Appendix 14.

2.4.3 Guasasa solar map

By zooming on the study area, the municipality of Guasasa, the raster resolution of the maps is evident. In order to emphasize the fluctuation, a very short range of color scale is set. Anyway, the Annual Global Horizontal Irradiation in Guasasa (map 2.2) appears to be almost constant all over the area considered. The black points represents the distribution of the buildings in the community. This result was predictable, since the morphology is basically flat and no obstacle to the sun rays can be found.

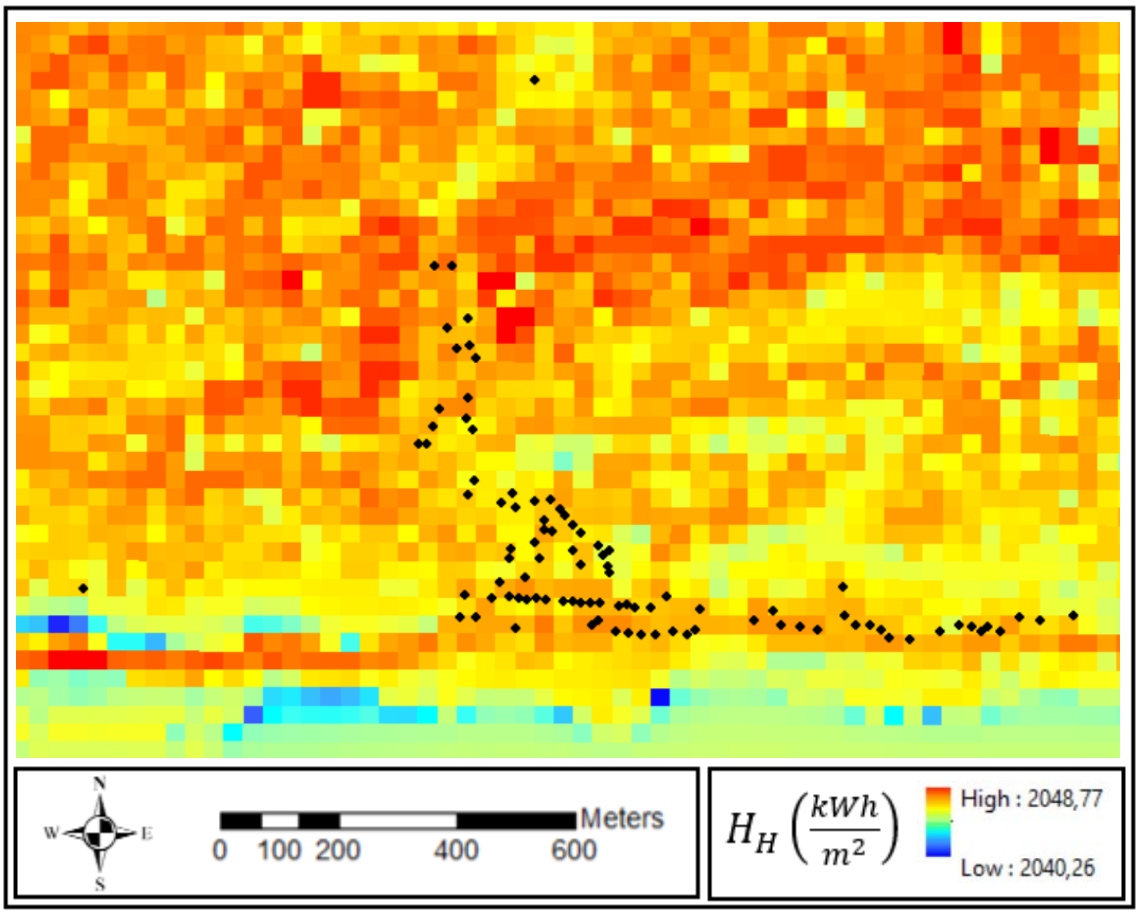

Map 2.2: Annual Global Horizontal Irradiation in Guasasa (own elaboration through ArcMap).

The calculated monthly solar maps of Guasasa can be found from Appendix 15 to Appendix 26.

2.4.4 Irradiation on tilted surface

The calculated maps are referred to the *Global Horizontal Radiation* (H_H). The required input of the LEC model is the solar radiation received by the solar panel surface, so on a tilted

surface. The surface angle considered is the optimal tilt angle (β_{opt}). In order to calculate the *Global Irradiation on optimal Tilted Surface* ($H_{\beta_{opt}}$) a correction factor is needed.

The Photovoltaic Geographic Information System (*PVGIS*) by The European Commission's science and knowledge service, provides a free and open access database of solar radiation values all over the world. Setting the coordinates of Guasasa, the monthly average values of Global Horizontal Irradiation and Global Irradiation on optimal Tilted Surface are downloaded. The period considered for the data collection is from 2001 to 2020. The ratio of each couple of values is calculated and the average value of each ratio is considered as correction factor K_β.

$$K_\beta = \frac{H_{\beta_{opt}}}{H_H} = 1.088$$

By multiplying the factor K_β for each pixel of the annual global horizontal radiation raster, a new raster representing the global irradiation on an optimal tilted surface is obtained.

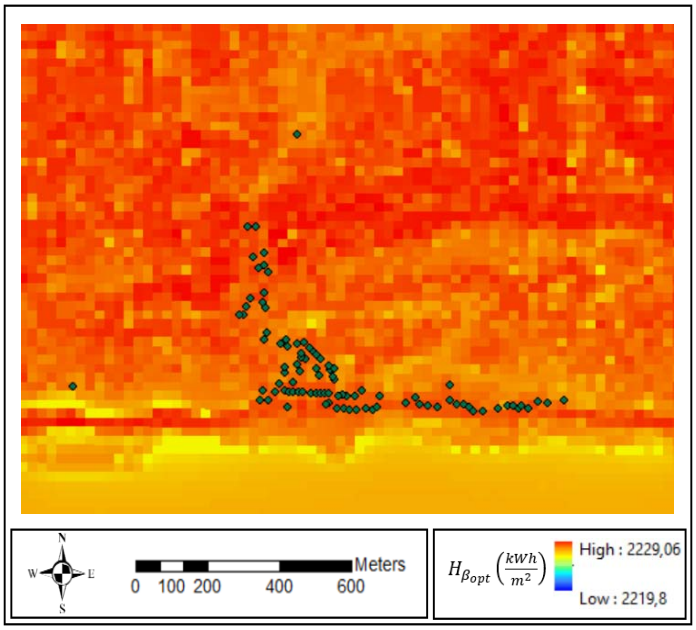

Map 2.3: Annual Global Irradiation on optimal Tilted Surface in Guasasa (own elaboration through ArcMap).

3 LEC model in ArcGIS environment

During the early stage of an electrification project, comparing alternative methods of energy production is fundamental. In this regard, an effective tool is the Levelized Energy Cost (LEC), an index to measure the cost of a generation plant per unit of total energy generated over its lifetime. It is calculated as the ratio between the total discounted costs of investment, fuel, operation and maintenance expenditures and the amount of electricity produced by the asset considered. The heterogeneity of energy resources and load distribution and their variability over time and space is a factor which can affect significantly the LEC of a power plant. Choosing the ideal energy mix and the most cost-effective system configuration is a challenging aspect which requires an assessment at a local level. The concept of using GIS technologies as a decision making tool for rural electrification allows to integrate the geographical and regional influence to the techno-economical evaluation, reducing the degree of approximation.

By using the application "ModelBuilder" by ArcGIS, it is possible to create a workflow of geoprocessing tools, that is an algorithm that calculates the desired output starting from GIS data. The present chapter will introduce a model created through "ModelBuilder" for the calculation of the LEC of different possible types of power plant. The input required is a point feature class[14] representing the group of buildings to be supplied, reporting in its attribute table[15] the specification of the energy demand of each load and some cost and lifetime assumptions (presented in details in chapter 4). Adapting the input to the specific case considered, the model can be applied to any selected group of loads.

The types of power plant admitted by the model are the following:

- Photovoltaic Stand-alone System (for each individual load);
- Photovoltaic Centralized System;
- Solar-Diesel Hybrid System (centralized system);
- Diesel Generator Set (centralized system).

In future possible developments, further typologies could be integrated, considering other energy resources to provide a complete picture of the viable electrification options.

[14] A feature class is a collection of geographic features that share the same geometry type (such as point, line, or polygon) and the same attribute fields for a common area (ArcGIS Desktop Help, 2019).

[15] In GIS science, an attribute table is a database or tabular file containing information about a set of geographic features. Attribute tables are often joined or related to spatial data layers and the attribute values they contain can be used to find, query and symbolize features or raster cells (ArcGIS Desktop Help, 2019).

3.1 Methodology

The present work applies the approach proposed by the group "gTIGER"[16] of CIEMAT, committed in the development of a GIS-based software tool to support the assessment of different options for rural electrification.

The origin of this methodology comes from the project SOLARGIS, financed by the Directorate General XII for Science, Research and Development of the European Commission that involved many research centers in the nineties. This project confirmed the importance of a local perspective in renewable energies integration processes and the great potential of GIS technologies in this contribution. A first update was released in the second phase of the project, SOLARGIS II, as part of the agreement between CIEMAT and the UPM (Polytechnic University of Madrid) with the aim of defining the degree of uncertainty of the model execution (Amador, 2000). With this basis, IntiGIS model was created: a plug-in of ArcGIS, developed without commercial purpose, to support the electrification planning of rural, isolated areas (Pinedo & Dominguez, 2011). At the actual stage, IntiGIS has been tested in different study sites and is still subject to improvements. The model allows to compare several technology options: photovoltaic, wind power, diesel generator, hybrid photovoltaic-diesel, hybrid wind-diesel. Further upgrades are under investigation, such as the addition of the biomass option. However, the main issue is now to improve the IT aspect, fixing some bugs that can undermine the smoothness of the operation. Because of the educational and humanitarian nature of the project, it was recently questioned the option of transferring the foreground to a free source (QGIS), in order to encourage the development and the use of IntiGIS by external contributors and stakeholders.

With these premises, it was agreed to adapt some of the equations used by IntiGIS to create an independent model in ArcGIS environment. This chapter will present the methodology applied for its implementation. The study focuses in solar energy in comparison with diesel power generation and their combination in a hybrid system. The main update introduced is designed to facilitate the comparison between individual and centralized systems. In the original model, the energy demand is expressed in the form of a raster representing the load density. The LEC calculation is performed pixel by pixel, allowing to visualize the most competitive technology to supply the energy demand of each cell.
In figure 3.1, an example of application of IntiGIS, tested for an isolated municipality in Spain (Domínguez & Pinedo, 2009).

[16] Grupo de Tecnologías de la Información Geográfica y Energías Renovables

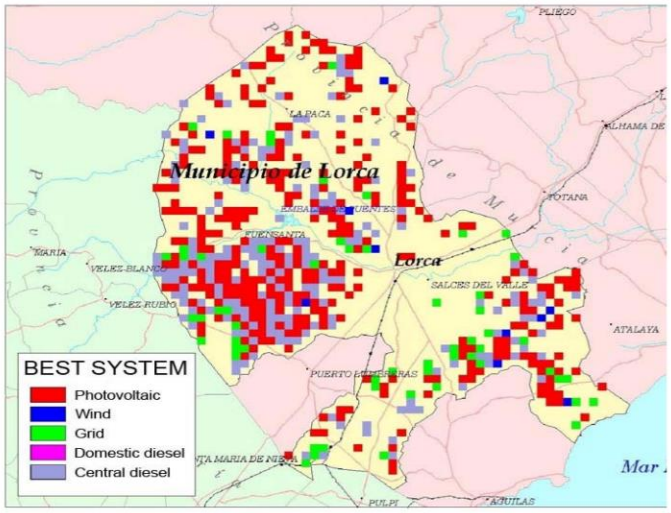

Figure 3.1: Result of IntiGIS execution in the municipality of Lorca (Murcia, Spain). Spatial distribution of the most competitive technologies for energy supply (Domínguez & Pinedo, 2009).

This approach provides an immediate visual impact in the comparison between different technologies. On the other hand, its weakness is not allowing a combination of different groups of loads in a mini-grid.

The new model proposes a solution to this issue. While introducing the input map that contains the energy demand distribution, the user can select a group of buildings to be supplied through a centralized power system. The unselected loads will be assigned by default to the individual system case. In this way, it is possible to simulate the techno-economic performance of different configurations of mini-grids and, at the same time, compare them with the individual option. Another change introduced for the centralized case consists on the visualization of the resulting LEC in a raster format. The choice of the installation site can have a high impact on the cost of generation, due to spatial variability of the resources combined with the distance from the main distribution line. In some cases, the most cost-effective solution does not correspond to the closest location to the central line. The resulting raster defines where it is more convenient to place the centralized plant. Each pixel represents the LEC value of an hypothetical plant placed in the same pixel, capable to fulfill the demand of the selected mini-grid.

The boundaries of the system considered for the centralized cases include the cost associated to the potential grid construction or extension. Being primarily designed for small communities, a low voltage grid is considered, so transmission lines and transformers are not included. Tax, subsides, environmental and public health impact are not taken into account in the cost assessment but could be considered for future developments.

3.1.1 General parameters

All the equation of the model are defined upon the following parameters:

- n_i [years]: *Expected Lifetime* of the subsystem "i";
- k: *Discount Rate;*
- $\tau(n_i)$: *Capital Recovery Factor* for the subsystem "i"

$$\tau(n) = \frac{k \cdot (1+k)^2}{(1+k)^n - 1} \tag{3.1}$$

- I_D(€/kW): *Capital Investment* for the diesel generator per unit of power;
- I_{pv}(€/kW_p): *Capital Investment* for the solar panels per unit of peak power;
- I_s (€/kWh): *Capital Investment* for the storage system per unit of capacity;
- I_{pc} (€/kW): *Capital Investment* for the power conditioning system per unit of power;
- I_l (€/km): *Capital Investment* for the distribution line per unit of length;
- I_{CN} (€/kW): *Capital Investment* for the grid connection per unit of power;
- OM_D (€/($h_{op} \cdot$ kW)): *Operation & Maintenance annual cost* for the diesel generator per units of operating hours per kW;
- OM_{pv} (€/kW_p): *Operation & Maintenance annual cost* for the solar panels per unit of peak power;
- OM_s (€/kW): *Operation & Maintenance annual cost* for the storage system per unit of capacity;
- OM_{pc} (€/kW): *Operation & Maintenance annual cost* for the power conditioning system per unit power;
- OM_l (€/kW): *Operation & Maintenance annual cost* for the distribution line per unit of length;
- $h_{year} = 8760$ (h): *Hours per year;*
- E_d (kWh): *Daily Energy Demand* for a single building;
- P (kW): *Contracted Power* for a single building;
- CF_i: *Capacity Factor* for the power generation technology "i"
- C_i (€cents/kWh): *Cost* of the subsystem "i" per unit of energy produced;
- LEC_i (€cents/kWh): *Levelized Energy Cost* of the power plant "i";

The *Capital Recovery Factor* is the ratio used to calculate the present value of an annuity (a series of equal annual cash flows).

The *Capacity Factor* is the ratio of the actual energy output over a period and the maximum possible energy output over the same period. The period considered is one year.

3.1.2 Individual power plants: PV stand-alone

The Levelized Energy Cost of a photovoltaic stand-alone power plant is calculated as the sum of the cost per kWh of three subsystems: PV modules ($C_{pv,ind}$) , Storage system ($C_{s,ind}$) and Power Conditioning system ($C_{pc,ind}$).

PV Levelized Energy Cost (€cents/kWh):

$$LEC_{pv,ind} = C_{pv,ind} + C_{s,ind} + C_{pc,ind} \tag{3.2}$$

The *PV Modules cost* (€cents/kWh) is calculated as follows:

$$C_{pv,ind} = \frac{\tau(n_{pv}) \cdot I_{pv} + OM_{pv}}{CF_{pv} \cdot h_{year}} \cdot 10^2 \tag{3.3}$$

CF_{pv} is the Capacity Factor of the photovoltaic system:

$$CF_{pv} = \frac{\eta_{pv} \cdot \eta_{stc} \cdot H_\beta \cdot A_{pv}}{P_{pv} \cdot h_{year}} \tag{3.4}$$

Where:

- η_{pv} is the global efficiency of the photovoltaic system;
- η_{stc} is the the maximum efficiency of the solar panel at standard conditions (Irradiance: $I_{stc} = 1\ \mathrm{kW/m^2}$; Temperature: $T_{stc} = 25\ ^\circ\mathrm{C}$; AM 1.5)
- A_{pv} is the total *Area* covered by the solar panels;
- H_β (kWh/m^2) is the average annual *Global Irradiation* on tilted surface (with inclination angle of the solar panel).
- P_{pv} is the *Peak Power* (kW) of the solar system, equal to:

$$P_{pv} = I_{stc} \cdot \eta_{stc} \cdot A_{pv} \tag{3.5}$$

Since the irradiance at standard conditions is equal to 1 kW/m^2, equation 3.4 can be simplified as follows:

$$CF_{pv} = \frac{\eta_{pv} \cdot H_\beta}{h_{year}} \tag{3.6}$$

The value of the annual global irradiation can be therefore expressed both in units of energy per squared meters (kWh/m^2) and in equivalent hours at 1 kW of irradiance ($h_{eq,stc}$). Once obtained the capacity factor of the photovoltaic system, the required installed power capacity (kW) can be calculated from:

$$P_{PV} = \frac{E_a}{CF_{PV} \cdot h_{year}} \tag{3.7}$$

Where:

- E_a is the annual energy demand for a single building ($E_a = E_d \cdot 365$) (kWh)

The *Storage system cost* (€cents/kWh) is calculated as follows:

$$C_{s,ind} = \frac{\tau(n_s) \cdot I_s + OM_s}{E_a} \cdot C \cdot 10^2 \tag{3.8}$$

C is the *Storage Capacity* (kWh):

$$C = \frac{d \cdot E_d}{\eta_s \cdot DoD} \tag{3.9}$$

Where:

- d [days] is the *autonomy* of the storage system. It represents the maximum period in which the battery can satisfy the energy demand by itself;
- DoD is the *Depth of Discharge* of the battery;
- η_s is the efficiency of the storage system.

The *Power Conditioning system cost* (€cents/kWh) is calculated as follows:

$$C_{pc,ind} = \frac{\tau(n_{pc}) \cdot I_{pc} + OM_{pc}}{LF_{i,pv} \cdot h_{year}} \cdot 10^2 \tag{3.10}$$

The Power Conditioning refers to the Balance of System excluding the storage system. It is mainly composed by the inverter.

$LF_{i,pv}$ is the *Inverter Load Factor* for a stand-alone PV system, which can be seen as the ratio between the average operating power and the maximum admissible power of the inverter. It is convenient to express this relation as a function of the energy load characteristics, which are described by the shape of the demand curve. The *Load Factor* (f_l) is the ratio between the *Average Load* ($\bar{P}$) and the *Peak Load* (P_{peak}) of the energy demand (Louie, 2018):

$$f_l = \frac{\bar{P}}{P_{peak}} \tag{3.11}$$

In the calculation of the inverter load factor, the conversion efficiency needs to be considered. The efficiency depends on the percentage of the load supply, on the type of inverter chosen and on the value of the input voltage (Borda et al., 2011). A correction factor (k_c) is therefore introduced which can include other adjustments experimentally derived in order to associate the proper weight to the cost of the power conditioning system. For example, the inverter is

normally designed with a higher maximum admissible power than the peak load, so an oversized coefficient affects the inverter load factor.

$$LF_{i,pv} = f_l \cdot \eta_{inv,pv} \cdot k_c \tag{3.12}$$

Where:

- $\eta_{inv,pv}$ is the nominal efficiency of the inverter for a PV stand-alone system.

3.1.3 Centralized power plants: Diesel, PV centralized, Hybrid Solar-Diesel

The LEC model considers three possible configurations for the centralized case:

1. Diesel generator set;
2. Photovoltaic centralized;
3. Solar-Diesel Hybrid system.

All the centralized configurations are defined by the same algorithm. The discriminating factors between one case and the others are the input settings of the model. In particular, a crucial parameter is the Renewable Fraction (f_r), representing the percentage of power generation from renewable sources in the total energy production:

1. $f_r = 0 \rightarrow$ Diesel generator set;
2. $f_r = 1 \rightarrow$ Photovoltaic centralized;
3. $0 < f_r < 1 \rightarrow$ Solar-Diesel Hybrid system.

The ArcMap model allows to select a group of loads to be supplied with a centralized power plant (further insights in chapter 3.2). The aggregated annual energy demand ($E_{a,centr}$) (kWh) is the sum of the annual energy demands of each building "i" selected ($365 \cdot E_{d,i}$) (kWh):

$$E_{a,centr} = 365 \cdot \sum_i E_{d,i} \tag{3.13}$$

Once established the renewable fraction, the annual energy produced by the photovoltaic system (E_{PV}) [kWh] can be calculated:

$$E_{PV} = f_r \cdot E_{a,centr} \tag{3.14}$$

The annual energy produced by the Diesel generator system (E_{Diesel}) (kWh) is the residual energy demand to be fulfilled:

$$E_{Diesel} = E_{a,centr} - E_{PV} \tag{3.15}$$

The Levelized Energy Cost of a centralized power plant, is calculated as the sum of the cost per kWh of seven subsystems: PV modules ($C_{pv,centr}$); Storage system ($C_{s,centr}$); Power Conditioning system ($C_{pc,centr}$); Diesel generator (C_D); Fuel (C_F); Line (C_l); Connections C_{CN}.

$$LEC_{centr} = C_{pv,centr} + C_{s,centr} + C_{pc,centr} + C_D + C_F + C_l + C_{CN} \tag{3.16}$$

The *centralized PV Modules cost* (€cents/kWh) is calculated as follows:

$$C_{pv,centr} = \frac{\tau(n_{pv,centr}) \cdot I_{pv,centr} + OM_{pv,centr}}{CF_{pv,centr} \cdot h_{year}} \cdot 10^2 \tag{3.20}$$

$CF_{pv,centr}$ is the Capacity Factor of the centralized photovoltaic system:

$$CF_{pv,centr} = \frac{\eta_{pv,centr} \cdot H_\beta}{h_{year}} \tag{3.21}$$

Where: $\eta_{pv,centr}$ is the global efficiency of the centralized photovoltaic system.

Once obtained the capacity factor of the centralized photovoltaic system is obtained, the required installed power capacity (kW) can be calculated from:

$$P_{PV,centr} = \frac{E_{PV}}{CF_{PV,centr} \cdot h_{year}} \tag{3.22}$$

The *centralized Storage system cost* (€cents/kWh) is calculated as follows:

$$C_{s,centr} = \frac{\tau(n_{s,centr}) \cdot I_{s,centr} + OM_{s,centr}}{E_{a,centr}} \cdot C_{centr} \cdot 10^2 \tag{3.23}$$

C_{centr} is the *centralized Storage Capacity* (kWh):

$$C_{centr} = \frac{d_{centr} \cdot \sum_i E_{d,i}}{\eta_{s,centr} \cdot DoD_{centr}} \tag{3.24}$$

Where:

- d_{centr} [days] is the *autonomy* of the centralized storage system. It represents the duration in which the battery can satisfy the aggregated energy demand by itself;
- DoD_{centr} is the *Depth of Discharge* of the battery used in the centralized storage system;
- $\eta_{s,centr}$ is the efficiency of the centralized storage system.

The *centralized Power Conditioning system cost* (€cents/kWh) is calculated as follows:

$$C_{pc,centr} = \frac{\tau(n_{pc,centr}) \cdot I_{pc,centr} + OM_{pc,centr}}{LF_{inv,c} \cdot h_{year}} \cdot 1.5 \cdot 10^2 \quad (3.25)$$

$LF_{pc,c}$ is the power conditioning Load Factor for a centralized system, for which the same considerations made for the inverter of the individual system are valid:

$$LF_{pc,c} = f_l \cdot \eta_{pc,centr} \cdot k_c \quad (3.26)$$

Where:

- $\eta_{pc,centr}$ is the conversion efficiency of the centralized power conditioning system. It includes in a single parameter the effect of the whole set of power electronics (inverters, rectifiers and/or bidirectional inverters)

A standard centralized system generates the power in AC current and feeds the load directly. In parallel, an AC to DC conversion is necessary to charge the battery. Finally, the central inverter converts again the output power of the storage. The contribution of the power conditioning to the LEC of a centralized plant is higher than an individual one. The investment for the rectifier system is taken as 50% of the cost associated to the central inverter (Borda et al.,2011). A correction factor of 1.5 is therefore applied to take into account the higher complexity of the centralized system in comparison to the individual case.

The *Diesel generator set cost* (€cents/kW) is composed by the generator cost (C_g) (€cents/kW) and the reconstruction cost (C_{rec}) (€cents/kW):

$$C_D = C_g + C_{rec} \cdot \frac{E_{Diesel}}{E_{a,centr}} \quad (3.27)$$

Such distinction in two factors was made in order to better reflect the cost associated to replacements of damaged components. For better reflecting the life cycle of a diesel set as the period before the first replacement needed was too penalizing compared to real cases. The separation of the reconstruction cost allowes to consider a higher value for the expected lifetime of the diesel generator. As a consequence, the capital investment cost has a wider distribution throughout the lifetime of the diesel set.

The *Diesel Generator cost* (€cents/kWh) is calculated as follows:

$$C_g = \left(\frac{\tau(n_D) \cdot I_D}{CF_D \cdot h_{year}} + OM_D \right) \cdot 10^2 \tag{3.28}$$

The *Reconstruction Cost* (€cents/kWh) is calculated as follows:

$$C_{rec} = \frac{\frac{\tau(n_D) \cdot (0.25 \cdot I_D)}{1 + k^{n_{rec}}}}{CF_D \cdot h_{year}} \cdot 10^2 \tag{3.29}$$

CF_D is the Capacity Factor of the Diesel generation set:

$$CF_D = \frac{E_{Diesel}}{P_D \cdot h_{year}} \tag{3.30}$$

P_D is the required installed Power capacity (kW) of the diesel generator set:

$$P_D = f_d \cdot \sum_i P_i \tag{3.31}$$

Where:

- P_i is the contracted power (kW) of each building to be supplied by the centralized power plant;
- f_d is the *Design Factor* of the diesel generator, to be set according to the simultaneity of the individual loads and an oversize factor.

The size of the diesel set needs to guarantee the supply of the aggregated load peak power with a safety margin. P_D should always exceed the load plus 2.5 or 3 times the power of the battery charger (Amador, 2000). For this reason, the design factor needs to have a higher value than the coincidence factor of the individual loads.

In the hybrid case, the diesel generator size does not depend on the renewable fraction of the system. It plays a backup role in the system, so it should be able to autonomously feed all the centralized loads in case of need.

The *Fuel Cost* (€cents/KWh) is calculated as follows:

$$C_F = CO_F \cdot F_p \cdot (1 - f_r) \cdot 10^2 \tag{3.32}$$

Where:

- CO_F is the *Fuel Consumption* (l/kWh) of the diesel generation set;
- F_p is the *Fuel Price* (€/l).

The *Line Cost* (€/kWh) is calculated as follows:

$$C_{LV} = \frac{\tau(n_l) \cdot I_l + OM_l}{E_{a,centr}} \cdot \frac{L_l}{10^3} \cdot 10^2 \tag{3.33}$$

L_l is the *Total line length* (m), automatically calculated by the ArcMap model and equal to:

$$L_l = L_{main_{line}} + d_{PowerPlant} \sum_i d_{load,i} \tag{3.34}$$

Where:

- L_{main_line} is the length of the central line;
- $d_{PowerPlant}$ is the distance between the installation site of the centralized power plant and the central line, following the shortest path;
- $d_{load,i}$ is the distance between the load "i" and the central line, following the shortest path.

Note that the requested line costs inputs are expressed in units of €/km.

The *Connection Cost* (€cents/KWh) is calculated as follows:

$$C_{CN} = \frac{\tau(n_D) \cdot I_{CN} \cdot \sum_i P_i}{E_{a,centr}} \cdot 10^2 \tag{3.35}$$

Such factor is associated with the expenditure for each load connection to the grid.

3.2 Model Structure

The model requires the following input data:

- Point feature class file representing the position of each building considered for the electrification project;
- Point feature class file representing the position of the group of building considered for the centralized system;
- Polyline feature class file representing the central distribution line of the mini-grid to which all the loads would be connected;
- Average annual global solar radiation raster on a tilted surface (solar panel inclination angle);
- Digital Elevation Model of the study area.

The point feature classes have to contain in their attribute table the value of the input parameters required by the equations defined in the previous paragraph: Energy Demand and Peak Power of the building, Investment and O&M cost for each subsystem and the series of f- indexes.

The algorithm is composed by a series of ArcMap tools interconnections. Every equation of the model introduces a new parameter which needs to be added as a new field in the attribute table (through the function "Add field"), before being calculated by a "Calculate field" function. The first operation executed is the separation of the group of centralized loads from the individual loads. Combining the function "Aggregate Points" with a "Buffer" of 50 meters, a polygon representing the area surrounding the centralized loads is created. Using this area to "clip" the central line, the portion of line required by the mini-grid can be extracted. In other words, once is selected the area of interest of the mini-grid, all the unnecessary line sections are eliminated. The same area can be used to isolate the group of individual loads from the total point feature class, using the function "Erase". Being excluded from the centralized system means that each of this load is supposed to be fed by an individual power plant (in this case, a stand-alone PV system). By applying "Extract Multi Values to Points" to the radiation raster, every building is associated to the value of solar radiation it annually receives.

At this point the LEC calculation for the individual case can be performed. The centralized system requires some extra step before the LEC calculation. First of all, the total grid length has to be calculated. It can be obtained by summing the central line length (calculated through the function "Add geometry"), the connection between the power plant and the central line and the sum of every connection between the loads and the central line. The second factor is calculated by the function "Near" which allows to obtain the shortest distance between points (the loads) and another feature (the central line). The third factor is obtained in form of raster by the function "Path Distance" which calculates, for each cell, the least accumulative distance from the selected source (the central line). The shortest path takes into account the altitude variations, thanks to the information provided by the DEM of the study area, which also defines the cell size and the edges of the resulting raster.

As previously discussed, the site of the centralized plant is left undefined in order to provide an extra hint for evaluation to the result. For this reason, the calculated distance has a fluctuating and spatially distributed value. The issue was to add the fixed value calculated by the sum of the first two factors to the raster obtained, cell by cell. A solution was found by combining the following sequence of function: "Feature to raster"+"Int"+ "Expand"+ "Raster calculator". Basically, this sequence allows to select the value of the desired field from point feature class and create a grid with that constant value for each pixel. Once converted the value in form of raster, it is ready to be used in raster calculations to obtain the line cost.

The PV centralized subsystem cost can be calculated in a raster form, avoiding the "extraction to points" feature which was necessary in the individual case.

All the other parameters required by the centralized LEC model are calculated as new attribute fields of the respective loads point features, similarly to the previous procedure. The important difference is that the calculations refer to the energy demand and the contracted power of the aggregated loads, obtained using "Summary Statistics" and added to the attribute table through "Join Field". The sum of all the subsystem costs per kWh is equal to the partial value of the LEC, that is the levelized cost of the centralized system without considering the PV modules and the line costs. Finally, the partial LEC value is converted in raster form (with the same procedure described earlier) and summed to the line and the PV modules subsystem costs, obtaining the total LEC for a centralized system.

In figure 3.2, the chart of the entire model as it stands in Model Builder format. In blue the input files, in yellow the ArcMap tool functions, in green the intermediate parameters, in red the relevant outputs.

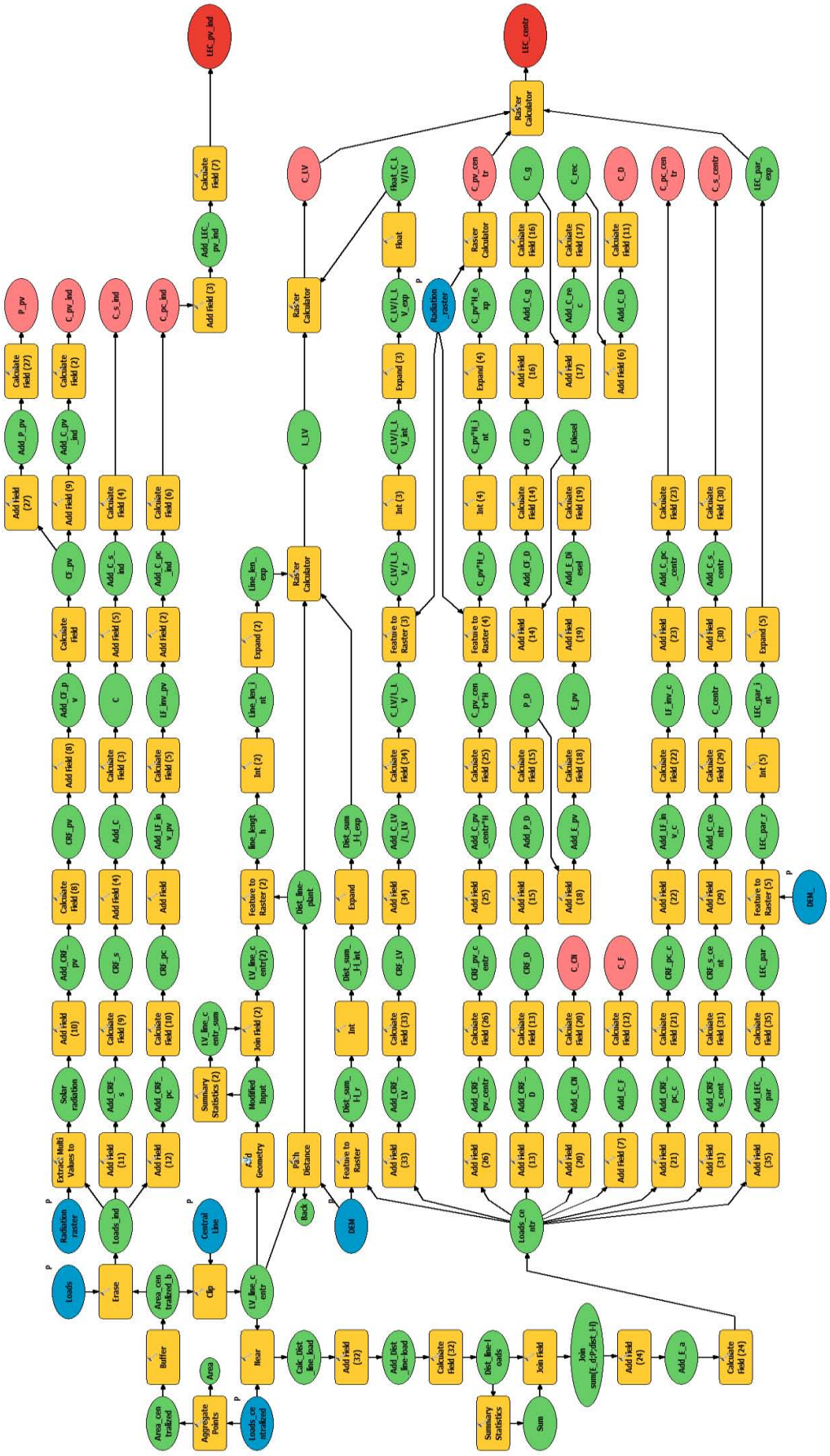

Figure 3.2: Chart of the new LEC model developed in ArcGIS environment

4 LEC calculation: the case of Guasasa

The LEC model has been tested for the case of Guasasa, a small isolated municipality of Ciego de Ávila in the southern coast of Matanzas province (Cuba).
As previously discussed in the introduction chapter, the electrification plan of the village is part of HIBRI2 project. Thanks to several researches carried out by partners institutions, a good baseline of knowledge is available. The results of this study are not meant to be a guideline for the specific project of Guasasa, which has already passed the preliminary phase and is now heading towards the purchase of the components. The model execution should be seen with a broader educational perspective, with the aim of proposing an approach replicable for any other case study.

The community is currently supplied for 12 hours a day by a diesel generator set. HIBRI2 project has the target of providing 24 hours of electricity through the integration of renewable energy sources in a hybrid system.

4.1 Components

Cubaenergía proposed the design of a micro-grid composed by the combination of (Cubaenergía, 2020):

- Diesel generator set (80 kW);
- Photovoltaic system (40 kW_p);
- Biomass gasification plant (10 kW);
- Aerogenerator (5 kW nominal at 12 m/s);

A set of bidirectional inverters with a three-phase power of approximately 60 kW and a 48 V battery with a storage capacity of 3257 Ah are needed. The daily estimated production by solar panels is 200 kWh, while the biomass plant would operate for 8 hours a day with a total daily production of about 80 kWh. The diesel generator is the current power source with a daily production of 265 kWh. Due to lack of data about the available wind source, the aerogenerator energy production is not accounted in the total estimation. With these conditions, the daily planned energy production would be of 545 kWh, so with a 25% of reserve respect the total estimated energy demand, equal to 437 kWh. The daily diesel generation could be reduced to 157 kWh to meet the demand, with a 60% decrease.

The components specification of the original project will be presented in the next paragraph and used as a reference for the techno-economic input assumptions of the LEC model. The biomass gasifier and the aerogenerator will be omitted since such technologies are not included in the model.

4.1.1 Diesel generator set

The diesel generator set is currently operative. With a power capacity of 80 kW and a reactive power of 100 kVA, it results to be overdimensioned for the actual maximum power consumption of the community (Caballero, 2019).

The license plate specifications are reported in the table 4.1:

Engine-drive AC Generator DENYO	
Model	DCA-100 ESI
Brushless AC Generator	
Model	DB-1101L
Phases	3
Wires	4
Rated Output	100 kVA
Rated Voltage	220 V
Rated Current	262 A
Frequency	60 Hz
Rating	Continuous
Power Factor	0.8
Poles	4
Engine	
Model	DB-6BG1T
Rated Output	91.3 kW – 1800 rpm
Piston displacement	6494 l
Fuel	Diesel

Table 4.1: License plate of the diesel generator set currently operating in Guasasa (Ciemat, 2020).

Figure 4.1 (left): The Engine-drive AC generator operating in Guasasa; Figure 4.2 (right): Diesel tank of the generator set in Guasasa (Ciemat, 2020).

4.1.2 PV solar panels

The proposed requirements for the photovoltaic installation include monocrystalline modules PERC, 18 % of minimum efficiency, with a minimum power of 300 W_p for a total of 40 kW_p connected to the grid.

A module that satisfies the requirements was chosen:

PV module Canadian Solar	
Model	SuperPower CS6K-295MS
Type	Monocrystalline
Temperature coefficient	-0.39 %/℃
Operating temperature	45 ℃
Efficiency	18.02 %
Global efficiency	80 %
Lifetime	25 years

Table 4.2: Technical specifications of the solar panel proposed for the project, meeting the requirements proposed by Cubenergía (Caballero, 2019).

4.1.3 Energy Storage System

The storage system proposed requires a total available capacity of 110 kWh and includes battery banks with a voltage of 48 V. A series of 6 battery banks with 8 batteries per bank with the following characteristics was chosen:

BAE Solar Battery	
Model	Secura PVS BLOCK
Type	Lead-Acid
Voltage	6 V
Nominal Capacity	2.17 kWh
Maximum Capacity	362 Ah
Capacity Ratio	0.36
Maximum Charge	55.8 A
Maximum Discharge	522 A
DoD	70 %
Efficiency	85 %
Lifetime	18 years

Table 4.3: Technical specifications of the battery model proposed for the project, meeting the requirements proposed by Cubaenergía (Caballero, 2019).

4.1.4 Power Conditioning System

A set of bidirectional inverters for the functioning in a micro-grid is needed. Cubaenergía has planned the installation of a Multicluster Box for the power conditioning of the hybrid system, together with the photovoltaic inverter and the bidirectional inverter of the battery. The

multicluster system is a three-phase AC distribution centre. The three-phase power is 60 kW approximately. The bidirectional inverter of the storage system controls the voltage and the frequency of the grid and manages the surplus energy produced to charge the batteries.
The following components have been proposed:

Multicluster Box SMA	
Model	Multicluster Box 12
Voltage	Three-phase 127/220 V
Frequency	60 Hz
PV Inverter SMA	
Model	Sunny Tripower 15000TL/20000TL/25000TL
Bidirectional Inverter Sunny Island	
Model	8.0H
Output Voltage	120 V
Frequency	60 Hz
Power Conditioning System	
Efficiency	95 %
Lifetime	15 years

Table 4.4: Technical specifications of the power conditioning components proposed for the project by Cubaenergía (Cubaenergía, 2020).

4.1.5 Grid

Guasasa is currently interconnected by a low voltage mini-grid, isolated from the national transmission line. The main characteristics of the line are reported in the following table:

Low Voltage Line	
Voltage	127/220 V (±10%)
Frequency	60 Hz (±0.6 Hz)
Type	Three-phase (3F+N) Single-phase

Table 4.5: Characteristic of the grid of Guasasa (Cubaenergía, 2020).

Figure 4.3 (left): Photo of the three-phase grid in Guasasa; Figure 4.4 (right): Photo of a single-phase line in Guasasa (Ciemat, 2020)

4.2 Energy demand

The population of Guasasa counts 214 inhabitants, distributed in 85 houses. All the buildings of the community are reported in the following table:

Building	n
House	85
Medical center	1
Pharmacy	1
School	1
Cellar	1
Canteen	1
Refrigerator	1
Video room	1
Social center	1
Water pump	1

Table 4.6: Buildings in Guasasa. Type and correspondent quantity (Caballero, 2019).

Cubaenergía studied the evolution of the daily energy demand using network analyzers for a week.

The current energy supply is limited to 12 hours a day divided into two periods: from 9 a.m. to 12 a.m. and from 3 p.m. to 12 p.m. Since the target of Hibridus project is to achieve 24 hours a day of energy supply, the load of the remaining hours has been estimated. A constant demand was considered from 1 a.m. to 6 p.m., while from 1 p.m. to 3 p.m. and from 6 a.m. to 9 a.m. a linear growth was estimated. The resulting demand curve is therefore a combination of the average measurements and estimations for the uncovered periods.

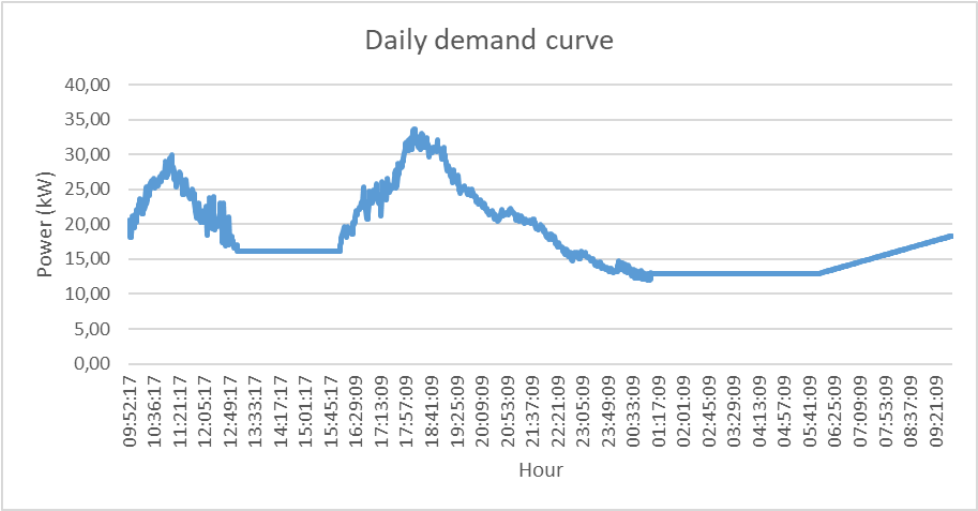

Figure 4.5: Daily demand curve of Guasasa obtained from network analysis (Cubaenergía, 2020)

In table 4.7, the main results derived from the network analysis.

Demand characterization			
Energy [kWh]		Power [kW]	
Actual (12 h)	265	Minimum	12
Total estimated	437	Peak	34

Table 4.7: Results of the energy demand analysis of the community of Guasasa (Cubaenergía, 2020).

It is possible to calculate the average energy demand by extracting information from the daily energy demand curve, hour by hour.

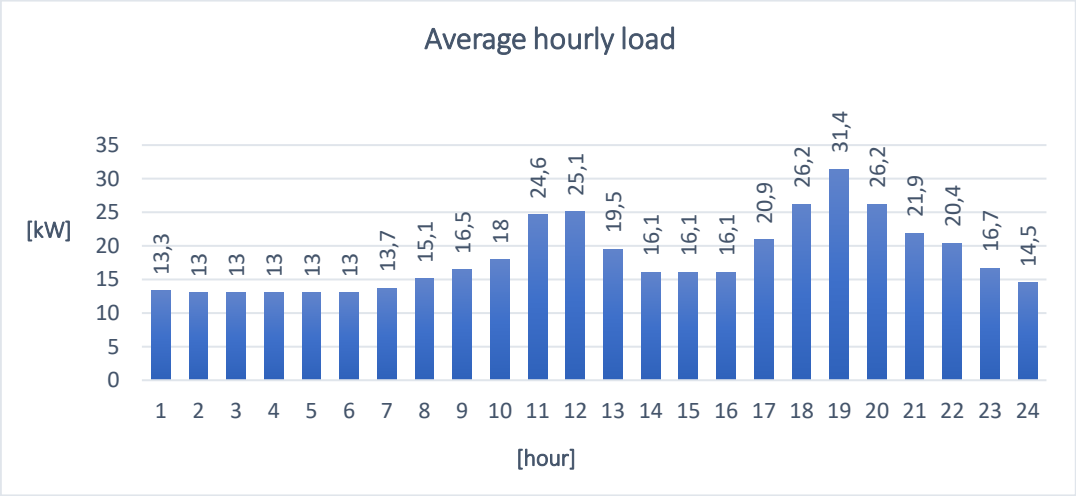

Table 4.8: Average hourly energy load for the community of Guasasa (Own elaboration).

Some useful parameters can be derived from this study. Knowing the value of the peak load (P_{peak}=34 kW) and calculating the average daily load ($\bar{P}$=18.2 kW), the load factor (f_l) can be calculated (equation 3.12):

$$f_l = \frac{\bar{P}}{P_{peak}} = \frac{18.2}{34} = 0.53$$

4.2.1 Allocation

One of the advantages of using GIS technologies in electrification planning is the possibility to consider the effect of spatial variability of the energy demand.

Especially for the comparison of individual cases or different groups of mini-grids, the distribution of the right amount of energy demand to each single load can have a significant effect on techno-economical assessments. In the study case, the only available information about the specific type of loads is the power of the public water pump ($P_{pump} = 2.5\ \text{kW}$), located in the northern part of the community.

Figure 4.6: Zoom on the satellite view of the areas of Guasasa characterized by different type of buildings (Source: Google Maps; Own elaboration)

All the other types of loads have been differentiated by distributing the total energy demand and the peak load. In this process, different weights have been assigned depending on the common usage of each type of facility.

The estimated peak load is 34 kW and refers to the aggregated peak load ($P_{peak,aggr}$) of the cummunity. By assigning a proper coincidence factor (f_c) (Benato & Fellin, 2011) we can calculate the total P_{peak} that is the sum of the individual peak loads ($P_{peak,i}$) and then allocate the peak power power of every facility.

$$P_{peak,tot} = \sum_i P_{peak,i} = \frac{P_{peak,aggr}}{f_c} = \frac{34}{0.4} = 85\ \text{kW}$$

Knowing the total daily energy demand and the sum of the peak load of each single facility, it is possible to complete the demand allocation, as reported in the table below.

Building	n	$E_{d,i}$ [kWh/day]	$E_{d,tot}$ [kWh/day]	$P_{peak,i}$ [kW]	$P_{peak,tot,i}$ [kW]	f_c	$P_{peak,aggr}$ [kW]
House	85	4.5	383.2	0.9	75.8	0.4	34
Medical center	1	4.5	4.5	0.9	0.9		
Pharmacy	1	2.3	2.3	0.4	0.4		
School	1	4.5	4.5	0.9	0.9		
Cellar	1	4.5	4.5	0.9	0.9		
Canteen	1	4.5	4.5	0.9	0.9		
Refrigerator	1	6.8	6.8	1.3	1.3		
Video room	1	2.3	2.3	0.4	0.4		
Social center	1	4.5	4.5	0.9	0.9		
Water pump	1	20.0	20.0	2.5	2.5		
Total	94		437.0		85.0		

Table 4.9: Daily energy demand and peak power allocation between the different types of facilities in Guasasa (Own elaboration).

4.3 Input assumptions

All the techno-economic assumptions have been defined according to previous studies performed in the context of the project HIBRI2 and other projects with similar analysis, technological state and experimental values.

An important economic index required by the model is the discount rate k, from which the capital recovery factor is derived (equation 3.1). The discount rate is commonly used in discounted cash flow analysis to estimate the value of an investment by the actualization of future expected cash flows. For the project, a nominal discount rate of 8.9% is detected (Caballero, 2019). Since an increase is expected in Cuba during the period 2016 - 2033 (Mesa, 2019), the present study considers a value of 10% for the nominal discount rate (k_n). However, the parameter used for the LEC assessment is the real discount rate (k_r), obtainable from k_n and the inflation rate (i) (Homer Pro 3.13):

$$k_r = \frac{k_n - i}{1 + i} \tag{3.36}$$

The resulting value is a real discount rate of 7 %.

ECONOMIC INDEXES	
Nominal Discount Rate	10 %
Inflation Rate	2.8 %
Real Discount Rate	7 %

Table 4.10: Indexes used for the economic assessment of the project in Guasasa.

All the cost assumptions have been converted from United States Dollars to Euros by a conversion rate of : $/€=0.89
Such value refers to the average conversion rate during 2019, according to the European Central Bank (ECB, 2020).

4.3.1 Photovoltaic modules

The capital expenditure for the solar modules estimated for the project HIBRI2 is equal to 1750 $/kW (Caballero, 2019). Since the project refers to a centralized power plant, a higher specific cost is expected for the case of individual stand-alone modules. The reason of this difference is attributed to economies of scale. NREL[17] proposes the following module prices valid for the USA, distinguishing between residential and commercial scale (NREL, 2019):

- Overnight capital cost for residential scale (<10 kW): 2511 $/kW;
- Overnight capital cost for commercial scale (>10 kW): 1601$/kW.

It is reasonable to consider the same proportion between residential and commercial scale to calculate the capital cost of a stand-alone module in Guasasa, obtaining the following result: 1750 ($/kW). Hence, the Investment costs considered for the execution of the model are:

- Stand-alone system investment cost: 2745 $/kW = 2443 €/kW;
- Centralized system investment cost: 1750 $/kW = 1557.5 €/kW.

For the annual Operation & Maintenance costs, the same source was considered (NREL, 2019):

- Stand-alone system O&M costs: 20 $/kW=17.8 €/kW ;
- Centralized system O&M costs: 16 $/kW= 14.2 €/kW.

The remaining technical parameters are taken from table 4.2. A lower global efficiency is considered for the stand-alone PV system:

- Stand-alone system efficiency: $\eta_{pv} = 65\%$;
- Centralized system efficiency: $\eta_{pv,centr} = 80\%$.

[17] National Renewable Energy Laboratory.

The input settings related to the solar systems are listed in the following tables.

n_{pv}	I_{pv} [€/kW$_p$]	OM_{pv}[€/kW$_p$]	η_{pv}
25	2443	18	65%

Table 4.11: Input settings for a PV stand-alone system.

$n_{pv,centr}$	$I_{pv,centr}$ [€/kW$_p$]	$OM_{pv,centr}$[€/kW$_p$]	$\eta_{pv,centr}$
25	1558	14	80%

Table 4.12: Input settings for a PV centralized system

4.3.2 Diesel

IRENA[18] proposes the following range for the price of a diesel generation set (IRENA, 2016): 200 €/kW<I_D<600 €/kW. As an average value in the suggested range, the capital expenditure considered for the case study of Guasasa is: I_D=400 €/kW.

For the cost of Operation & Maintenance, a value of 0.02 euros for each hour of operation and per units of power size of the diesel generator is chosen: OM_D=0.02 \$/($h_{operation}$·kW) (Caballero, 2019).

Due to shortage of supply for the isolated location, the diesel price is particularly high: 2 CUP/l, equal to 2 \$/l (Caballero, 2019). From the consumption analysis of the actual generator set, a value of 0.4 l/kWh is detected for the fuel consumption (Caballero, 2019).

- Fuel price: F_p= 2 \$/l = 1.78 €/l;
- Fuel consumption: CO_F= 0.4 l/kWh.

As design factor of the electric machine, a higher value than the coincidence factor of the loads is taken, for reasons of security margin:

- Design factor: f_d=0.77.

The expected lifetime is 20 years (n_D =20), while major maintenances is estimated to be needed every 5 years (n_r =5).

The input settings related to the diesel generator set are listed in the following table.

n_D	n_{rec}	I_D [€/kW]	OM_D [€/(h_{op}·kW)]	f_d
20	5	400	0.02	0.77

F_p [€/l]	CO_F [l/kWh]
1.78	0.40

Table 4.13: Input settings for the diesel generator set.

[18] International Renewable Energy Agency

4.3.3 Storage

The reference cost considered for the storage system in Guasasa is 3500 $ per bank of batteries (Caballero, 2019). Each bank is composed by 8 batteries of 2.17 kWh of nonimal capacity each. So the investment cost per units of capacity is equal to: I_s=201.6 $/kWh=179.4 €/kWh.

The annual Operation & Maintenance costs considered are 80 $ per bank of batteries (Caballero, 2019). Repeating the calculation, the cost per kWh can be obtained: OM_s=4.6 $/kWh=4.1 €/kWh.

For the photovoltaic systems, the days of autonomy should be enough to guarantee the desired reliability, covering the maximum estimated strings of consecutive non-solar days. A value of 3 days is used both for the individual and the centralized case. For a hybrid system, the reliability is guaranteed by the diesel generator, so the storage system capacity can be lower. Two hybrid configurations will be tested in the next paragraph, different for percentage of renewable fraction. For the hybrid system with 50% of renewable fraction, 1 day of battery autonomy is considered sufficient. For the hybrid system with 75% of renewable fraction, the intervention of the diesel generator needs to be limited, so 2 days of battery autonomy are set. Due to the modular nature of batteries, no distinctions are considered between the costs of individual and centralized systems. The remaining technical parameters are taken from table 4.3.
The input settings related to storage system are listed in the following tables:

n_s	I_s[€/kWh]	OM_s[€/kWh]	η_s	d [days]	DoD
18	180	4	85%	3	70%

Table 4.14: : Input settings for the energy storage of the solar systems.

$n_{s,centr}$	$I_{s,centr}$ [€/kWh]	$OM_{s,centr}$[€/kWh]	$\eta_{s,centr}$	d_{centr} [days]	DoD_{centr}
18	180	4	85%	2	70%

Table 4.15: : Input settings for the energy storage of the hybrid systems with 75% of renewable fraction.

$n_{s,centr}$	$I_{s,centr}$ [€/kWh]	$OM_{s,centr}$[€/kWh]	$\eta_{s,centr}$	d_{centr} [days]	DoD_{centr}
18	180	4	85%	1	70%

Table 4.16: : Input settings for the energy storage of the hybrid systems with 50% of renewable fraction.

4.3.4 Power Conditioning

For the power conditioning, the same investment cost is associated for the individual and the centralized case. However, the greater complexity of the centralized system is weighted thanks to the correction factor present in equation 3.23:

$I_{pc,ind}$=$I_{pc,centr}$: 300 $/kW=267 €/kW (Caballero, 2019).

No Operation & Maintenance costs are considered. The remaining technical parameters are taken from table 4.4.

The input settings related to storage system are listed in the following tables:

$n_{pc,ind}$	$I_{pc,ind}$ [€/kW]	$OM_{pc,ind}$[€/kW]	$\eta_{inv,pv}$
15	267	0	95%

Table 4.17: Input settings for the power conditioning of an individual system.

$n_{pc,centr}$	$I_{pc,centr}$ [€/kW]	$OM_{pc,centr}$[€/kW]	$\eta_{pc,centr}$
15	267	0	95%

Table 4.18: Table 4.19: : Input settings for the power conditioning of a centralized system.

4.3.5 Grid

The grid actually operating in Guasasa is a low voltage system. For the hypothetical condition of complete electrification, only the low voltage line investment is implemented in the model, considering the small distances to be covered.

Louie proposes the following range of construction costs for a low voltage line in isolated areas: 10000 \$/km<I_{LV}<18000 \$/km (Louie, 2018). The line costs per unit of distance tends to increase for smaller grids, due to the effect of fixed costs, so the highest value of the range suggested is considered: I_{LV}=18000 \$/km=16000 €/km.

The annual O&M costs are assumed as 1% of the capital cost: OM_{LV}=160 €/km.

As costs of connection, a value of 100 €/kW is defined.

The expected lifetime is 30 years.

The input settings related to the grid are listed in the following table:

n_{LV}	I_{LV}[€/km]	OM_{LV}[€/km]	I_{CN}[€/kW]
30	16000	160	100

Table 4.20: : Input settings for the distribution line and connection system

4.4 Model test

Once defined all the inputs, the model can be tested.
Five layers of GIS data are required, as introduced in chapter 3.2:

- Point layer of the whole community. Each point represents a building and is characterized by an attribute table reporting all the techno-economic assumption and the load energy demand previously discussed;
- Point layer of the group of loads to be centralized in a mini-grid. It is obtained as a selection of the total point layer, so it is characterized by the same attribute table;
- Line layer of the central distribution line supposed for the ideal case of complete electrification needed;
- Digital Surface Model of the terrain of Guasasa, extracted from the DSM used in chapter 2, with a resolution of 30x30 meters (figure 2.6);
- Global solar radiation raster on optimal angle tilted surface, with a high spatial resolution (30x30 m), obtained in paragraph 2.4.3.

The type of configuration is determined by the group of loads selection in the second point layer. In general, three cases can be simulated:

- All the loads selected: centralized system to feed the whole community;
- No selection: all the loads supplied by stand-alone PV systems;
- A group of loads selected: centralized system to feed the mini-grid, while the remaining loads supplied by stand-alone PV systems.

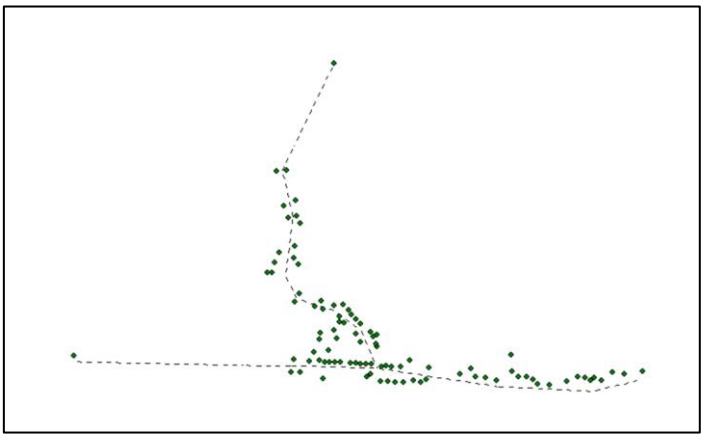

Figure 4.7: Point layer of the buildings in Guasasa (in green) and line layer of the central distribution line (dotted). (ArcGIS, own elaboration).

Introducing the group of centralized loads points, the model automatically selects the area in their surrounding and properly extract the portion of distribution line needed by the mini-grid.

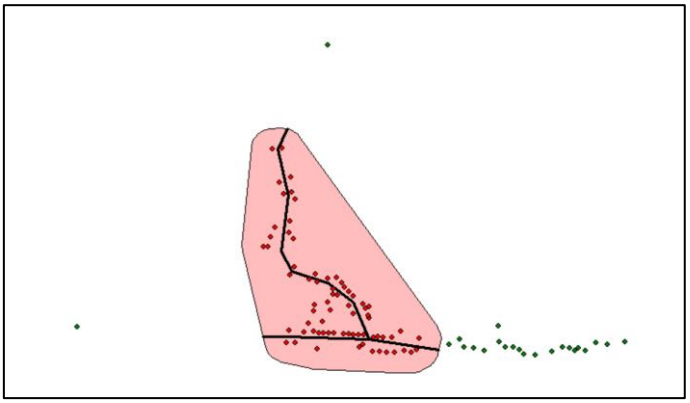

Figure 4.8: Point layer of the group of building to be centralized (in red) and portion of distribution line needed by the mini grid (in black). Also in red, the area used to extract the portion of line from the total (ArcGIS, own elaboration).

Three different conditions will be considered in the model execution:

1) Total case: a complete electrification is needed. The ideal starting point considered is a total absence of power generation and distribution facilities;
2) Partial case: same hypothetical condition of the first case but a combination of the centralized and the individual solution is considered (stand-alone + centralized);
3) Real case: The starting point considered is the actual level of electrification in Guasasa and the actual facilities are kept.

For each of the three conditions, all the available types of power plant implemented will be investigated, always assuming the target of 24 h/day of energy supply for the whole community. Note that a specific location in the map is considered for the numerical results reported in the following chapter. For the case of the centralized systems it corresponds to the planned project site of HIBRI2, visible in figure 4.6. Anyway, information about the resulting LEC of a power plant located in any other area is provided by a graphical representation. Similarly, to simplify the review, the numerical results of only one building is considered for the individual systems. The choice falls on the isolated house in the extreme south east of the village.

In the results visualization, the weight of each subsystem in to the total cost per kWh is displayed in different colors. The category "Grid" includes the sum of the line and the connection costs.

4.4.1 PV stand-alone

The first run is related to a stand-alone photovoltaic system for every building. All the input settings are reported in the table below:

n_{pv}	I_{pv} [€/kW]	OM_{pv} [€/kW]	η_{pv}	n_s	I_s [€/kWh]	OM_s [€/kWh]	η_S	d [days]	DoD	$n_{pc,ind}$	$I_{pc,ind}$ [€/kW]	$OM_{pc,ind}$ [€/kW]	$\eta_{inv,pv}$
25	2443	18	65%	18	180	4	85%	3	70%	15	267	0	95%

Table 4.21: Input settings of the LEC model for a PV stand-alone system.

The calculation for the chosen reference house produced the following results:

C_D [€cents/kWh]	C_F [€cents/kWh]	C_{PV} [€cents/kWh]	C_s [€cents/kWh]	C_{pc} [€cents/kWh]	C_{LV} [€cents/kWh]	C_{CN} [€cents/kWh]
-	-	4.3	13.9	2.8	-	-
E_{Diesel} [kWh/year]	P_{Diesel} [kW]	CF_{Diesel}	E_{PV} [kWh/year]	P_{PV} [kW]	CF_{pv}	LEC_{pv} [€cents/kWh]
-	-	-	1642.5	1.1	16.5%.	21.0

Table 4.22: Results of the calculation for a PV stand-alone system referred to a single house.

A LEC of 21 €cents/kWh was obtained. As can be noticed by the diagram of the cost contributions, the storage system results the subsystem that affects the most the total costs.

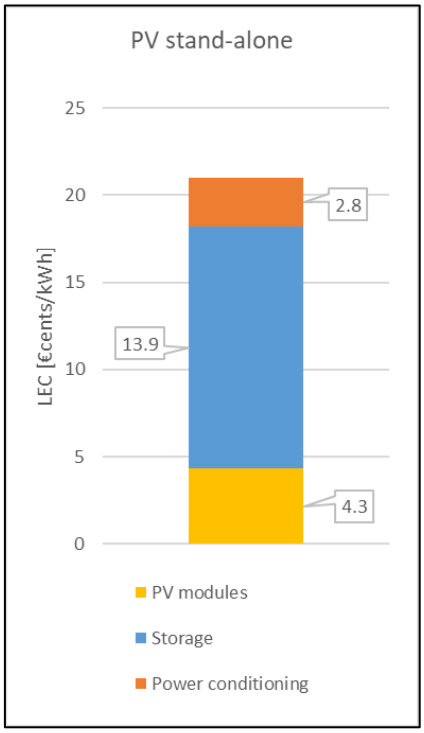

Figure 4.9: Cost contribution of each subsystem to the total LEC of a PV stand-alone system in Guasasa.

The power capacity required by each building mainly depends on the allocation of the energy demand (made in paragraph 4.2.1) and has the following distribution in the community:

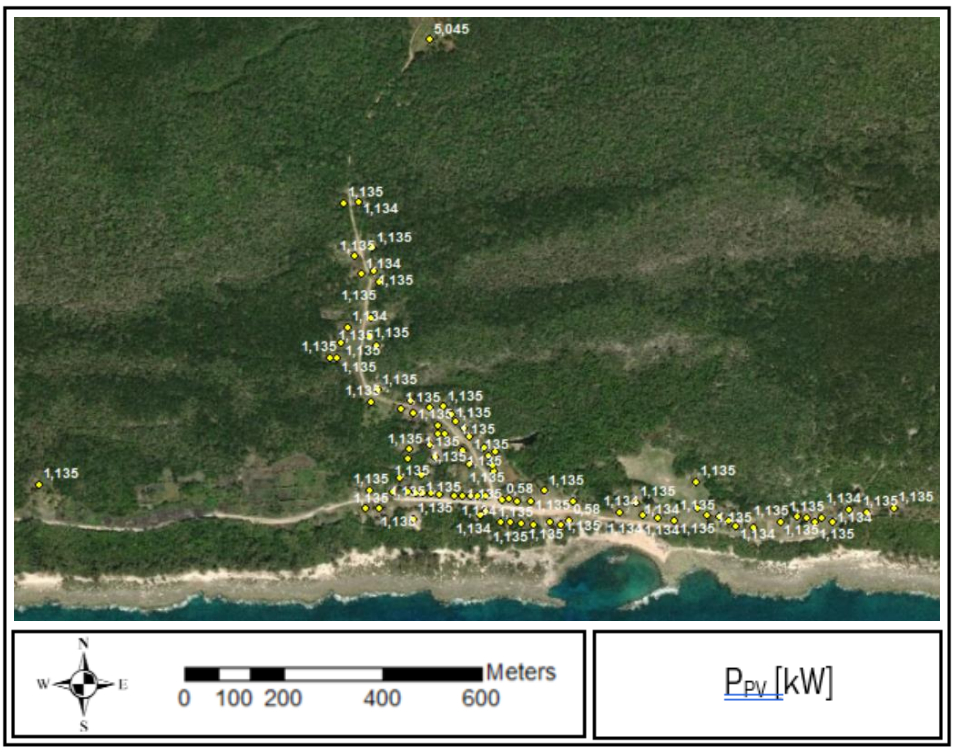

Map 4.1: Installed power capacity required by each building of Guasasa, referred to a PV stand-alone system.

The capacity factor calculated for each PV system is reported in the following map:

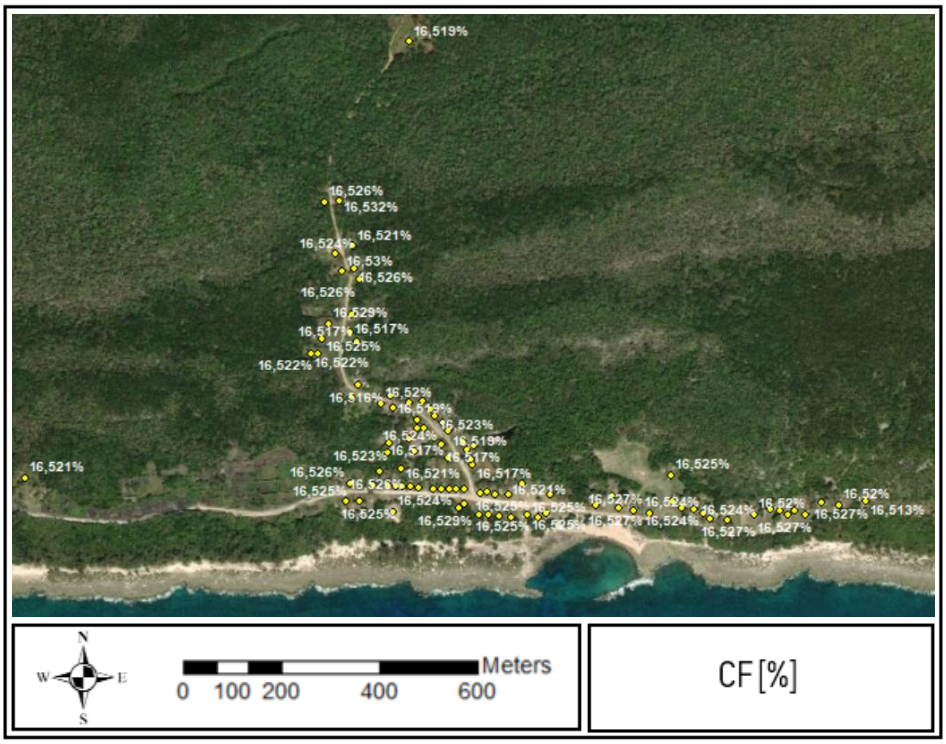

Map 4.2: Capacity factor of the PV stand-alone systems required to feed each energy load of Guasasa.

The incoming solar radiation is very uniform along the whole study area, due to morphological characteristics (substantially flat) and the absence of shading obstacles.
As a consequence, both the capacity factor and the LEC obtained for each individual power plant have a homogeneous distribution.

In the map below, the LEC obtained for a PV stand-alone system installed to supply the demand of each building of the community.

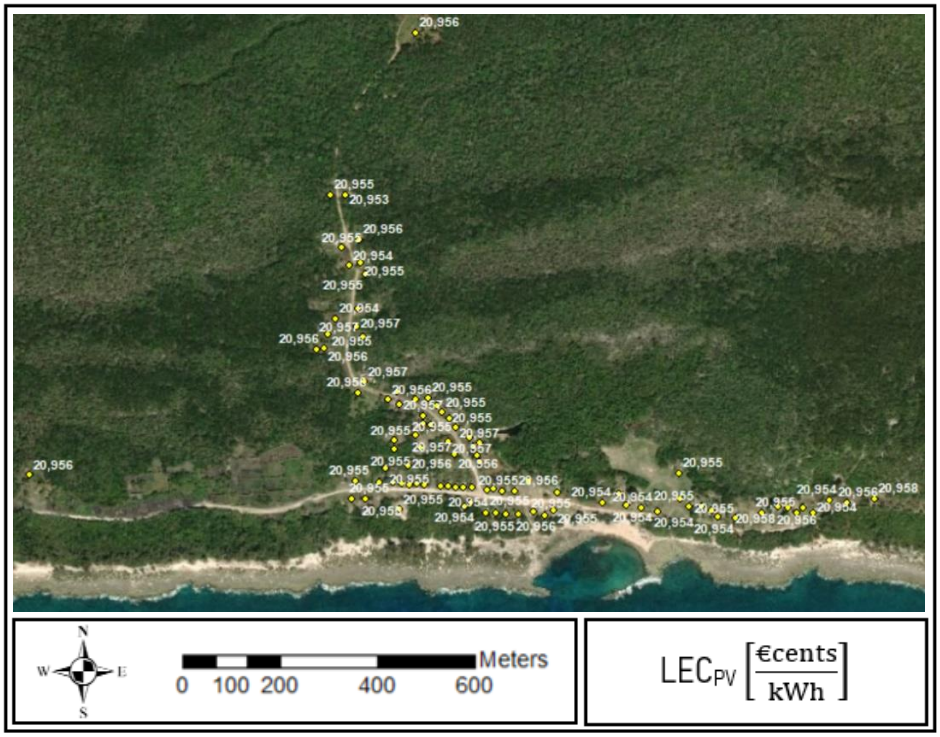

Map 4.3: LEC of the PV stand-alone systems required to feed each energy load of Guasasa.

As can be noticed, the variation between different values is negligible, but it is present. It means that in a condition of higher spatial fluctuation of the available resource, the differences would be more evident and would provide more useful information to the user.

4.4.2 PV centralized

The model execution for the centralized cases includes three runs, corresponding to the three cases previously introduced. Between the first case (total) and the second case (partial) the inputs related to the centralized PV system are the same because they both refers to a condition of absence of any electrification equipment as starting point. However, the partial case also requires the introduction of the inputs for the stand-alone systems, since the group of loads excluded by the centralization performs simultaneously the individual LEC calculation.

The third case refers to the real case, where the distribution system is already operative. So the investment costs for the low voltage line and the connection costs are null.

A summary of the input settings for the three runs referred to a PV centralized system is reported in the following tables.

1) Total case:

$n_{pv,centr}$	$l_{pv,centr}$ [€/kW]	$OM_{pv,centr}$ [€/kW]	$\eta_{pv,centr}$	$n_{s,centr}$	$l_{s,centr}$ [€/kWh]	$OM_{s,centr}$ [€/kWh]	$\eta_{s,centr}$	d_{centr} [days]	DoD_{centr}	$n_{pc,centr}$	$l_{pc,centr}$ [€/kW]	$OM_{pc,centr}$ [€/kW]	$\eta_{pc,centr}$
25	1558	14	80%	18	180	4	85%	3	70%	15	267	0	95%
n_D	n_{rec}	l_D [€/kW]	OM_D [€/(h·kW)]	f_d	F_p [€/l]	CO_F [l/kWh]	n_{LV}	l_{LV} [€/km]	OM_{LV} [€/km]	l_{CN} [€/kW]	f_l	f_r	Type
-	-	-	-	-	-	-	30	16000	160	100	0.53	100%	PV

Table 4.23: Input settings of the LEC model for a PV centralized system including all the community (ideal case).

2) Partial case:

n_{pv}	l_{pv} [€/kW]	OM_{pv} [€/kW]	η_{pv}	n_s	l_s [€/kWh]	OM_s [€/kWh]	η_S	d [days]	DoD	$n_{pc,ind}$	$l_{pc,ind}$ [€/kW]	$OM_{pc,ind}$ [€/kW]	$\eta_{inv,pv}$
25	2443	18	65%	18	180	4	85%	3	70%	15	267	0	95%
$n_{pv,centr}$	$l_{pv,centr}$ [€/kW]	$OM_{pv,centr}$ [€/kW]	$\eta_{pv,centr}$	$n_{s,centr}$	$l_{s,centr}$ [€/kWh]	$OM_{s,centr}$ [€/kWh]	$\eta_{s,centr}$	d_{centr} [days]	DoD_{centr}	$n_{pc,centr}$	$l_{pc,centr}$ [€/kW]	$OM_{pc,centr}$ [€/kW]	$\eta_{pc,centr}$
25	1558	14	80%	18	180	4	85%	3	70%	15	267	0	95%
n_D	n_{rec}	l_D [€/kW]	OM_D [€/(h·kW)]	f_d	F_p [€/l]	CO_F [l/kWh]	n_{LV}	l_{LV} [€/km]	OM_{LV} [€/km]	l_{CN} [€/kW]	f_l	f_r	Type
-	-	-	-	-	-	-	30	16000	160	100	0.53	100%	PV

Table 4.24: Input settings of the LEC model for a PV centralized system with partial centralization (ideal case).

3) Real case:

$n_{pv,centr}$	$l_{pv,centr}$ [€/kW]	$OM_{pv,centr}$ [€/kW]	$\eta_{pv,centr}$	$n_{s,centr}$	$l_{s,centr}$ [€/kWh]	$OM_{s,centr}$ [€/kWh]	$\eta_{s,centr}$	d_{centr} [days]	DoD_{centr}	$n_{pc,centr}$	$l_{pc,centr}$ [€/kW]	$OM_{pc,centr}$ [€/kW]	$\eta_{pc,centr}$
25	1558	14	80%	18	180	4	85%	3	70%	15	267	0	95%
n_D	n_{rec}	l_D [€/kW]	OM_D [€/(h·kW)]	f_d	F_p [€/l]	CO_F [l/kWh]	n_{LV}	l_{LV} [€/km]	OM_{LV} [€/km]	l_{CN} [€/kW]	f_l	f_r	Type
-	-	-	-	-	-	-	30	-	160	-	0.53	100%	PV

Table 4.25: Input settings of the LEC model for a PV centralized system including all the community in the real case.

The resulting LEC obtained for each case is respectively: 21.6 €cents/kWh, 21.4 €cents/kWh and 20.9 cents/kWh. The difference between total and partial centralization is determined by lower line costs which are not particularly relevant due to the limited dimensions of the area considered. Also, from the ideal to the real condition, the decrease is associated to lower line costs which in the real case derives just from operation and maintenance.The higher efficiency of the centralized system compared to the stand-alone case leads to a higher capacity factor, equal to 20.3%, compared to the 16.5% detected for the individual system.

A summary of the results of the model execution for the three cases is reported in the following tables:

1) Total case

C_D [€cents/kWh]	C_F [€cents/kWh]	C_{PV} [€cents/kWh]	C_s [€cents/kWh]	C_{pc} [€cents/kWh]	C_{LV} [€cents/kWh]	C_{CN} [€cents/kWh]
-	-	2.4	13.9	4.1	1.07	0.15
E_{Diesel} [kWh/year]	P_{Diesel} [kW]	CF_{Diesel}	E_{PV} [kWh/year]	P_{PV} [kW]	CF_{pv}	LEC_{centr} [€cents/kWh]
-	-	-	160928.5	90.4	20.3%.	21.6

Table 4.26: Results of the LEC model execution for a PV centralized system including all the community (ideal case).

2) Partial case:

C_D [€cents/kWh]	C_F [€cents/kWh]	C_{PV} [€cents/kWh]	C_s [€cents/kWh]	C_{pc} [€cents/kWh]	C_{LV} [€cents/kWh]	C_{CN} [€cents/kWh]
-	-	2.4	13.9	4.1	0.87	0.15
E_{Diesel} [kWh/year]	P_{Diesel} [kW]	CF_{Diesel}	E_{PV} [kWh/year]	P_{PV} [kW]	CF_{pv}	LEC_{centr} [€cents/kWh]
-	-	-	115851	65.1	20.3%.	21.4

Table 4.27: Results of the LEC model execution for a PV centralized system with partial centralization (ideal case).

3) Real case:

C_D [€cents/kWh]	C_F [€cents/kWh]	C_{PV} [€cents/kWh]	C_s [€cents/kWh]	C_{pc} [€cents/kWh]	C_{LV} [€cents/kWh]	C_{CN} [€cents/kWh]
-	-	2.4	13.9	4.1	0.48	-
E_{Diesel} [kWh/year]	P_{Diesel} [kW]	CF_{Diesel}	E_{PV} [kWh/year]	P_{PV} [kW]	CF_{pv}	LEC_{centr} [€cents/kWh]
-	-	-	115851	65.1	20.3%.	20.9

Table 4.28: Results of the LEC model execution for a PV centralized system including all the community in the real case.

In the following diagrams, the cost contribution of each subsystem in the three cases tested.

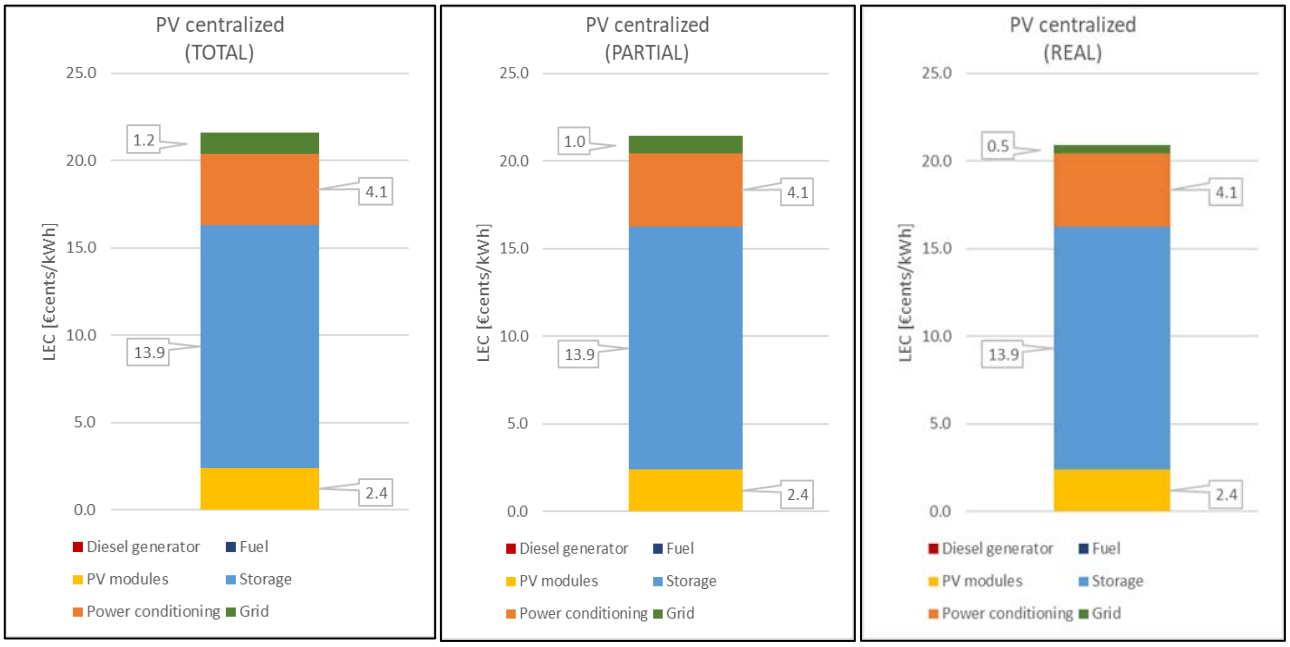

Figure 4.10: Cost contribution of each subsystem to the total LEC of a PV centralized system for the three cases tested.

In the maps below, the resulting raster representation of the LEC obtained for the three cases tested, in terms of location of the centralized system.

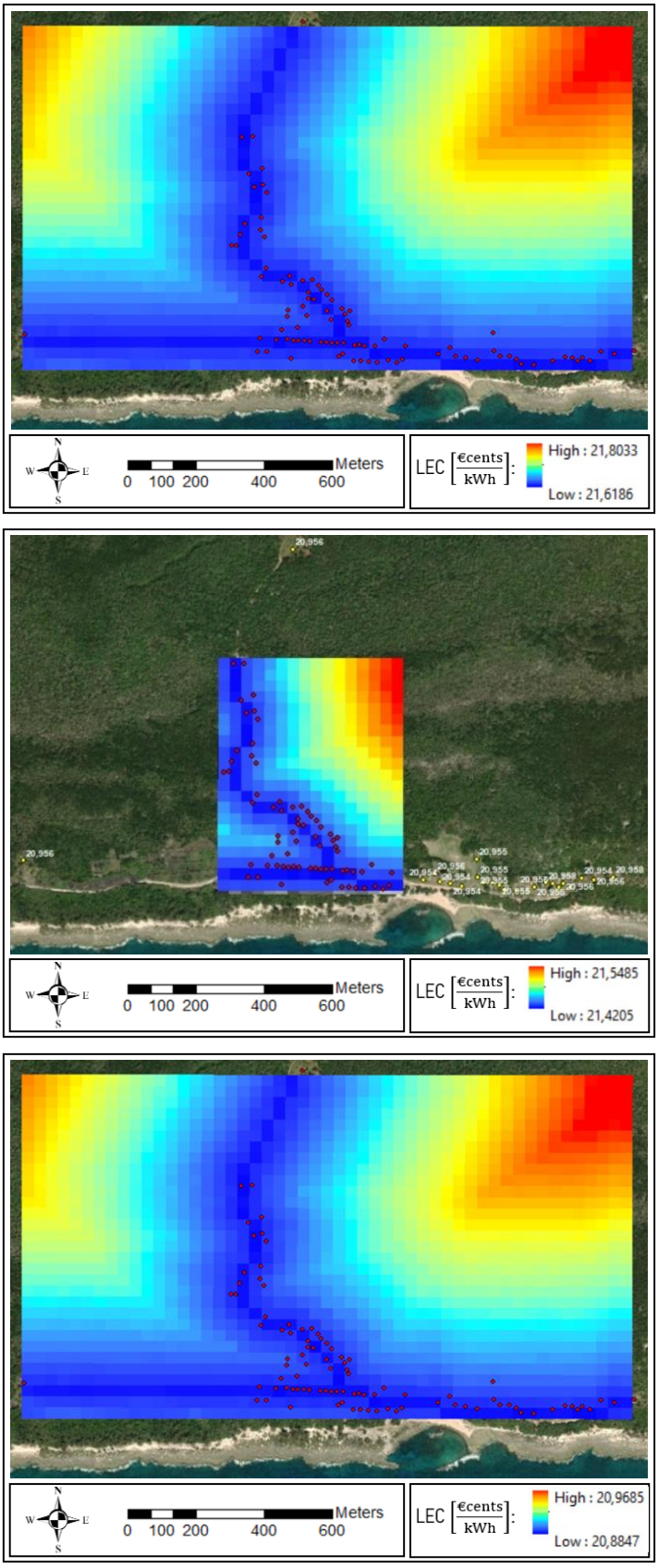

Map 4.4: LEC of a PV centralized system for the total case (up), for the partial case (middle) and the real case (down).

4.4.3 Hybrid Diesel-PV f_r 75%

The first hybrid Diesel-PV power plant considered has a renewable fraction of 75%.
The input settings follow the same conditions as the three previous cases, adding the parameters relative to the diesel generator and the fuel costs.
For the real case, no investment costs are defined for the diesel generator, which is currently operative in Guasasa.

A summary of the input settings for the three runs executed is reported in the following tables:

1) Total case

$n_{pv,centr}$	$I_{pv,centr}$ [€/kW]	$OM_{pv,centr}$ [€/kW]	$\eta_{pv,centr}$	$n_{s,centr}$	$I_{s,centr}$ [€/kWh]	$OM_{s,centr}$ [€/kWh]	$\eta_{s,centr}$	d_{centr} [days]	DoD_{centr}	$n_{pc,centr}$	$I_{pc,centr}$ [€/kW]	$OM_{pc,centr}$ [€/kW]	$\eta_{pc,centr}$
25	1558	14	80%	18	180	4	85%	2	70%	15	267	0	95%
n_D	n_{rec}	I_D [€/kW]	OM_D [€/(h·kW)]	f_d	F_p [€/l]	CO_F [l/kWh]	n_{LV}	I_{LV} [€/km]	OM_{LV} [€/km]	I_{CN} [€/kW]	f_l	f_r	Type
20	5	400	0.02	0.77	1.78	0.40	30	16000	160	100	0.53	75%	H

Table 4.29: Input settings of the LEC model for a diesel-PV (r.f.75%) system including all the community (ideal case).

2) Partial case:

n_{pv}	I_{pv} [€/kW]	OM_{pv} [€/kW]	η_{pv}	n_s	I_s [€/kWh]	OM_s [€/kWh]	η_s	d [days]	DoD	$n_{pc,ind}$	$I_{pc,ind}$ [€/kW]	$OM_{pc,ind}$ [€/kW]	$\eta_{inv,pv}$
25	2443	18	65%	18	180	4	85%	3	70%	15	267	0	95%
$n_{pv,centr}$	$I_{pv,centr}$ [€/kW]	$OM_{pv,centr}$ [€/kW]	$\eta_{pv,centr}$	$n_{s,centr}$	$I_{s,centr}$ [€/kWh]	$OM_{s,centr}$ [€/kWh]	$\eta_{s,centr}$	d_{centr} [days]	DoD_{centr}	$n_{pc,centr}$	$I_{pc,centr}$ [€/kW]	$OM_{pc,centr}$ [€/kW]	$\eta_{pc,centr}$
25	1558	14	80%	18	180	4	85%	2	70%	15	267	0	95%
n_D	n_{rec}	I_D [€/kW]	OM_D [€/(h·kW)]	f_d	F_p [€/l]	CO_F [l/kWh]	n_{LV}	I_{LV} [€/km]	OM_{LV} [€/km]	I_{CN} [€/kW]	f_l	f_r	Type
20	5	400	0.02	0.77	1.78	0.40	30	16000	160	100	0.53	75%	H

Table 4.30: Input settings of the LEC model for a diesel-PV (r.f..75%) system with partial centralization (ideal case).

3) Real case:

$n_{pv,centr}$	$I_{pv,centr}$ [€/kW]	$OM_{pv,centr}$ [€/kW]	$\eta_{pv,centr}$	$n_{s,centr}$	$I_{s,centr}$ [€/kWh]	$OM_{s,centr}$ [€/kWh]	$\eta_{s,centr}$	d_{centr} [days]	DoD_{centr}	$n_{pc,centr}$	$I_{pc,centr}$ [€/kW]	$OM_{pc,centr}$ [€/kW]	$\eta_{pc,centr}$
25	1558	14	80%	18	180	4	85%	2	70%	15	267	0	95%
n_D	n_{rec}	I_D [€/kW]	OM_D [€/(h·kW)]	f_d	F_p [€/l]	CO_F [l/kWh]	n_{LV}	I_{LV} [€/km]	OM_{LV} [€/km]	I_{CN} [€/kW]	f_l	f_r	Type
20	5	-	0.02	0.77	1.78	0.40	30	-	160	-	0.53	75%	H

Table 4.31: Input settings of the LEC model for a diesel-PV (r.f.75%) system including all the community in the real case.

The resulting LEC obtained for each case is respectively: 38.8 €cents/kWh, 38.6 €cents/kWh and 36.1 €cents/kWh. In addition to the decrease of the line costs, with the same trend presented in the previous paragraph, a reduction can be noticed in the diesel subsystem. Between the ideal cases and the real one, the costs associated to the diesel generator decrease, since in the last case only the operation and maintenance expenditures are considered.

A summary of the results of the model execution for the three cases is reported in the following tables:

1) Total case:

C_D [€cents/kWh]	C_F [€cents/kWh]	C_{PV} [€cents/kWh]	C_s [€cents/kWh]	C_{pc} [€cents/kWh]	C_{LV} [€cents/kWh]	C_{CN} [€cents/kWh]
4.0	17.8	2.4	9.3	4.1	1.07	0.15
E_{Diesel} [kWh/year]	P_{Diesel} [kW]	CF_{Diesel}	E_{PV} [kWh/year]	P_{PV} [kW]	CF_{PV}	LEC_{centr} [€cents/kWh]
40232.1	66.6	6.9%	120696.4	67.8	20.3%	38.8

Table 4.32: Results of the LEC model execution for a diesel-PV (r.f.75%) system feeding the whole community (ideal case).

2) Partial case:

C_D [€cents/kWh]	C_F [€cents/kWh]	C_{PV} [€cents/kWh]	C_s [€cents/kWh]	C_{pc} [€cents/kWh]	C_{LV} [€cents/kWh]	C_{CN} [€cents/kWh]
4.0	17.8	2.4	9.3	4.1	0.87	0.15
E_{Diesel} [kWh/year]	P_{Diesel} [kW]	CF_{Diesel}	E_{PV} [kWh/year]	P_{PV} [kW]	CF_{PV}	LEC_{centr} [€cents/kWh]
28962.8	48.7	6.8%	86888.25	48.8	20.3%	38.6

Table 4.33: Results of the LEC model execution for a diesel-PV (r.f.75%) system with partial centralization (ideal case).

3) Real case:

C_D [€cents/kWh]	C_F [€cents/kWh]	C_{PV} [€cents/kWh]	C_s [€cents/kWh]	C_{pc} [€cents/kWh]	C_{LV} [€cents/kWh]	C_{CN} [€cents/kWh]
2	17.8	2.4	9.3	4.1	0.48	-
E_{Diesel} [kWh/year]	P_{Diesel} [kW]	CF_{Diesel}	E_{PV} [kWh/year]	P_{PV} [kW]	CF_{PV}	LEC_{centr} [€cents/kWh]
40232.1	80	5.7%	120696.4	67.8	20.3%	36.1

Table 4.34: Results of the LEC model execution for a diesel-PV (f.r.75%) feeding the whole community in the real case.

In the following diagrams, the cost contribution of each subsystem in the three cases tested.

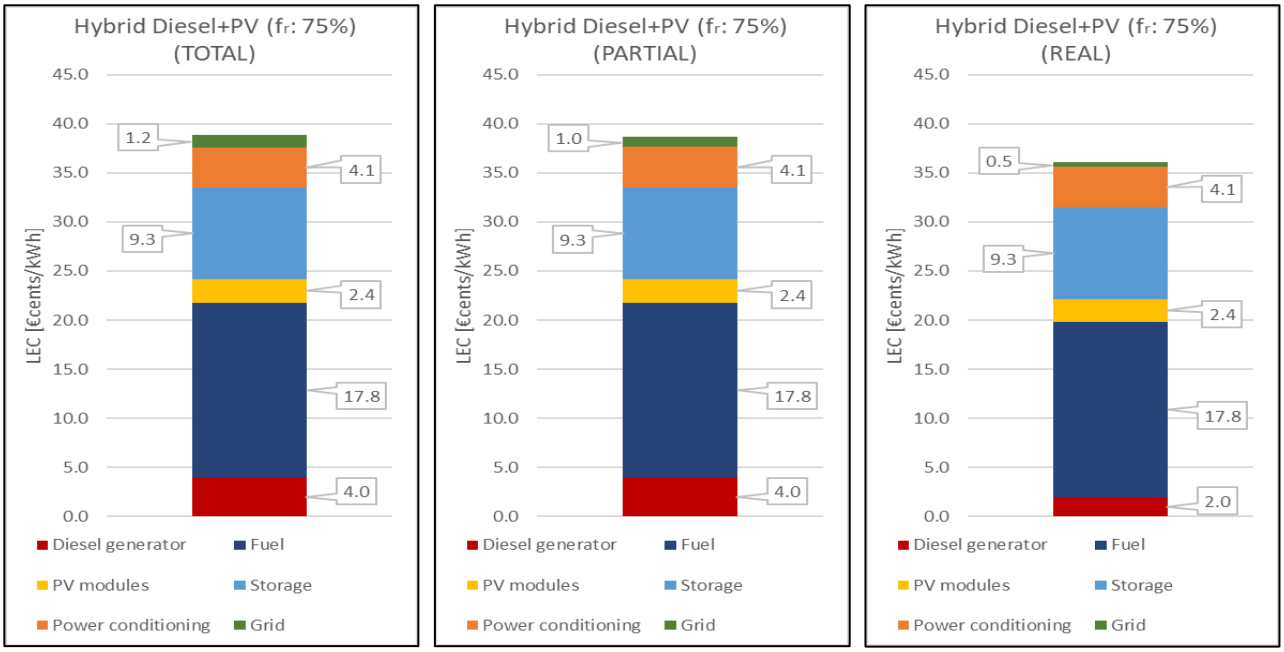

Figure 4.11: Cost contribution of each subsystem to the total LEC of a diesel-PV(f.r.75%) system for the three cases tested.

In the maps below, the resulting raster representation of the LEC obtained for the three cases tested, in terms of placement of the centralized system.

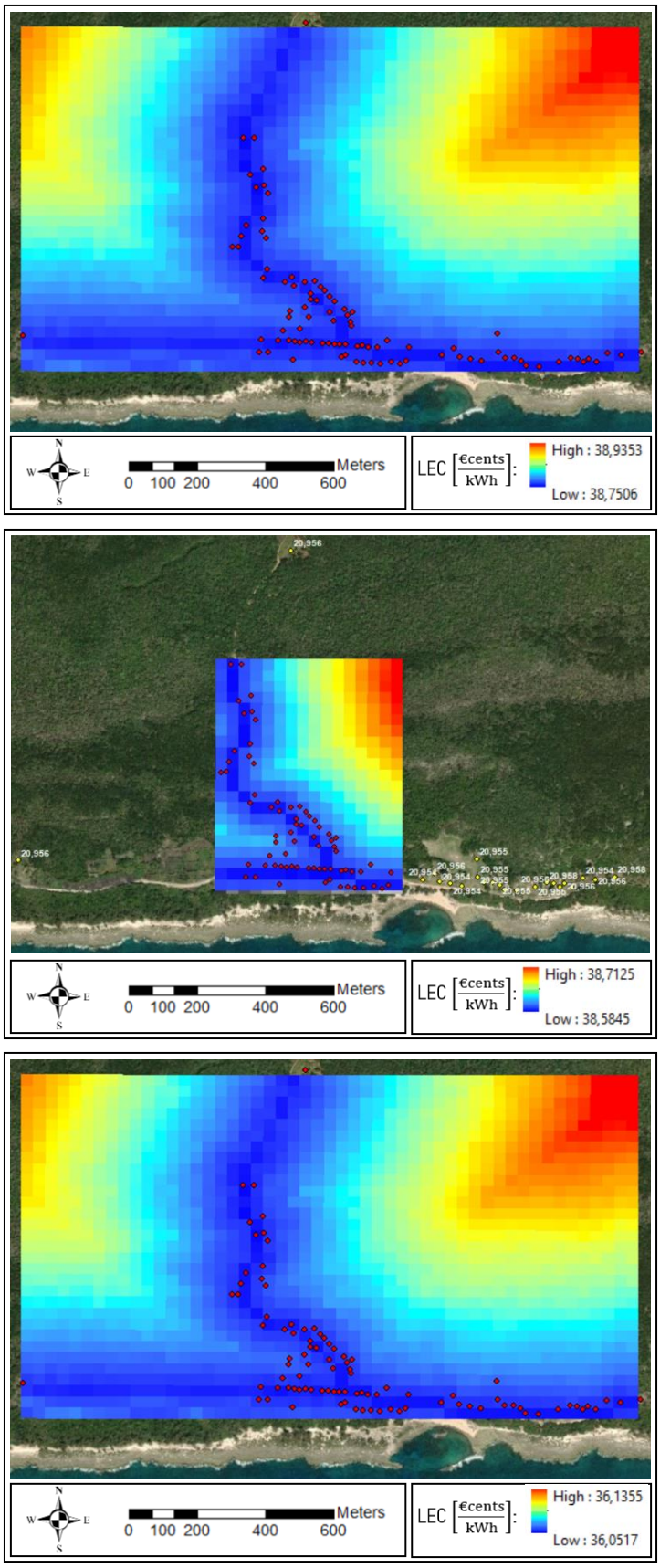

Figure 4.12: : LEC of a diesel-PV(f.r.75%) system for the total case (up), for the partial case (mid.) and the real case (down).

4.4.4 Hybrid Diesel-PV f_r 50%

The important setting change in the hybrid system passing from one configuration to the other is the battery autonomy. As previously motivated, one day of autonomy is considered sufficient for the reliability of a diesel-PV system with 50% of renewable fraction, rather than the two days set for the 75% case.

A summary of the input settings for the three runs referred is reported in the following tables:

1) Total case:

$n_{pv,centr}$	$I_{pv,centr}$ [€/kW]	$OM_{pv,centr}$ [€/kW]	$\eta_{pv,centr}$	$n_{s,centr}$	$I_{s,centr}$ [€/kWh]	$OM_{s,centr}$ [€/kWh]	$\eta_{s,centr}$	d_{centr} [days]	DoD_{centr}	$n_{pc,centr}$	$I_{pc,centr}$ [€/kW]	$OM_{pc,centr}$ [€/kW]	$\eta_{pc,centr}$
25	1558	14	80%	18	180	4	85%	1	70%	15	267	0	95%
n_D	n_{rec}	I_D [€/kW]	OM_D [€/(h·kW)]	f_d	F_p [€/l]	CO_F [l/kWh]	n_{LV}	I_{LV} [€/km]	OM_{LV} [€/km]	I_{CN} [€/kW]	f_l	f_r	Type
20	5	400	0.02	0.77	1.78	0.40	30	16000	160	100	0.53	50%	H

Table 4.35: Input settings of the LEC model for a diesel-PV (r.f.50%) system including all the community (ideal case).

2) Partial case:

n_{pv}	I_{pv} [€/kW]	OM_{pv} [€/kW]	η_{pv}	n_s	I_s [€/kWh]	OM_s [€/kWh]	η_S	d [days]	DoD	$n_{pc,ind}$	$I_{pc,ind}$ [€/kW]	$OM_{pc,ind}$ [€/kW]	$\eta_{inv,pv}$
25	2443	18	65%	18	180	4	85%	3	70%	15	267	0	95%
$n_{pv,centr}$	$I_{pv,centr}$ [€/kW]	$OM_{pv,centr}$ [€/kW]	$\eta_{pv,centr}$	$n_{s,centr}$	$I_{s,centr}$ [€/kWh]	$OM_{s,centr}$ [€/kWh]	$\eta_{s,centr}$	d_{centr} [days]	DoD_{centr}	$n_{pc,centr}$	$I_{pc,centr}$ [€/kW]	$OM_{pc,centr}$ [€/kW]	$\eta_{pc,centr}$
25	1558	14	80%	18	180	4	85%	1	70%	15	267	0	95%
n_D	n_{rec}	I_D [€/kW]	OM_D [€/(h·kW)]	f_d	F_p [€/l]	CO_F [l/kWh]	n_{LV}	I_{LV} [€/km]	OM_{LV} [€/km]	I_{CN} [€/kW]	f_l	f_r	Type
20	5	400	0.02	0.77	1.78	0.40	30	16000	160	100	0.53	50%	H

Table 4.36: Input settings of the LEC model for a diesel-PV (r.f..50%) system with partial centralization (ideal case).

3) Real case

$n_{pv,centr}$	$I_{pv,centr}$ [€/kW]	$OM_{pv,centr}$ [€/kW]	$\eta_{pv,centr}$	$n_{s,centr}$	$I_{s,centr}$ [€/kWh]	$OM_{s,centr}$ [€/kWh]	$\eta_{s,centr}$	d_{centr} [days]	DoD_{centr}	$n_{pc,centr}$	$I_{pc,centr}$ [€/kW]	$OM_{pc,centr}$ [€/kW]	$\eta_{pc,centr}$
25	1558	14	80%	18	180	4	85%	1	70%	15	267	0	95%
n_D	n_{rec}	I_D [€/kW]	OM_D [€/(h·kW)]	f_d	F_p [€/l]	CO_F [l/kWh]	n_{LV}	I_{LV} [€/km]	OM_{LV} [€/km]	I_{CN} [€/kW]	f_l	f_r	Type
20	5	-	0.02	0.77	1.78	0.40	30	-	160	-	0.53	50%	H

Table 4.37: Input settings of the LEC model for a diesel-PV (r.f.50%) system including all the community in the real case.

The resulting LEC obtained for each case is respectively: 51.0 €cents/kWh, 50.8 €cents/kWh and 49.2 €cents/kWh.

The observations derivable by the comparison of the three cases are the same encountered in the other hybrid system: a decrease of the line costs and of the diesel generator costs.
The comparison between the two hybrid systems (f_r 75% and 50%) is more significant. As expected, in this last case the storage costs decrease, while the fuel costs increase, since the diesel contribution in the energy generation balance is doubled. The increase of the capacity factor implies a decrease of the diesel subsystem cost. Overall, the raise prevails, leading to a higher total LEC value.

A summary of the results of the model execution for the three cases is reported in the following tables:

1) Total case:

C_D [€cents/kWh]	C_F [€cents/kWh]	C_{PV} [€cents/kWh]	C_s [€cents/kWh]	C_{pc} [€cents/kWh]	C_{LV} [€cents/kWh]	C_{CN} [€cents/kWh]
3.1	35.6	2.4	4.6	4.1	1.07	0.15
E_{Diesel} [kWh/year]	P_{Diesel} [kW]	CF_{Diesel}	E_{PV} [kWh/year]	P_{PV} [kW]	CF_{PV}	LEC_{centr} [€cents/kWh]
80464.3	66.6	13.8%	80464.3	45.2	20.3%	51.0

Table 4.38: Results of the LEC model execution for a diesel-PV (r.f.50%) system feeding the whole community (ideal case).

2) Partial case:

C_D [€cents/kWh]	C_F [€cents/kWh]	C_{PV} [€cents/kWh]	C_s [€cents/kWh]	C_{pc} [€cents/kWh]	C_{LV} [€cents/kWh]	C_{CN} [€cents/kWh]
3.1	35.6	2.4	4.6	4.1	0.87	0.15
E_{Diesel} [kWh/year]	P_{Diesel} [kW]	CF_{Diesel}	E_{PV} [kWh/year]	P_{PV} [kW]	CF_{pv}	LEC_{centr} [€cents/kWh]
57925.5	48.7	13.6%	57925.5	32.53	20.3%	50.8

Table 4.39: : Results of the LEC model execution for a diesel-PV (r.f.50%) system with partial centralization (ideal case).

3) Real case:

C_D [€cents/kWh]	C_F [€cents/kWh]	C_{PV} [€cents/kWh]	C_s [€cents/kWh]	C_{pc} [€cents/kWh]	C_{LV} [€cents/kWh]	C_{CN} [€cents/kWh]
2	35.6	2.4	4.6	4.1	0.48	-
E_{Diesel} [kWh/year]	P_{Diesel} [kW]	CF_{Diesel}	E_{PV} [kWh/year]	P_{PV} [kW]	CF_{PV}	LEC_{centr} [€cents/kWh]
80464.3	80	11.5%	80464.3	45.2	20.3%	49.2

Table 4.40: Results of the LEC model execution for a diesel-PV (f.r.50%) feeding the whole community the real case.

In the following diagrams, the cost contribution of each subsystem in the three cases tested.

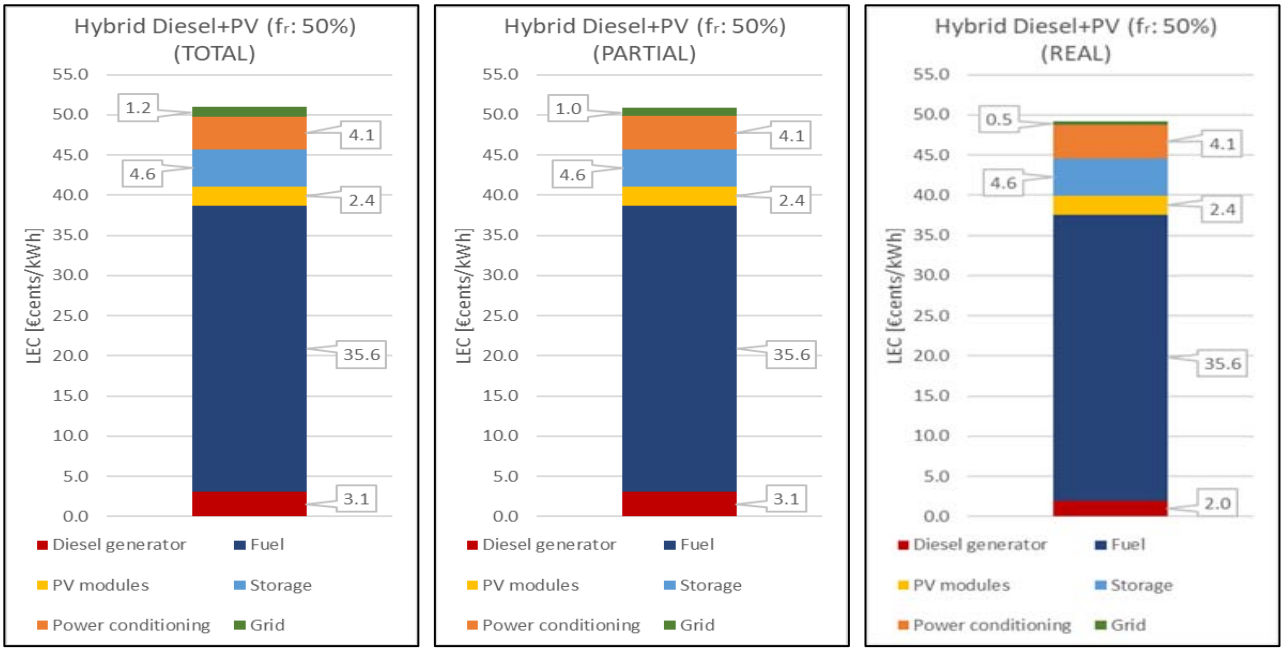

Figure 4.13: : Cost contribution of each subsystem to the total LEC of a diesel-PV(f.r.50%) system for the three cases tested.

In the maps below, the resulting raster representation of the LEC obtained for the three cases tested, in terms of placement of the centralized system.

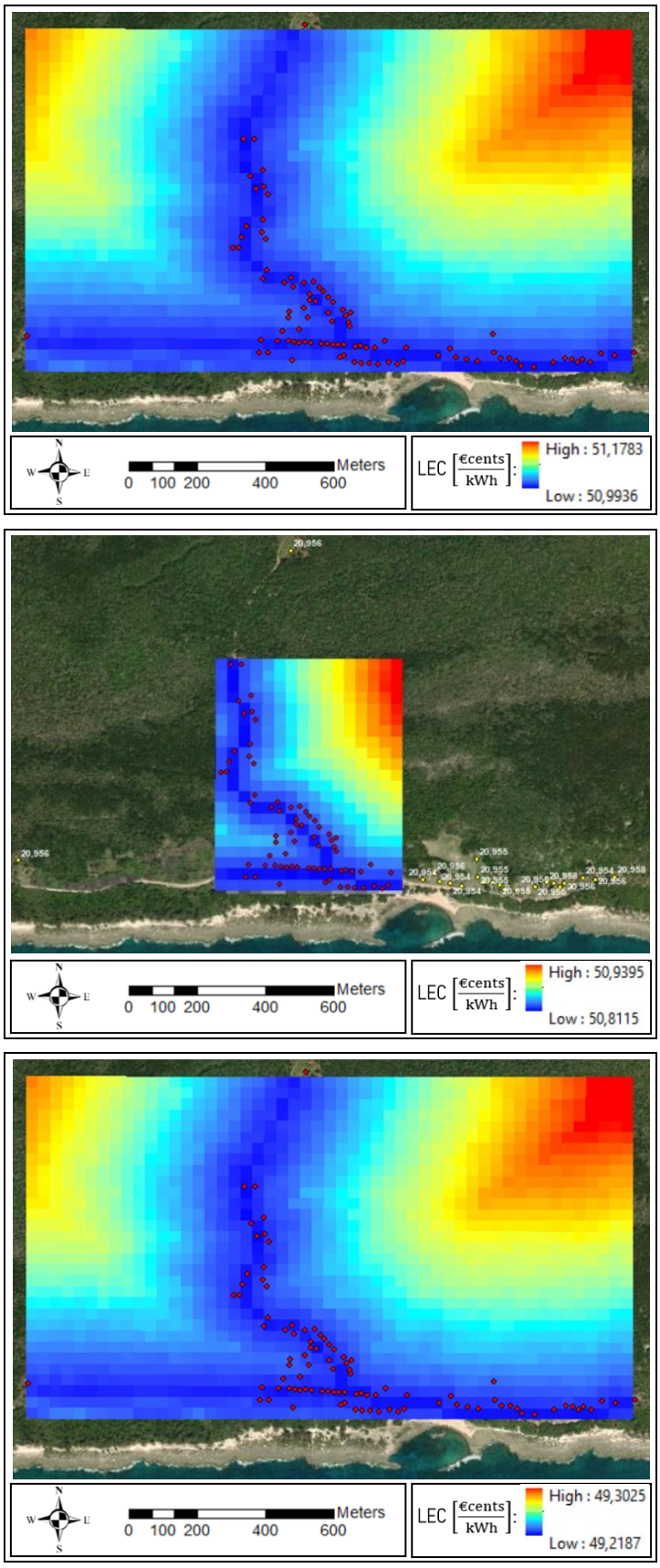

Figure 4.14: LEC of a diesel-PV(f.r.50%) system for the total case (up), for the partial case (mid.) and the real case (down).

4.4.5 Diesel genset

The last type of configuration considered is a diesel generator set that directly feeds all the energy demand considered, without any storage or external power conditioning system. In particular, the real case represents an increase of the diesel genset use from the actual 12 hours/day of operation to a continuous operation.
A summary of the input settings for the three runs referred is reported in the following tables:

1) Total case:

n_D	n_{rec}	I_D [€/kW]	OM_D [€/(h·kW)]	f_d	F_p [€/l]	CO_F [l/kWh]	n_{LV}	I_{LV} [€/km]	OM_{LV} [€/km]	I_{CN} [€/kW]	f_l	f_r	Type
20	5	400	0.02	0.77	1.78	0.40	30	16000	160	100	0.53	0%	D

Table 4.41: Input settings of the LEC model for a diesel genset feeding all the community (ideal case).

2) Partial case:

n_{pv}	I_{pv} [€/kW]	OM_{pv} [€/kW]	η_{pv}	n_s	I_s [€/kWh]	OM_s [€/kWh]	η_s	d [days]	DoD	$n_{pc,ind}$	$I_{pc,ind}$ [€/kW]	$OM_{pc,ind}$ [€/kW]	$\eta_{inv,pv}$
25	2443	18	65%	18	180	4	85%	3	70%	15	267	0	95%
n_D	n_{rec}	I_D [€/kW]	OM_D [€/(h·kW)]	f_d	F_p [€/l]	CO_F [l/kWh]	n_{LV}	I_{LV} [€/km]	OM_{LV} [€/km]	I_{CN} [€/kW]	f_l	f_r	Type
20	5	400	0.02	0.77	1.78	0.40	30	16000	160	100	0.53	0%	D

Table 4.42:: Input settings of the LEC model for a diesel genset with partial centralization (ideal case).

3) Real case:

n_D	n_{rec}	I_D [€/kW]	OM_D [€/(h·kW)]	f_d	F_p [€/l]	CO_F [l/kWh]	n_{LV}	I_{LV} [€/km]	OM_{LV} [€/km]	I_{CN} [€/kW]	f_l	f_r	Type
20	5	-	0.02	0.77	1.78	0.40	30	-	160	-	0.53	0%	D

Table 4.43: : Input settings of the LEC model for a diesel genset feedingg all the community in the real case.

The resulting LEC obtained for each case is respectively: 75.0 €cents/kWh, 74.8 €cents/kWh and 73.7 €cents/kWh. Despite the absence of several cost contributors and a most efficient use of the diesel generator, the total LEC appears to be the highest in all the three cases. It is evident that the cause is the high cost associated to the fuel consumption. Even omitting any environmental issues, the present investigation, with the assumption made, identifies the diesel generator set as the least cost-effective solution for the case study.

A summary of the results of the model execution for the three cases is reported in the following tables:

1) Total case:

C_D [€cents/kWh]	C_F [€cents/kWh]	C_{PV} [€cents/kWh]	C_s [€cents/kWh]	C_{pc} [€cents/kWh]	C_{LV} [€cents/kWh]	C_{CN} [€cents/kWh]
2.6	71.2	-	-	-	1.07	0.15
E_{Diesel} [kWh/year]	P_{Diesel} [kW]	CF_{Diesel}	E_{PV} [kWh/year]	P_{PV} [kW]	CF_{PV}	LEC_{centr} [€cents/kWh]
160928.5	66.6	27.6%	-	-	-	75.0

Table 4.44: Results of the LEC model execution for a diesel generator feeding the whole community (ideal case).

2) Partial case:

C_D [€cents/kWh]	C_F [€cents/kWh]	C_{PV} [€cents/kWh]	C_s [€cents/kWh]	C_{pc} [€cents/kWh]	C_{LV} [€cents/kWh]	C_{CN} [€cents/kWh]
2.6	71.2	-	-	-	0.87	0.15
E_{Diesel} [kWh/year]	P_{Diesel} [kW]	CF_{Diesel}	E_{PV} [kWh/year]	P_{PV} [kW]	CF_{PV}	LEC_{centr} [€cents/kWh]
115851	48.7	27.1%	-	-	-	74.8

Table 4.45: Results of the LEC model execution for a diesel generator set with partial centralization (ideal case).

3) Real case:

C_D [€cents/kWh]	C_F [€cents/kWh]	C_{PV} [€cents/kWh]	C_s [€cents/kWh]	C_{pc} [€cents/kWh]	C_{LV} [€cents/kWh]	C_{CN} [€cents/kWh]
2	71.2	-	-	-	0.48	-
E_{Diesel} [kWh/year]	P_{Diesel} [kW]	CF_{Diesel}	E_{PV} [kWh/year]	P_{PV} [kW]	CF_{PV}	LEC_{centr} [€cents/kWh]
160928.5	80	23%	-	-	-	73.7

Table 4.46: : Results of the LEC model execution for a diesel generator set feeding the whole community in the real case.

In the following diagrams, the cost contribution of each subsystem in the three cases tested.

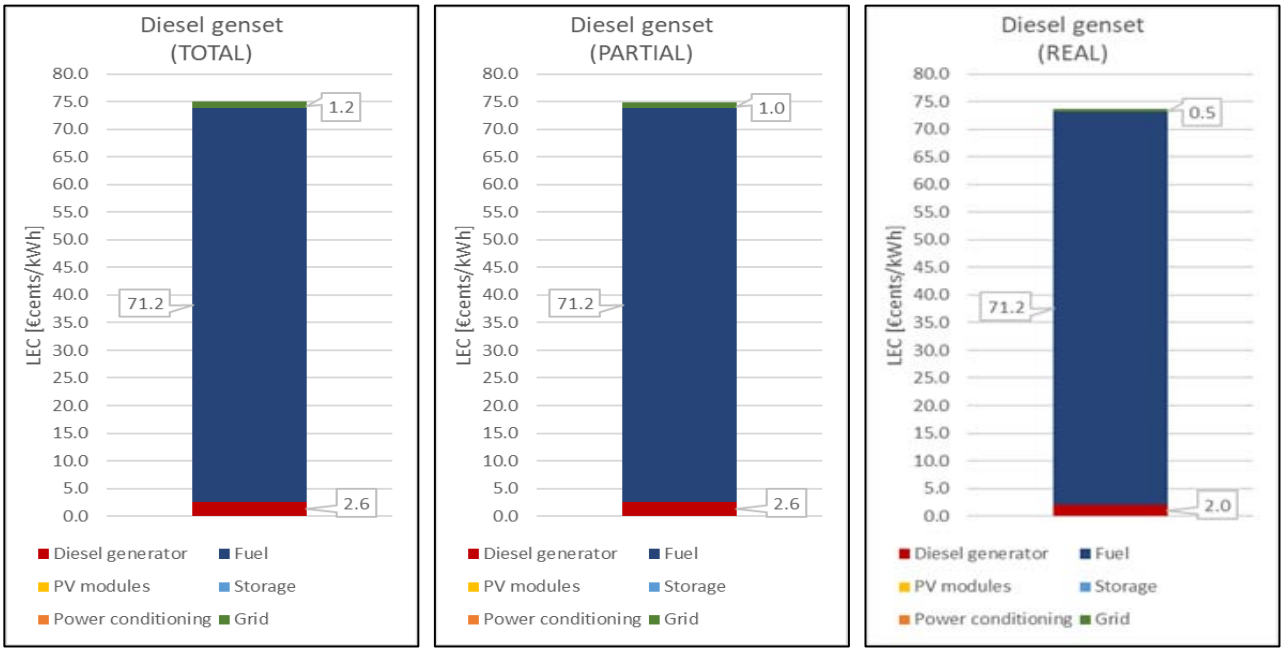

Figure 4.15: Cost contribution of each subsystem to the total LEC of a diesel generator set or the three cases tested.

In the maps below, the resulting raster representation of the LEC obtained for the three cases tested, in terms of placement of the centralized system.

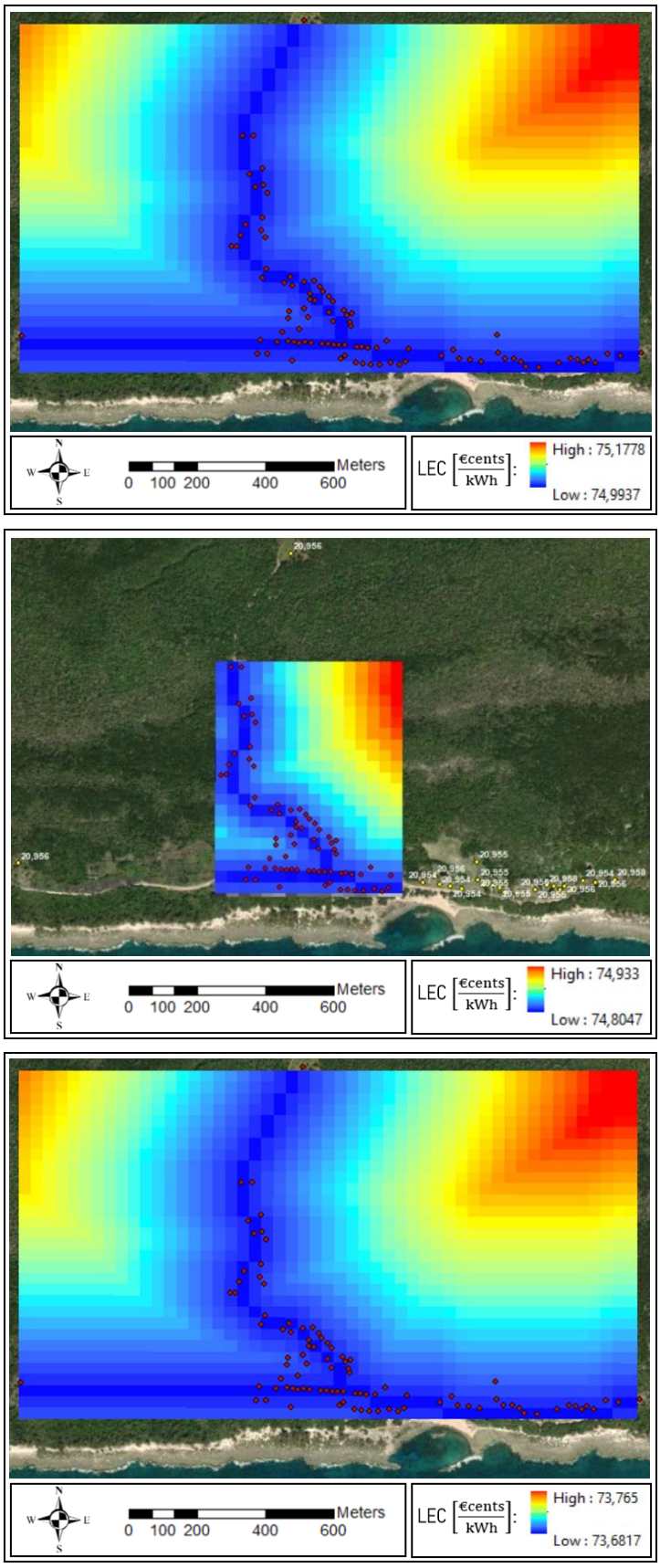

Figure 4.16: LEC of a diesel generator set for the total case (up), for the partial case (mid.) and the real case (down).

4.5 Results comparison

The approach proposed by the new model created allows to perform the assessment of different configuration on multiple levels of comparison. The previous paragraph was focused in showing how the initial condition considered can affect the calculation.

The differences revealed by the comparison of three cases are almost irrelevant but in a different context they could be significant. The limited size of the study area is reflected in a low impact of the line costs, which would increase considerably if higher voltage systems were required. Also, the size of the required power plants does not justify a possible cost variation due to economies of scale, as it is the case between the stand-alone and the centralized solar system. In case of higher powers involved, the transition from a complete centralization to various configurations of mini-grids would have a more evident effect on cost evaluation. The characteristic and the size of the study areas do not involve sensible fluctuation of the solar resource from a spatial point of view. For this reason, the information about the best installation site location for a centralized system (provided by the raster format of the LEC) results to be mainly driven by the distance from the line, which has a low impact. Integrating the hybrid model with other types of renewable-based power plant would increase the spatial variability of the available resources. This would take the most advantage the versatility of the LEC model created as a decision-making instrument. Another effective comparison that deserves a closer look is between the different type of power generation systems investigated.

The LEC of the two solar system types appears to be mainly equal. The lower cost per kWh associated to the solar panel of the centralized system are balanced by the higher cost of the power conditioning system and by the cost associated to the grid. From the PV centralized system to the diesel generator set and the two types of hybrid system, the same trend can be noticed. The higher the renewable fraction is, the more the storage cost and the diesel generator cost increase, while the fuel consumption decreases. The storage costs are related to the required reliability of the power plant. The diesel generator costs depend on its capacity factor. Since its size is fixed by the total energy demand, an increase of contribution in the total energy production clearly leads to a lower associated cost per kWh produced. The weight assumed by each of the subsystems involved determine the overall evolution of this trend. In this case study the fuel subsystem results to have a very high impact in the total cost. It is justified by the high price of the diesel considered, motivated by the isolated location of Guasasa. It can be noticed that a lower fuel price would definitely increase the competitiveness of the hybrid system as electrification option. The trend is evident in all the three cases previously investigated. The following paragraph will further highlight the comparison between the different configurations.

4.5.1 Total centralization

In table and diagram below, the LEC comparison among the different types of power plant and the contribution of each subsystem cost investigated. The case considered is the complete centralization, starting from the ideal condition of absence of any electrification equipment.

TOTAL	Diesel [€cents/kWh]	PV [€cents/kWh]	Storage [€cents/kWh]	PC [€cents/kWh]	Fuel [€cents/kWh]	Line [€cents/kWh]	Total [€cents/kWh]
PV stand-alone	0	4.3	13.9	2.8	0	0	21.0
PV centralized	0	2.4	13.9	4.1	0	1.2	21.6
Hybrid 75% PV	4.0	2.4	9.3	4.1	17.8	1.2	38.8
Hybrid 50% PV	3.1	2.4	4.6	4.1	35.6	1.2	51.0
Diesel genset	2.6	0	0	0	71.2	1.2	75.0

Table 4.47: LEC of different types of power plant and contribution of each subsystem cost considering the ideal case and total centralization.

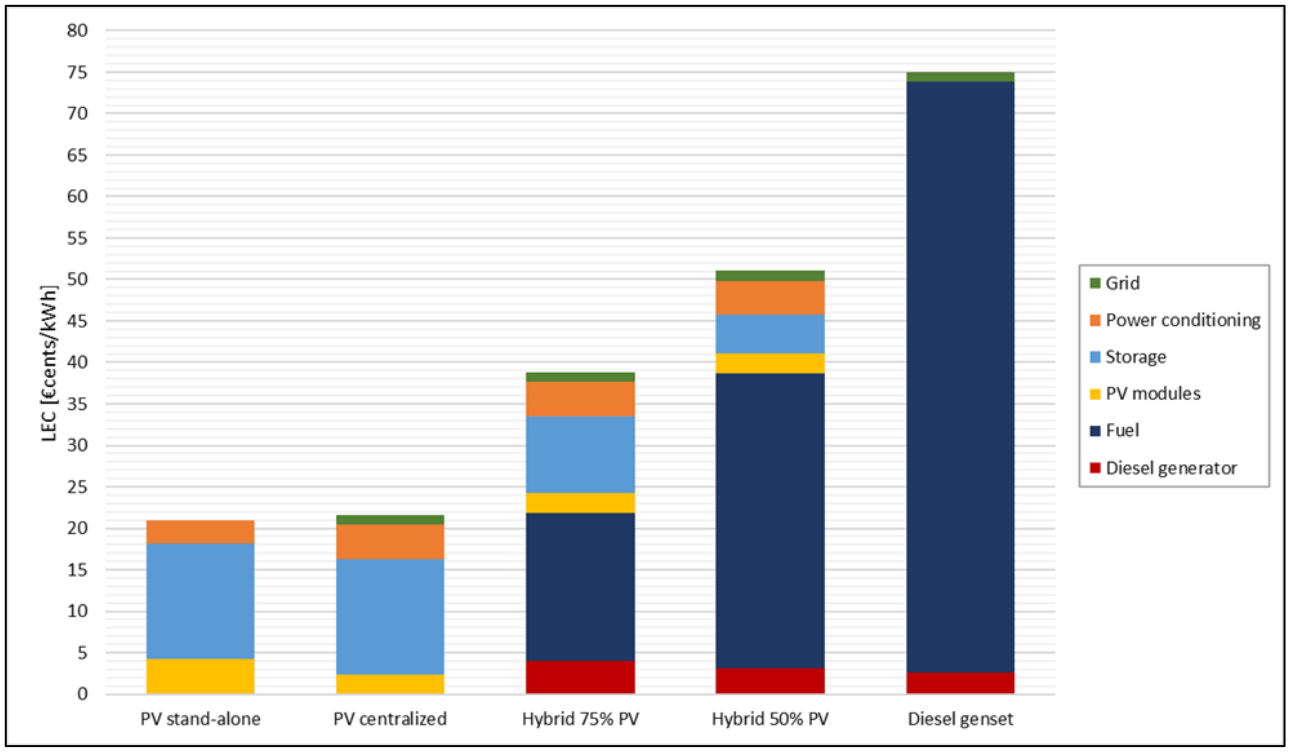

Figure 4.17: LEC comparison of different types of power plant and contribution of each subsystem cost considering the ideal case and total centralization.

4.5.2 Partial centralization

In table and diagram below, the LEC comparison among the different types of power plant and the contribution of each subsystem cost is investigated. The case considered is the partial centralization, starting from the ideal condition of absence of any electrification equipment. The loads excluded by the centralized system are considered supplied by a PV stand-alone system.

PARTIAL	Diesel [€cents/kWh]	PV [€cents/kWh]	Storage [€cents/kWh]	PC [€cents/kWh]	Fuel [€cents/kWh]	Line [€cents/kWh]	Total [€cents/kWh]
PV stand-alone	0	4.3	13.9	2.8	0	0	21.0
PV centralized	0	2.4	13.9	4.1	0	1.0	21.4
Hybrid 75% PV	4.0	2.4	9.3	4.1	17.8	1.0	38.6
Hybrid 50% PV	3.1	2.4	4.6	4.1	35.6	1.0	50.8
Diesel genset	2.6	0	0	0	71.2	1.0	74.8

Table 4.48: LEC of different types of power plant and contribution of each subsystem cost considering the ideal case and partial centralization.

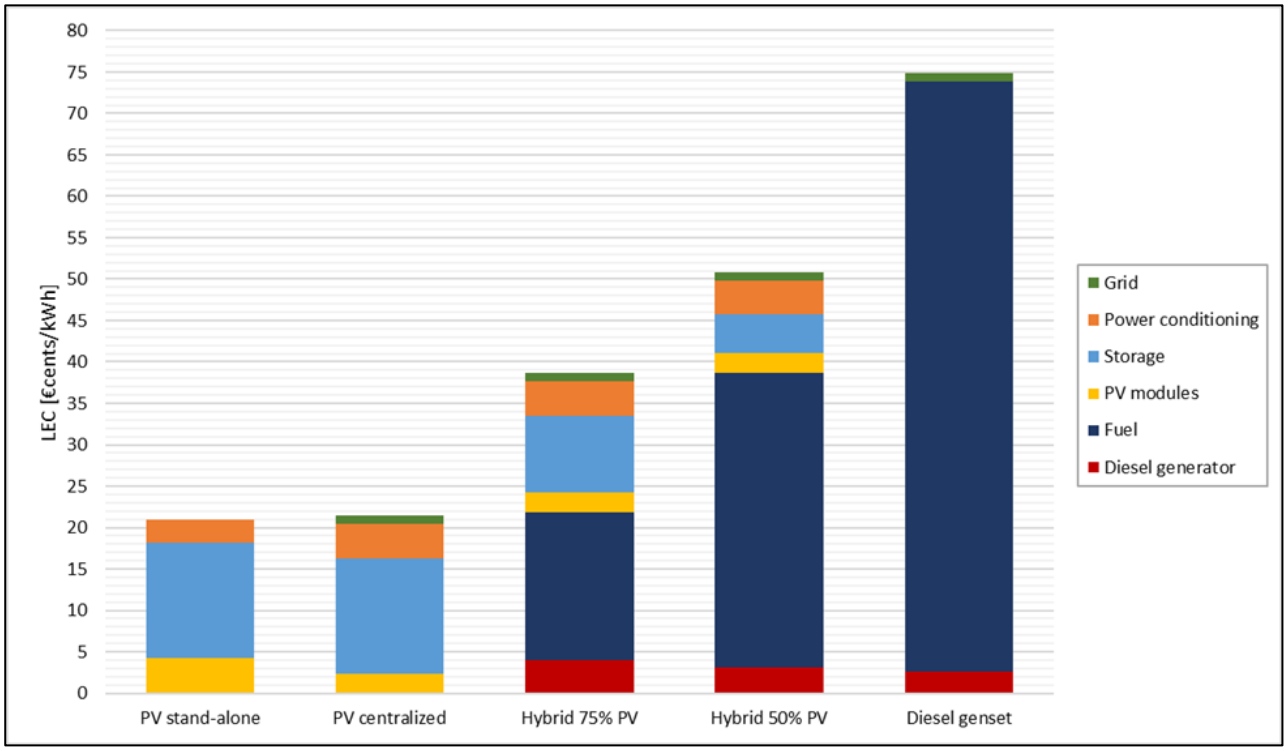

Figure 4.18: LEC comparison of different types of power plant and contribution of each subsystem cost considering the ideal case and partial centralization.

4.5.3 Real case

In table and diagram below, the LEC comparison among the different types of power plant and the contribution of each subsystem cost investigated. The case considered is the actual electrification condition in Guasasa.

REAL	Diesel [€cents/kWh]	PV [€cents/kWh]	Storage [€cents/kWh]	PC [€cents/kWh]	Fuel [€cents/kWh]	Line [€cents/kWh]	Total [€cents/kWh]
PV stand-alone	0	4.3	13.9	2.8	0	0	21.0
PV centralized	0	2.4	13.9	4.1	0	0.5	20.9
Hybrid 75% PV	2.0	2.4	9.3	4.1	17.8	0.5	36.1
Hybrid 50% PV	2.0	2.4	4.6	4.1	35.6	0.5	49.2
Diesel genset	2.0	0	0	0	71.2	0.5	73.7

Table 4.49: LEC of different types of power plant and contribution of each subsystem cost considering the real case.

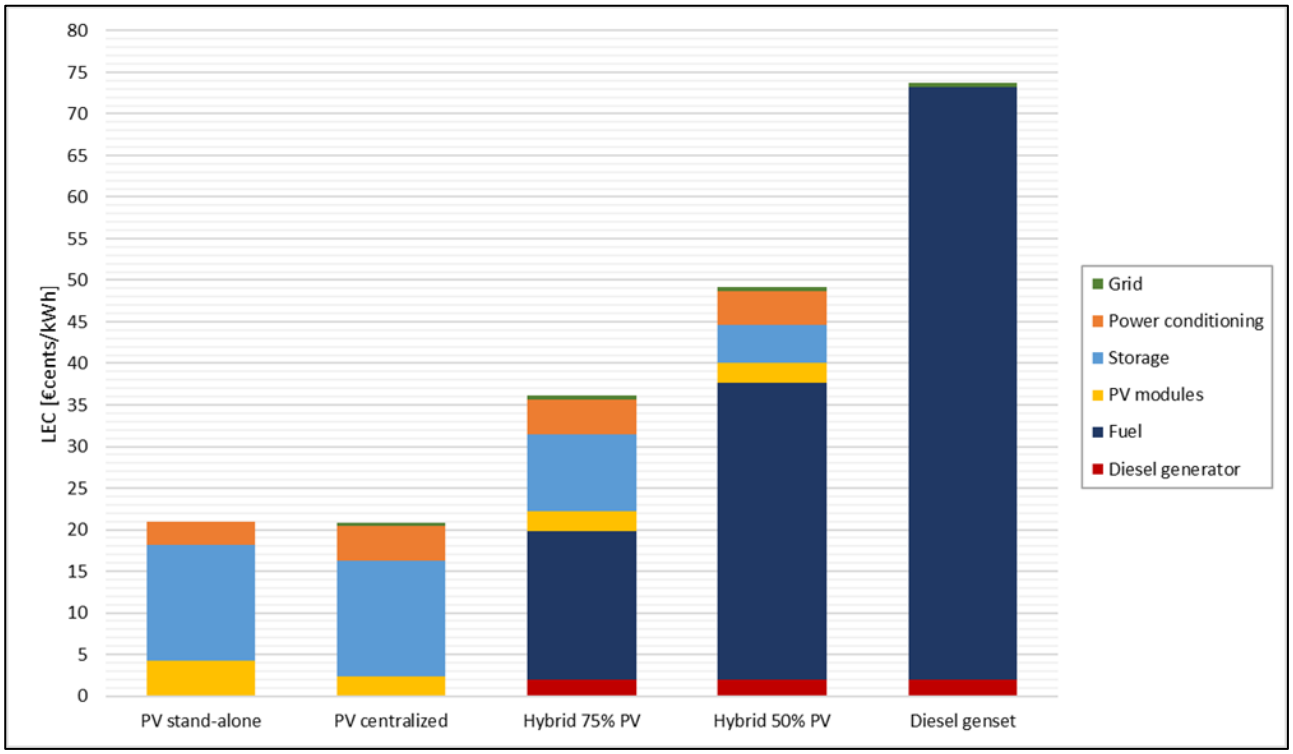

Figure 4.19: LEC comparison of different types of power plant and contribution of each subsystem cost considering the real case.

5 Conclusion

A GIS-based model is proposed for the LEC assessment of different types of power generators: solar, diesel or hybrid systems. The core of the approach is the incorporation of the territorial reality of the study area by taking into account the distribution of the energy demand to feed and of the available solar resource. The objective is providing a suitable groundwork for future developments of a tool for decision-making processes in rural electrification. While creating the required inputs of the model, a method for the generation of high-resolution solar radiation maps has been proposed, representing a collateral objective of the thesis. Both the solar map generation method and the LEC model are designed with a focus on replicability: for any case study, the input settings are easily adaptable.

The model introduces some innovation to the structure of the IntiGIS model, from which part of the equations have been extracted and adapted. The main change is the possibility of managing the load clusters in centralized or individual systems, providing another level of results comparison. In addition to the effect of changing the type of energy generation, the techno-economic impact of different configurations of mini-grids can be investigated. A second change is the visualization of the results as a function of all the possible installation sites for the centralized power plant.

The relevance of these upgrades is not particularly evident in the case study of Guasasa. Indeed, the small size of the area considered and the uniformity of the receiving solar radiation lead to a low influence of spatial variation on the cost associated to the PV module ant the line costs subsystems. Anyway, the evolution of the resulting LEC complies with the expectation, even though in a smaller scale. For sure, a more complex topography would better highlight the impact of the innovations introduced.

The application to the case of Guasasa represents a good simulation of the model reliability, thanks to the background knowledge provided by the existing studies. However, a certain degree of simplification must be considered while analyzing the results, as inevitably happens dealing with LEC calculations. A good way to reduce the effect of approximations is focusing on the results comparison of the different tests, rather than on the individual output values. The results obtained are plausible and the pattern of the LEC variation case by case can be justified. With all the assumptions made, the photovoltaic systems, both for the centralized and the individual configurations, turn out to be the most convenient option. The decisive factor in the overall balance is the cost associated to the diesel consumption, which is particularly onerous due to unfavorable conditions of supply. Assuming a lower fuel price would definitely increase the competitiveness of the hybrid solution, which have the potential to represent the most cost-effective option for the electrification of Guasasa.

Of course, a complete assessment should also consider other factors, like the system reliability or the environmental impact. The first factor encourages the presence of a conventional system as back-up power source, while considering taxations and subsides would predictably reward a massive use of renewable resources. In future developments, evaluating the externalities would surely provide a more comprehensive overview. For further improvements of the model, several types of power sources could be integrated, contributing on the creation of an effective tool for electrification projects.

Bibliography

Amador, J. G. (2000). *Análisis de los parámetros técnicos en la aplicación de los sistemas de información geográfica a la integración regional de las energías renovables en la producción descentralizada de electricidad.* Tesis Doctoral: Universidad Politécnica de Madrid - Departamento de Ingeniería Eléctrica.

ArcGIS for Desktop 10.7.1 - ArcMap. (2019). *ArcGIS Desktop Help 10.7.1.* Environmental Systems Research Institute (ESRI).

Benato, R., & Fellin, L. (2011). Impianti elettrici. Milano: Wolter Kluwer.

Borda, A., Domínguez, J., Amador, J., Arribas, L., & Pinedo, I. (2011). *Characterization of Hybrid Systems for Rural Electrification with Renewable Energies Using Geographic Information Systems (GIS).* Madrid: Informes Técnicos Ciemat.

Caballero, L. M. (2019). *Estudio de la introdución de sistemas basados en energías renovables en Guasasa (Cuba).* Proyecto Fin de Máster: Universidad Politécnica de Madrid - Master en Energías Renovables y Medio Ambiente.

Ciemat. (2020). *Aula Virtual - Hibri2.* Obtenido de Ciemat: http://avformacion.ciemat.es

Comini, G., & Savino, S. (2013). *La Captazione dell'Energia Solare.* Udine: International Centre for Mechanical Sciences Monografie CISM.

Cubaenergía - Centro de Gestión de la Información y Desarollo de la Energía. (2020). *Mejora del servicio eléctrico en la comunidad de Guasasa por medio de una microred eléctrica con fuentes renovables de energia - Descripción Técnica.*

De Carvalho Alves, M., Sanches, L., de Souza, J., & Mattos Silva, V. A. (2013). Effects od Sky Conditions Measured by the Clearness Index on the Estimation of Solar Radiation Using a DIgital ELevation Model. *Atmospheric and Climate Sciences*, 3: 618-626.

De Floriani, L., & Magillo, P. (2018). Digital Elevetion Models. En L. Liu, & M. T. Özsu, *Encyclopedia od Database Systems.* New York: Springer.

Domínguez Bravo, J. (2000). *Breve Introducción a la Cartografía y a los Sistemas de Información Geográfica (SIG).* Madrid: CIEMAT.

Domínguez Bravo, J. (2002). *La integración económica y territorial de las energías renovables y los sistemas de información geográfica.* Madrid: Universidad

Complutense de Madrid - Facultad de Geografía e Historia - Departamento de Geografía Humana.

Domínguez, J., & Pinedo, I. (2009). GIS Tool for Rural Electrification with Renewable Energies in Latin America. *Advanced Geographic Information Systems & Web Services International Conference.* Cancun, Mexico: IEEE Xplore.

Duffie, J. A., & Beckman, W. A. (2013). *Solar Engineering of Thermal Processes, Fourth Edition.* Hoboken: John Wiley & Sonsc, Inc.

European Central Bank. (2020). *ECB euro reference exchange rate: US dollar (USD).* https://www.ecb.europa.eu/stats/policy_and_exchange_rates/euro_reference_exchange_rates.

European Commission. (2020). *PVGIS - Photovoltaic Geographical Information System.* Obtenido de https://ec.europa.eu/

European Commission's science and knowledge service. (s.f.). Obtenido de PVGIS - Photovoltaic Geographical Information System: https://ec.europa.eu/

Fu, P., & Rich, P. (1999). Design and Implementation of the Solar Analyst: an ArcView extension for modeling solar radiation at landscape scales. *Nineteenth Annual ESRI User Conference.*

Homer Pro 3.13. (s.f.). *Glossary.* https://www.homerenergy.com/products/pro/docs/latest/real_discount_rate.

International Energy Agency. (2019). *World Energy Outlook 2019.*

IRENA. (2016). *Innovation Outlook: Renewable Mini-grids.* Abu Dhabi.

Louie, H. (2018). *Off-Grid Electrical System in Developing Countries.* Seattle: Springer.

Lovett, A. A. (2000). GIS and Environmental Management. In T. O'Riordan, *Environmental Science for Environmental Management* (pp. 267-285). Routledge.

Mesa, C. (2019). El enfriamiento de la economia cubama. *Nueva sociedad, 279.*

Meteonorm - Global Meteorological Database - Version 7.1. (July 2015). *Handbook part II: Theory.* Meteotest AG.

Meteonorm - Global Meteorological Database - Version 7.1. (July 2016). *Handbook Part I: Software.* Meteotest AG.

Mora-Lopez, L., Piliougine, M., Carretero, J. E., & Sidrach-de Cardona, M. (2010). Integration of Statistical and Machine Learnig Models for Short-term Forecastinng of the Atmospheric Clearness Index. *International Congrss on Environmental Modelling*

and Software Modelling for Environmental's Sake, Fifth Biennal Meeting. Ottawa: International Environmental Modelling and Software Sociaety (iEMSs).

NREL. (2019). *2019 Annual Technology Baseline.* Golden, CO: https://atb.nrel.gov/electricity/2019.

Padovan, A., & Del Col, D. (2010). Measurements and modeling of solar irradiance components on horizontal and tilted panels. *Solar Energy* , 84: 2068-2084.

Pinedo, I., & Dominguez, J. (2011). INTIGIS: Evaluación de Alternativas de Electrificación Rural basada en Sistemas de Información Geográfica. *XXII Congreso de Geógrafos Españoles - AGE.* Alicante.

Simpson, R. A. (1997). Optical depth. En *Encyclopedia of Planetary Science. Encyclopedia of Planetary Earth Science.* Dordrecht: Springer.

Singh, J., Bimal, K. B., Manoj, K., & Kaniska, M. (2013). Modelling monthly diffuse solar radiation fraction and its validity over the Indiansub-tropics. *Internationl Journal of Climatology*, 33: 77-86.

Appendix

Appendix 1: Example of the Script for the Point Solar Radiation execution referred to the period of January (pag.30).

```
# PointsSolarRadiation
# Requirements: Spatial Analyst Extension

# Import system modules
import arcpy
from arcpy import env
from arcpy.sa import *

month="jan"
folder_PointSolar="C:\\Users\\Carlo\\Desktop\\Script\\Point_Solar\\"
folder_Location=folder_PointSolar+"Location\\"
folder_Month=folder_PointSolar+month+"\\"

global_merge=folder_Month+"Merge\\{}_glob".format(month)
direct_merge=folder_Month+"Merge\\{}_dir".format(month)
diffuse_merge=folder_Month+"Merge\\{}_dif".format(month)
# Set environment settings
env.workspace =folder_Month
# Check out the ArcGIS Spatial Analyst extension license
arcpy.CheckOutExtension("Spatial")

# Set local variables
skySize = 400
timeConfig = TimeMultipleDays(2020, 1, 32)
dayInterval = 14
hourInterval = 0.5
zFactor = 1
calcDirections = 32
zenithDivisions = 16
azimuthDivisions = 16

dict = {}
file = open('Lat.txt', 'r')
for line in file.readlines():
        lat = [float(i) for i in line.split('\t')]
file = open('Kt_{}.txt'.format(month), 'r')
for line in file.readlines():
        kt = [float(i) for i in line.split('\t')]
file = open('Kd_{}.txt'.format(month), 'r')
for line in file.readlines():
        kd = [float(i) for i in line.split('\t')]
dictList = [None]*len(lat)
for i in range(len(lat)):
        dictList[i] = {'point': folder_Location+"{}.shp".format(i),
                       'cell':folder_Location+"dsm_split{}.TIF".format(i),
                       'lat':lat[i],'kt':kt[i],'kd':kd[i]}

listGlobal=[]
listDirect=[]
listDiffuse=[]
for i in range(len(lat)):
        inPntFC = dictList[i]['point']
        inRaster = dictList[i]['cell']
        latitude = dictList[i]['lat']
        transmittivity = dictList[i]['kt']
        diffuseProp = dictList[i]['kd']

        name_global="Glob_{}".format(i)
        outFeatures=folder_Month+name_global
        listGlobal.append(name_global+".shp")

        name_dif="Dif_{}".format(i)
        outDiffuseRad=folder_Month+name_dif
        listDiffuse.append(name_dif+".shp")

        name_dir="Dir_{}".format(i)
        outDirectRad=folder_Month+name_dir
        listDirect.append(name_dir+".shp")

        outDirectDur = ""

        # Execute PointsSolarRadiation
        PointsSolarRadiation(inRaster, inPntFC, outFeatures, "", latitude, skySize,
                    timeConfig, dayInterval, hourInterval, "INTERVAL",
                    zFactor, "FROM_DEM", calcDirections, zenithDivisions,
                    azimuthDivisions,"STANDARD_OVERCAST_SKY", diffuseProp,
                    transmittivity, outDirectRad, outDiffuseRad, outDirectDur)


arcpy.Merge_management(listGlobal, global_merge)
arcpy.Merge_management(listDirect, direct_merge)
arcpy.Merge_management(listDiffuse, diffuse_merge)
```

Appendix 2: Example of the Script for the Area Solar Radiation execution referred to the period of January (pag. 37).

```
# Import system modules
import arcpy
from arcpy import env
from arcpy.sa import *

# Set local variables
inRaster = "C:\Users\Carlo\Desktop\MADRID\Arcgis\Finale\mds_sagoma"
skySize = 400
timeConfig = TimeMultipleDays(2020, 1, 32)
dayInterval = 1
hourInterval = 0.5
zFactor = 1
calcDirections = 32
zenithDivisions = 16
azimuthDivisions = 16
outDirectRad = ""
outDiffuseRad = ""
outDirectDur = ""
# Set environment settings
def init_my_env():
    arcpy.ResetEnvironments()
    env.workspace = "C:\Users\Carlo\Desktop\MADRID\Arcgis\Finale\Script\Solar_Radiation"

    # Check out the ArcGIS Spatial Analyst extension license
    arcpy.CheckOutExtension("Spatial")

init_my_env()

file_input= open('Var_jan.txt', 'r')
cellList=[]
for line in file_input.readlines():
        var = [float(i) for i in line.split('\t')]
        cell={'lat':var[0],'kt':var[1],'kd':var[2],'Xmin':var[3],'Ymin':var[4],'Xmax':var[5],'Ymax':var[6]}
        cellList.append(cell)
i=0
outputList=""
for cell in cellList:
        arcpy.env.extent =arcpy.Extent(cell['Xmin'],cell['Ymin'], cell['Xmax'], cell['Ymax'])
        latitude = cell['lat']
        transmittivity = cell['kt']
        diffuseProp = cell['kd']
        # Execute AreaSolarRadiation
        outGlobalRad = AreaSolarRadiation(inRaster, latitude, skySize, timeConfig, dayInterval, hourInterval,
                                          "NOINTERVAL", zFactor, "FROM_DEM", calcDirections, zenithDivisions,
                                          azimuthDivisions, "STANDARD_OVERCAST_SKY", diffuseProp, transmittivity,
                                          outDirectRad, outDiffuseRad, outDirectDur)
        output_file = "Jan_{}".format(i)
        i+=1
        outGlobalRad.save(output_file)
        outputList+= "{};".format(output_file)
outputList = outputList[:-1]

init_my_env()

arcpy.MosaicToNewRaster_management(outputList, "Solar_Radiation", "Jan","", "32_BIT_FLOAT","", "1", "MEAN","FIRST")
```

Appendix 3: Monthly Global Horizontal Irradiation in Matanzas during January.

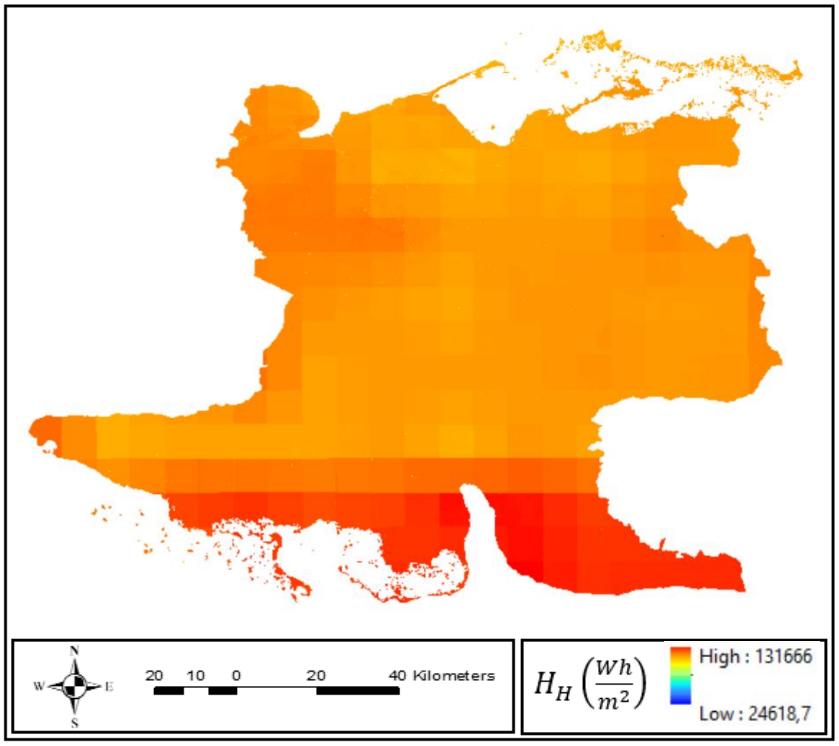

Appendix 4: Monthly Global Horizontal Irradiation in Matanzas during February.

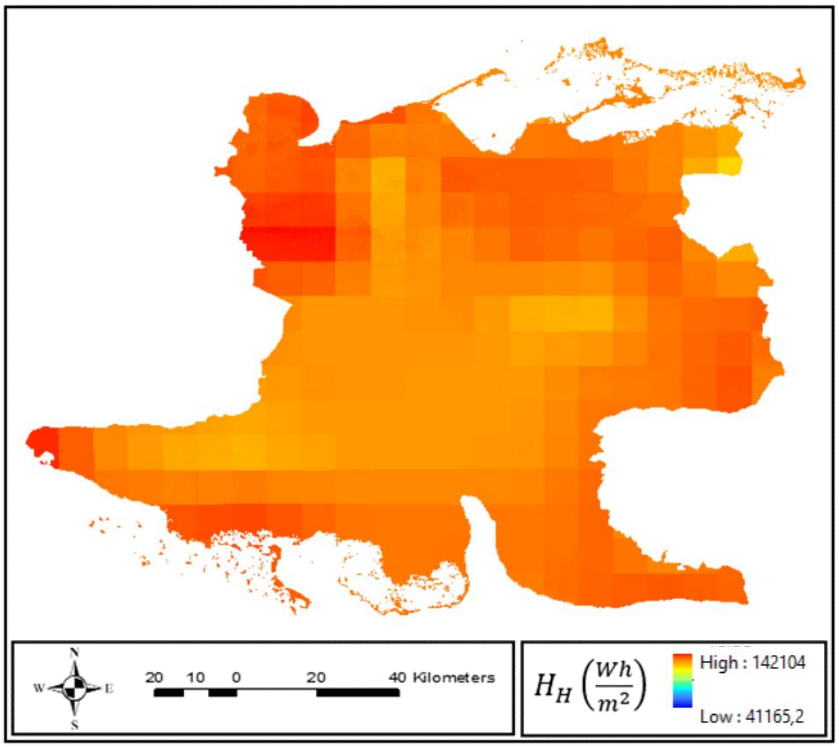

Appendix 5: Monthly Global Horizontal Irradiation in Matanzas during March.

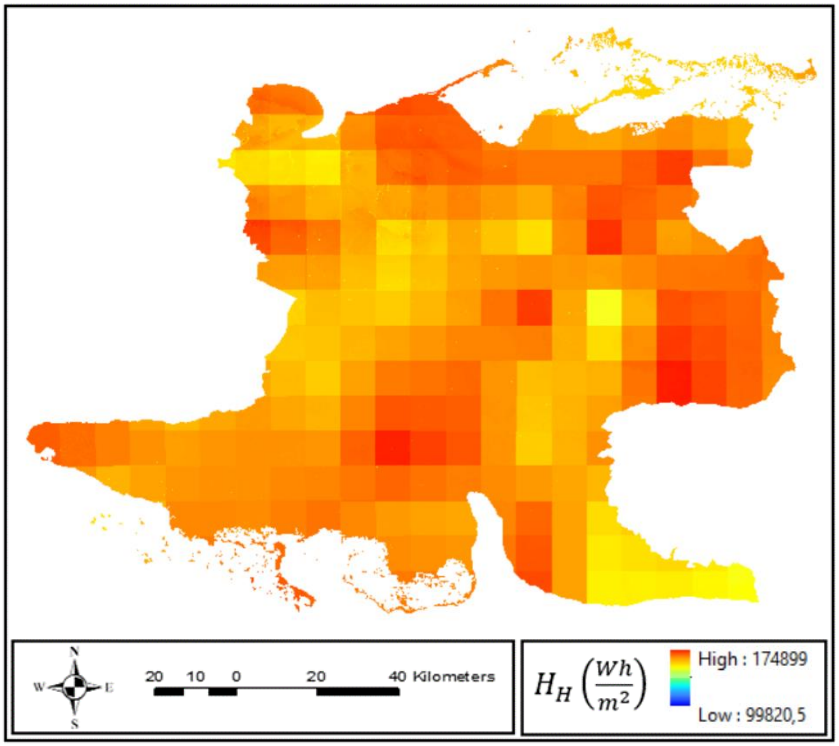

Appendix 6: Monthly Global Horizontal Irradiation in Matanzas during April.

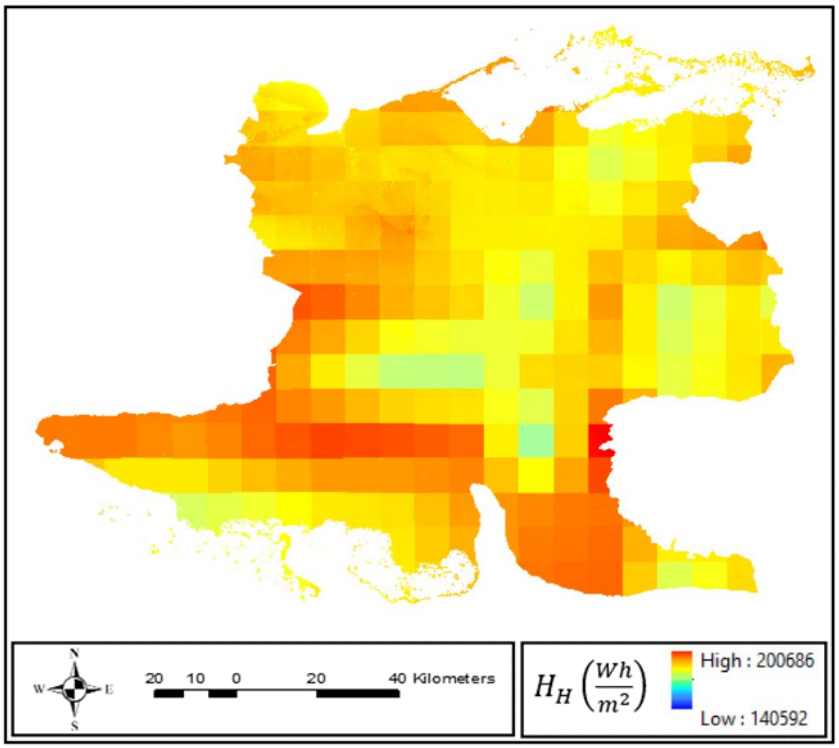

Appendix 7: Monthly Global Horizontal Irradiation in Matanzas during May.

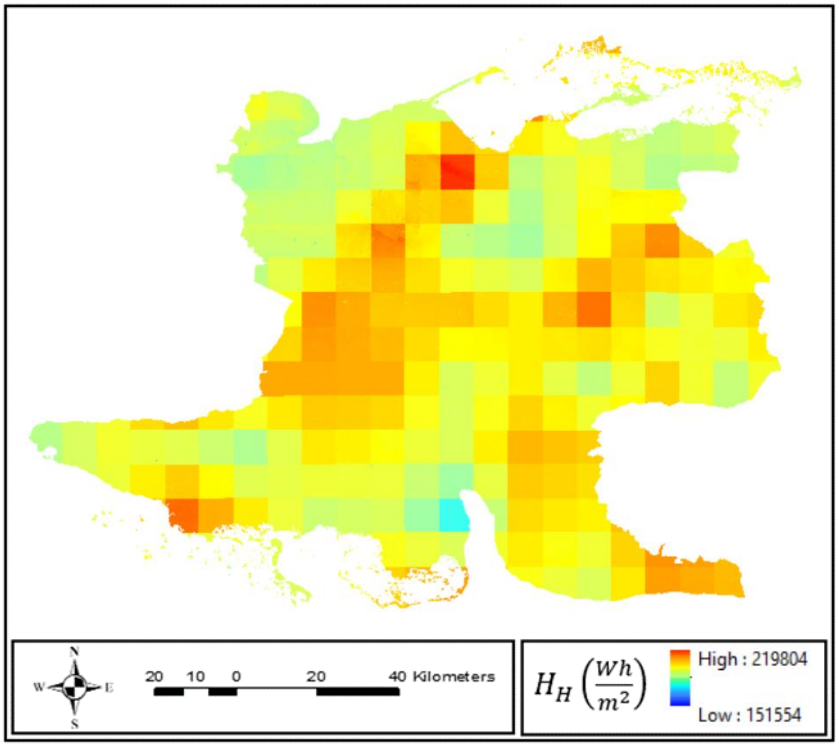

Appendix 8: Monthly Global Horizontal Irradiation in Matanzas during June.

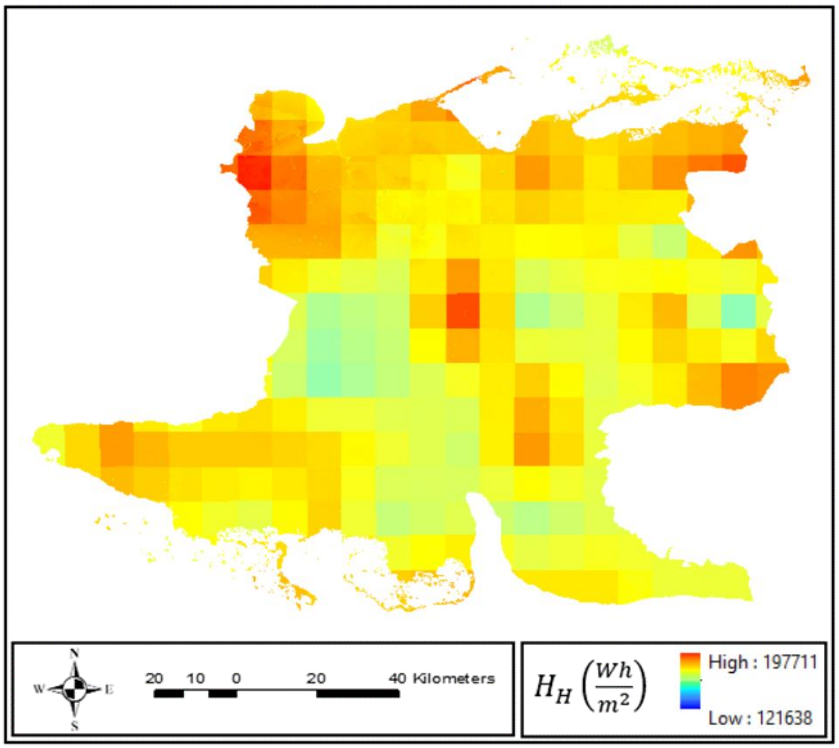

Appendix 9: Monthly Global Horizontal Irradiation in Matanzas during July.

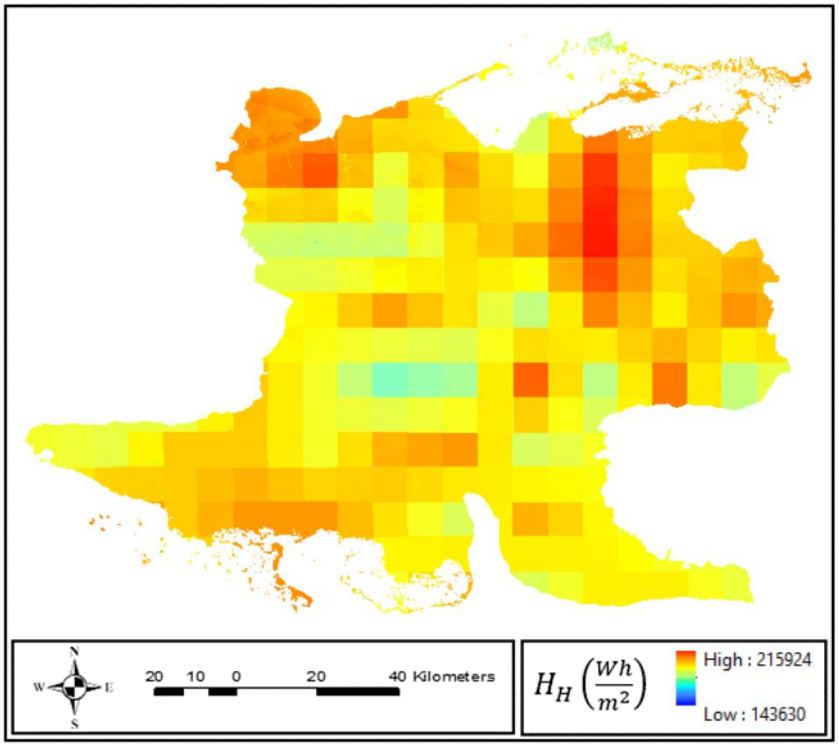

Appendix 10: Monthly Global Horizontal Irradiation in Matanzas during August.

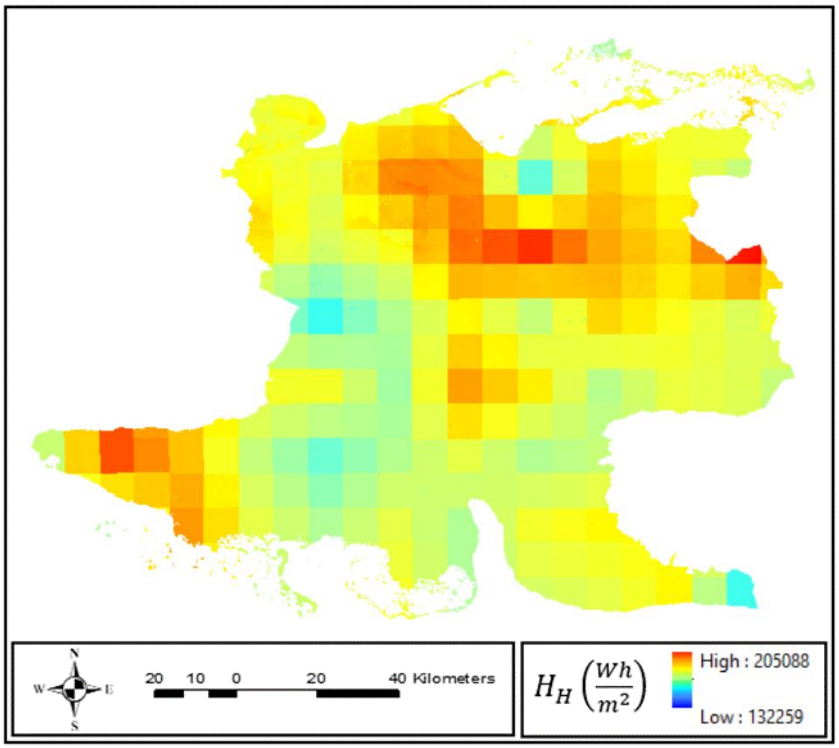

Appendix 11: Monthly Global Horizontal Irradiation in Matanzas during September.

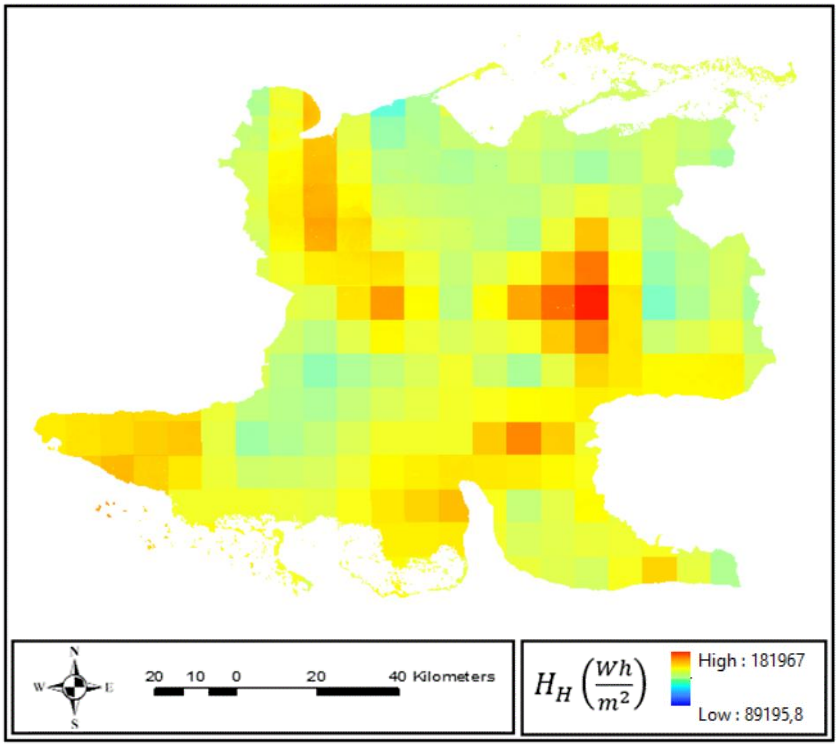

Appendix 12: Monthly Global Horizontal Irradiation in Matanzas during October.

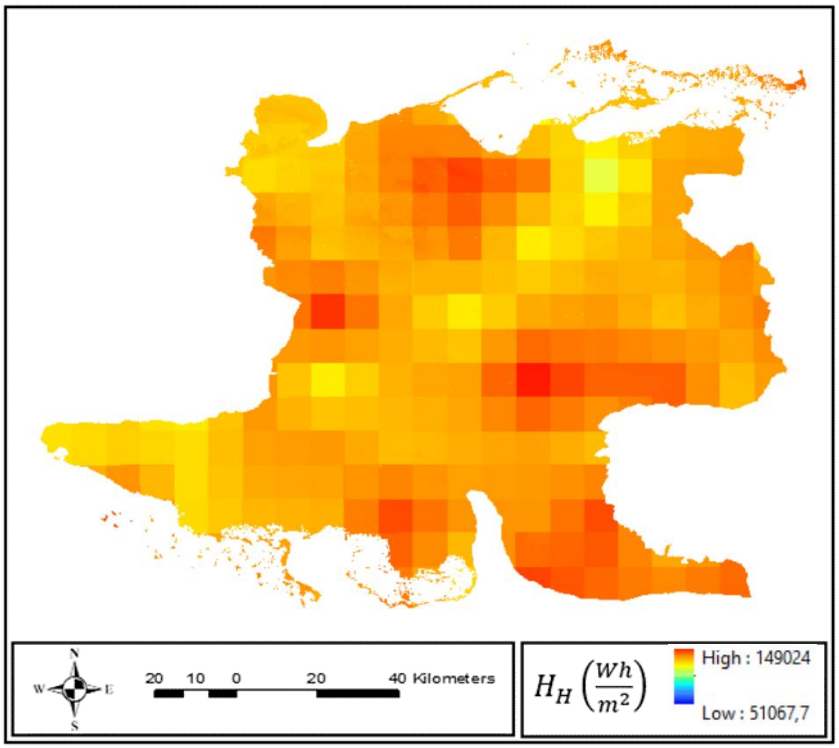

Appendix 13: Monthly Global Horizontal Irradiation in Matanzas during November.

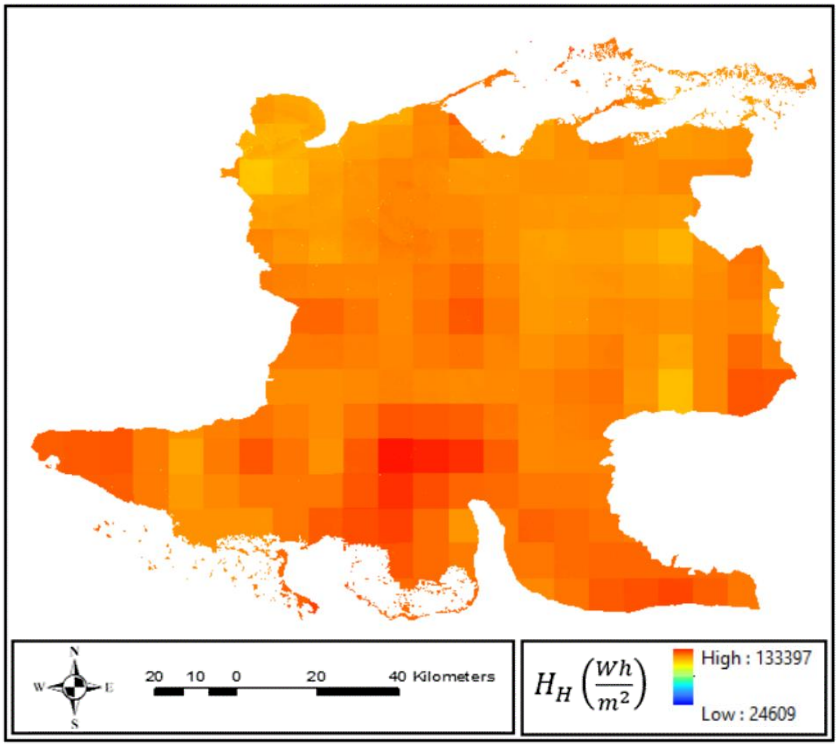

Appendix 14: Monthly Global Horizontal Irradiation in Matanzas during December.

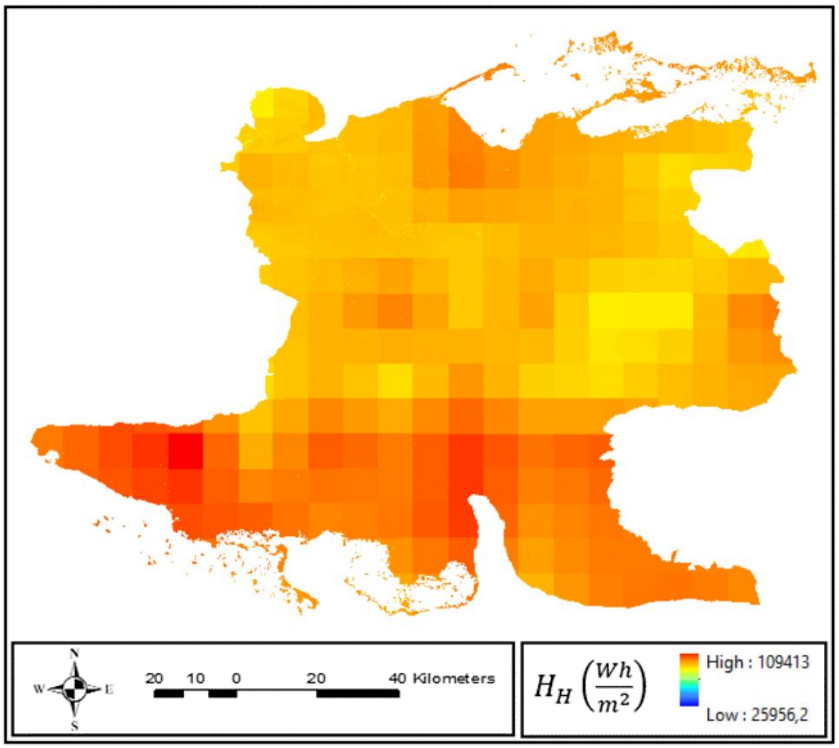

Appendix 15: Monthly Global Horizontal Irradiation in Guasasa during January.

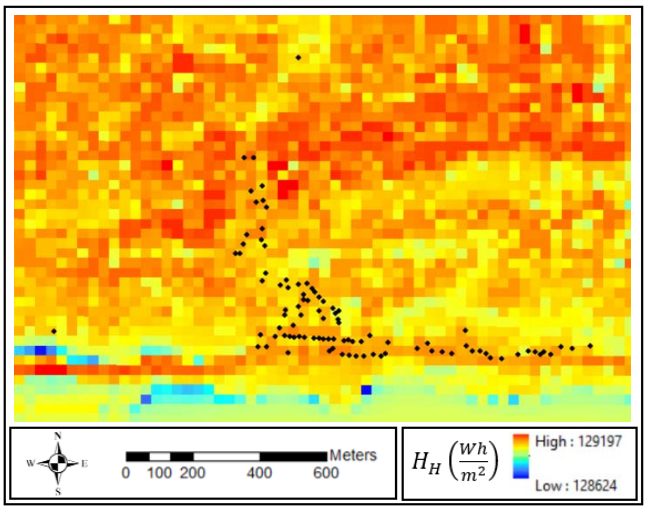

Appendix 16: Monthly Global Horizontal Irradiation in Guasasa during February.

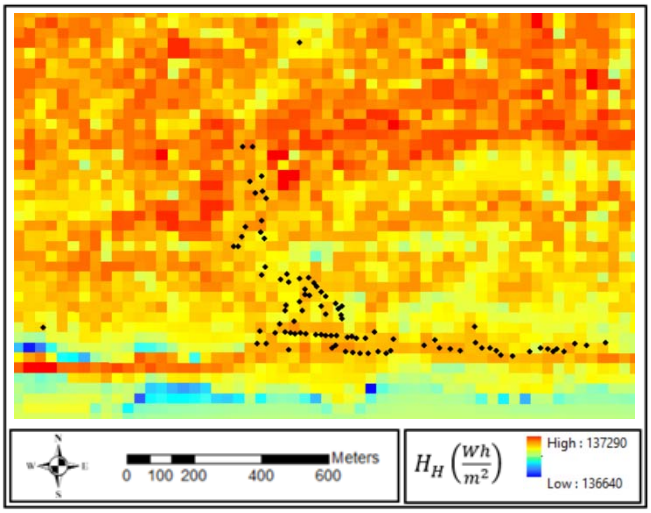

Appendix 17: Monthly Global Horizontal Irradiation in Guasasa during March.

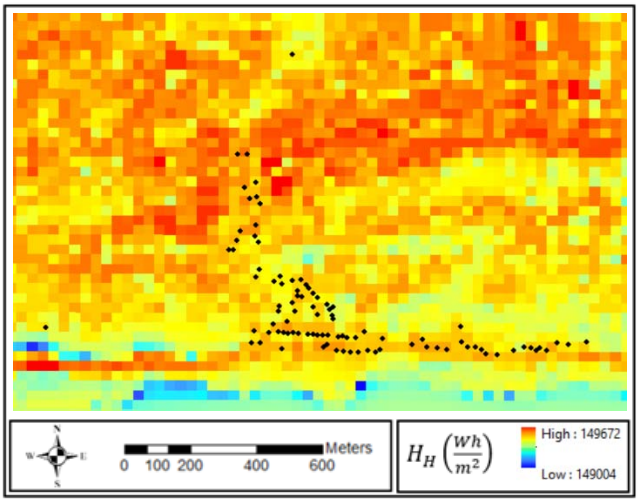

Appendix 18: Monthly Global Horizontal Irradiation in Guasasa during April.

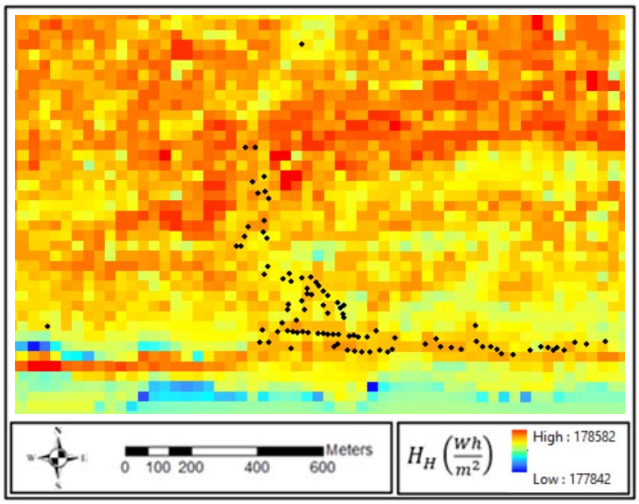

Appendix 19: Monthly Global Horizontal Irradiation in Guasasa during May.

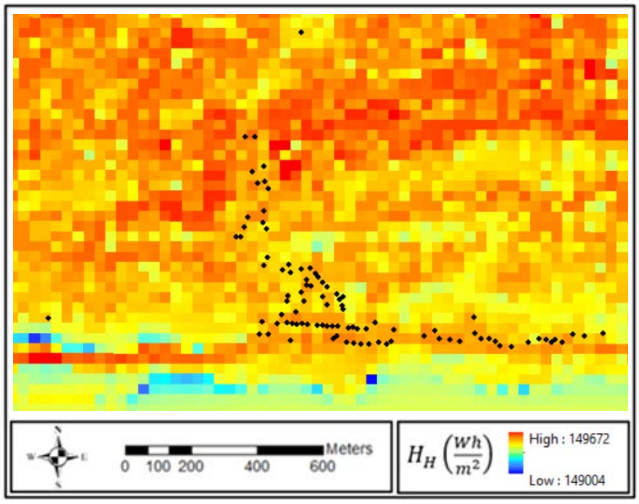

Appendix 20: Monthly Global Horizontal Irradiation in Guasasa during June.

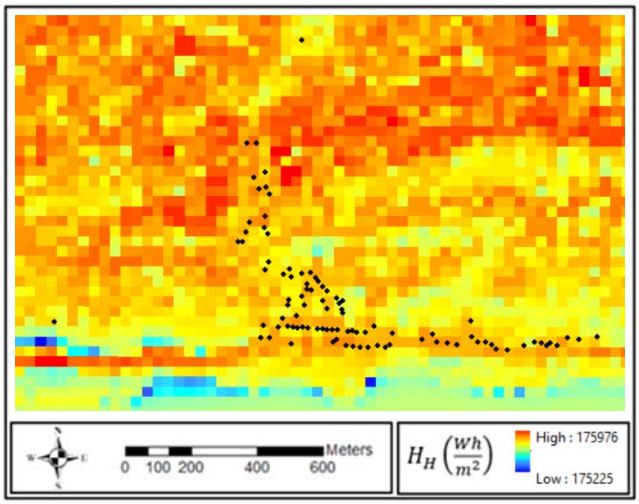

Appendix 21: Monthly Global Horizontal Irradiation in Guasasa during July.

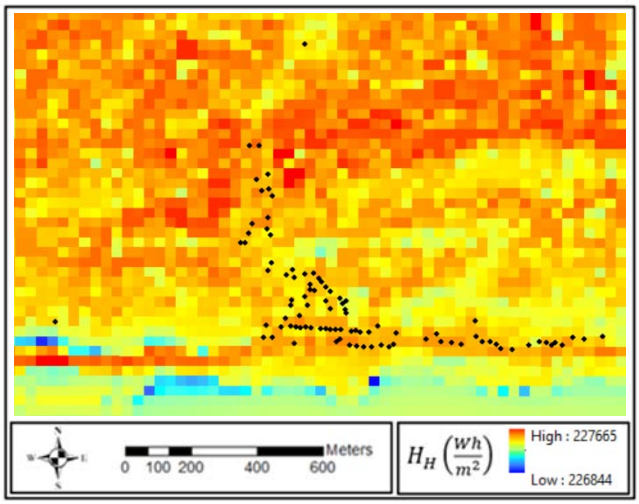

Appendix 22: Monthly Global Horizontal Irradiation in Guasasa during August.

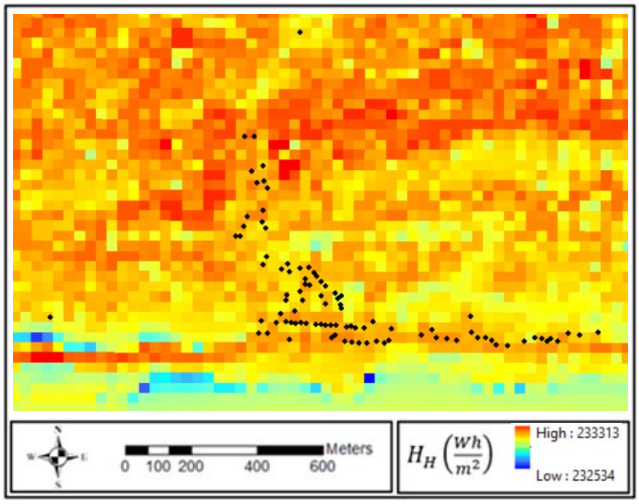

Appendix 23: Monthly Global Horizontal Irradiation in Guasasa during September.

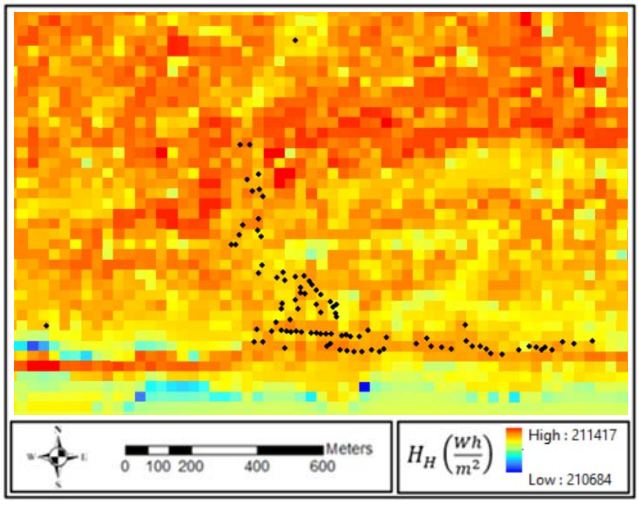

Appendix 24: Monthly Global Horizontal Irradiation in Guasasa during October.

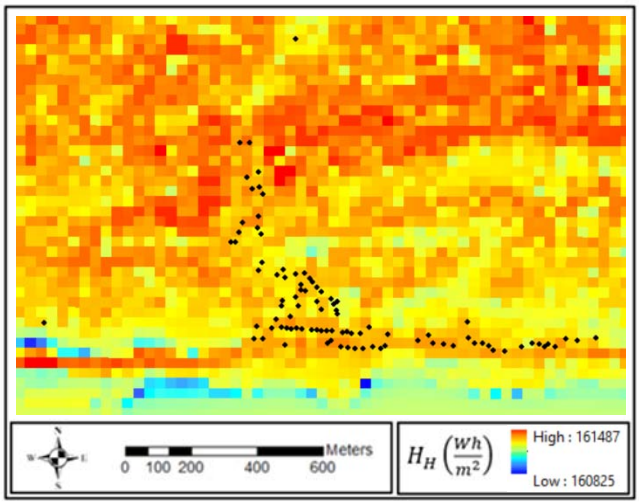

Appendix 25: Monthly Global Horizontal Irradiation in Guasasa during November.

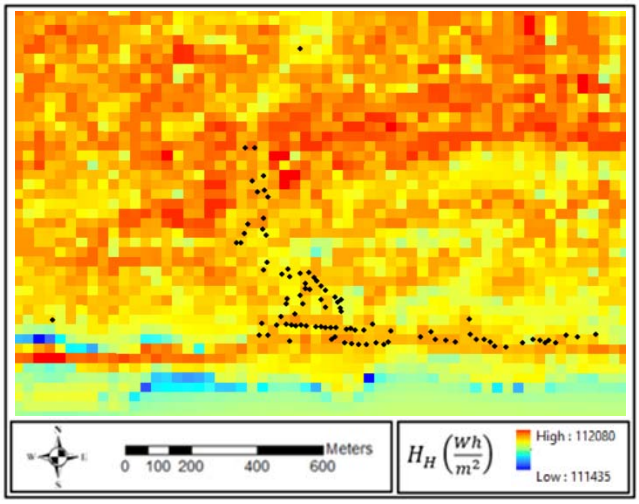

Appendix 26: Monthly Global Horizontal Irradiation in Guasasa during December.